

Microwave spectroscopy and multi-channel quantum defect analysis of ytterbium Rydberg states

Rin Kuroda,^{1, 2,*} Vernon M. Hughes,^{1, 2,*} Martin Poitrinal,¹ Michael Peper,^{1, †} and Jeff D. Thompson^{1, ‡}

¹*Department of Electrical and Computer Engineering,
Princeton University, Princeton, NJ 08544, USA*

²*Department of Physics, Princeton University, Princeton, NJ 08544, USA*

(Dated: July 16, 2025)

The complex Rydberg structure of ytterbium atoms is shaped by multiple low-lying ion-core-excited states and strong channel interactions, which presents both opportunities and challenges for quantum information processing and precision metrology. In this work, we extend high-resolution microwave spectroscopy and multichannel quantum defect theory (MQDT) modeling of singly excited $6snl$ Rydberg states in ^{174}Yb and ^{171}Yb to include the $\ell = 3$ (f) and $\ell = 4$ (g) series. Our measurements reveal p - f mixing in odd-parity Rydberg states of ^{171}Yb , which we incorporate by combined MQDT models for $6snp$ and $6snf$ series. Additionally, we observe that for $\ell = 4$ the spin-orbit interaction dominates over the exchange interaction, such that the $6sng$ states are more accurately described in a jj -coupled basis. We validate our models by comparing the predicted Landé g -factors and static dipole polarizabilities with experimental measurements, finding excellent agreement. These results provide important input for designing high-fidelity entangling gates with ytterbium atoms.

I. INTRODUCTION

Ytterbium (Yb) atoms provide a powerful and versatile platform for quantum computing and simulation [1–5], and precision metrology [6–8] due to their unique electronic structure and favorable atomic properties. In particular, the fermionic isotope ^{171}Yb , with nuclear spin $I = 1/2$, supports high-fidelity qubits using either the ground-state nuclear spin or the metastable $6s6p\,{}^3P_0$ state.

Encoding the qubit in the metastable 3P_0 state allows for midcircuit operations on atoms in the ground state, enabling efficient erasure error conversion [2, 9–11]. Combined with continuous coherent atom replacement [12] and fast, high-fidelity entanglement via single-photon Rydberg excitation [3, 5, 13] ytterbium atoms represent a promising candidate for scalable quantum technologies.

However, the energies and wavefunctions of Rydberg states in divalent atoms are modified by interactions with low-lying doubly excited *perturber* states [14–16]. Furthermore, in isotopes with non-zero nuclear spin, hyperfine coupling in the ionic core leads to additional mixing and level splittings within the Rydberg series [17–19]. These effects can be accurately captured through precision spectroscopy and modeling using multichannel quantum defect theory (MQDT) [20–23].

Previous studies of singly-excited $6snl$ Rydberg states in ytterbium have reported low- ℓ MQDT models to reproduce the observed energy spectra [13, 24–32]. A comprehensive study in Ref. [13] unified and refined the models for Rydberg series with $\ell \leq 2$, enabling the accurate

prediction of static dipole polarizabilities and interaction potentials of $6sns$ Rydberg states, leading to improved Rydberg gate fidelities. There have been several studies of higher angular momentum Rydberg series ($\ell \geq 3$) in ^{174}Yb [26, 30, 31, 33]. However, many series with $\ell \geq 3$ have not yet been measured, and there are no measurements of states with $\ell \geq 3$ in ^{171}Yb . Completing this picture would enable the prediction of properties of $6snd$ Rydberg states such as static dipole polarizabilities and Rydberg-Rydberg interactions.

In this article, we present three main results. First, in Sec. III and Sec. IV we extend the comprehensive microwave spectroscopy of ^{174}Yb and ^{171}Yb to $\ell = 3$ Rydberg series. We validate the accuracy of the presented models by comparison to measurements of g -factors. We observe that the $6snp$ and $6snf$ Rydberg series in ^{171}Yb are mixed for $F = 3/2$ and $F = 5/2$ due to configuration interactions, and demonstrate that combined MQDT models for these states resolve a previously reported deviation between the experimental and MQDT energies in the $6snp$ ($F = 3/2$) series [13].

Next, in Sec. V and Sec. VI we measure several previously unobserved $\ell = 4$ series in both ^{174}Yb and ^{171}Yb and develop MQDT models for these series. We find that for $\ell = 4$ the spin-orbit interaction dominates over the exchange interaction, such that the $6sng$ series are best described in jj instead of LS coupling, unlike the $\ell \leq 3$ states.

Finally, in Sec. VII, we validate the MQDT energies and wavefunction predictions for the $6snp$ and $6snf$ series in ^{174}Yb and ^{171}Yb by measuring the static dipole polarizabilities of $6snd$ states. We find excellent agreement between the measured polarizabilities and those predicted by the model. This confirms the model accuracy, enabling the predictions of Rydberg-Rydberg interactions involving $6snd$ states, which we discuss in Sec. VIII.

* These authors contributed equally to this work.

† michael.peper@princeton.edu

‡ jdthompson@princeton.edu

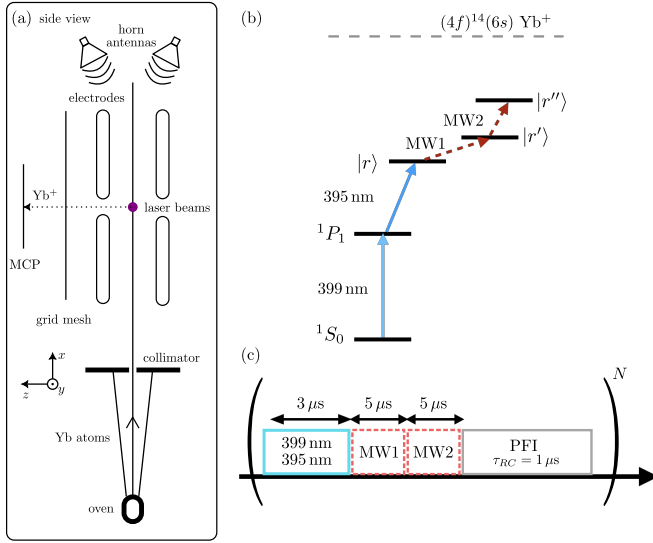


Figure 1. (a) Schematic diagram of the spectroscopy setup adapted from Ref. [13]. A collimated atomic beam interacts with the laser beams and microwave pulses near the center of the vacuum chamber. The atoms are ionized by PFI and detected by the MCP. (b) Schematic level diagram depicting the typical transition scheme to probe Rydberg states of interest. Details described in the text. (c) Typical pulse sequence. The laser pulses are simultaneously applied for $3\ \mu\text{s}$, followed by the microwave pulses for $5\ \mu\text{s}$ each. Subsequently, the Rydberg atoms are ionized by PFI and the time-of-flight of the resulting ions to the MCP is recorded using an oscilloscope. The experimental sequence is repeated at a rate of 1000 cycles per second, with each data point averaged over typically $N = 1500$ repetitions.

II. METHODS

A. Experimental setup

The experimental setup and methods used in this work follow those of Ref. [13]. A sketch of the experimental setup is presented in Fig. 1(a). In summary, an atomic beam of Yb is generated from an effusive oven and collimated using a pinhole aperture. We excite to $6snf$ and $6sng$ Rydberg states via a two-photon transition through the intermediate $6s6p\ ^1P_1$ state using counter-propagating laser beams at 399 nm and ≈ 395 nm, generated by frequency-doubled Ti:sapphire lasers. The laser beams are applied perpendicular to the atomic beam to minimize Doppler shifts. Using the isotope shift of the $6s6p\ ^1P_1$ transition, we selectively probe either ^{171}Yb ($I = 1/2$) or ^{174}Yb ($I = 0$) Rydberg states.

Rydberg population is detected via state-selective pulsed-field ionization (PFI) [34] followed by time-resolved ion detection on a microchannel plate (MCP). To probe laser-inaccessible $6sn\ell$ Rydberg states, including those with $\ell = \{1, 3, 4\}$, transitions between Rydberg states are driven using microwaves from 20–170 GHz, generated via frequency multiplication and ap-

plied through horn antennas. Laser and multi-step microwave pulses are applied consecutively in time. The microwave intensity is deliberately kept low to eliminate residual light shifts. A simplified level diagram showing the transition scheme and a typical pulse sequence of the spectroscopy experiment is shown in Fig. 1(b) and (c).

Static electric fields are controlled by a set of electrodes placed inside the vacuum chamber. Static magnetic fields are controlled by three pairs of Helmholtz coils. Residual electric fields and magnetic fields in the spectroscopy region are compensated as needed via dc Stark and Zeeman shift measurements.

B. MQDT modeling

We extend the MQDT framework described in Ref. [13] to $6snf$ and $6sng$ Rydberg states of ytterbium. The ^{174}Yb MQDT model parameters are determined as part of a global weighted optimization of all the $\ell \leq 4$ model parameters using previous and new spectroscopic data of ^{174}Yb , as compiled in Ref. [13] and App. C, respectively.

For ^{171}Yb , we prepare an initial guess based on the ^{174}Yb MQDT models and include the hyperfine interaction through a frame transformation [13, 35, 36]. We then optimize the ^{171}Yb MQDT parameters in a global weighted fit to all previous and new spectroscopic data of ^{171}Yb $\ell \leq 4$ states, as compiled in Ref. [13] and App. C, respectively.

III. ^{174}YB $6snf$ STATES

In ^{174}Yb , there are four distinct $6snf$ Rydberg series, which in LS coupling are labeled as 1F_3 , 3F_3 , 3F_2 , and 3F_4 . In this work, we present new microwave spectroscopic data on all four series and analyze them in conjunction with previously reported laser [26, 30] and microwave [31] spectroscopic data using single- and multi-channel quantum defect models. Series-specific details and comparisons are discussed in the following subsections.

An overview of the modeled spectroscopic data of the $6snf$ states of ^{174}Yb is presented in Fig. 2.

A. $6snf\ ^1,^3F_3$

The $6snf\ ^1,^3F_3$ Rydberg series in ^{174}Yb exhibit complex perturbations that have been partially characterized in earlier spectroscopic work [26, 30, 31, 37, 38]. Aymar et al. [26] reported state energies for $6snf\ ^1,^3F_3$ states in the range of $16 \leq n \leq 51$ with 3 GHz accuracy, and identified a single perturbing state at $50\ 228.09\ \text{cm}^{-1}$, which they attributed to a $4f^{13}5d^26s$ ($J = 3$) state. The laser spectroscopic data in Ref. [26] was modeled by a three channel MQDT model optimized for $6snf$ states in the range of $16 \leq n \leq 51$. Ali et al. [30] reported

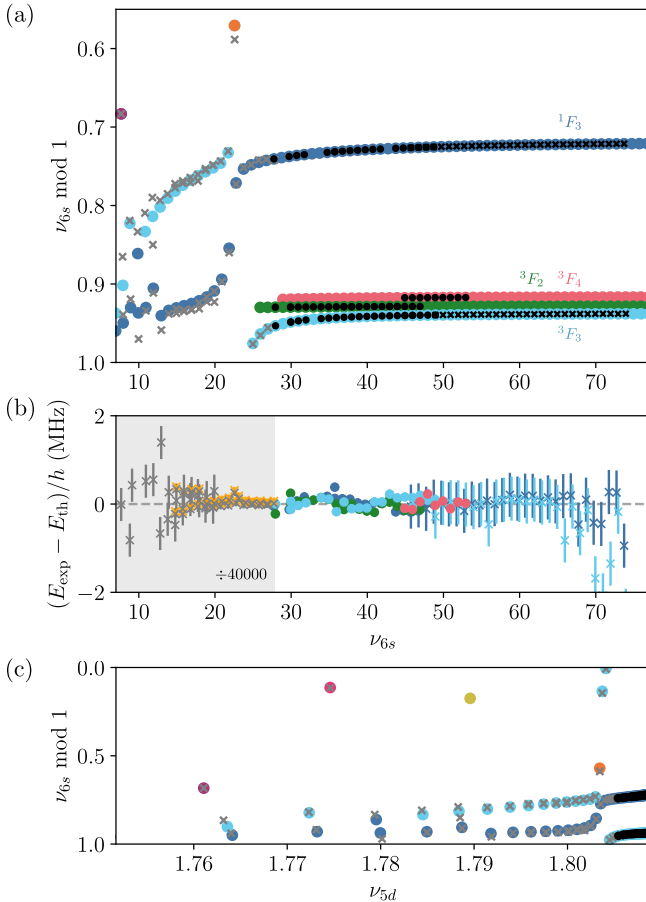


Figure 2. (a) Lu-Fano-type plot of ^{174}Yb odd-parity $6snf$ Rydberg states. The colored circles correspond to MQDT model predictions. Black crosses indicate microwave spectroscopic data obtained in Ref. [31]. The black points are experimentally measured energies by microwave spectroscopy reported in this work. The gray crosses are laser spectroscopy data from Refs. [26, 30]. The effect of a global offset of -2.4 GHz to the term values reported in Ref. [26] is discussed in the text. The $6snf\ ^{1,3}F_3$ series are mixed due to spin-orbit coupling, but the states are categorized based on their dominant character. (b) Deviation between experimental energies and the MQDT model predictions. Deviations of laser spectroscopy data (gray crosses) are divided by 40000, and the orange crosses are the deviations before the global offset was added. (c) Lu-Fano plot of the $6snf\ ^{1,3}F_3$ Rydberg states as a function of the effective principal quantum number ν_{5d} with respect to the $4f^{13}5d6s\ ^{1,3}D$ ionization threshold. The four non-blue-colored points denote the four perturbers discussed in Sec. III A, as reported in Refs. [26, 30].

additional lower lying $6snf\ ^{1,3}F_3$ Rydberg states with $9 \leq n \leq 30$ to 15 GHz accuracy, as well as three additional perturbers at $48\ 584.1\text{ cm}^{-1}$, $49\ 122.4\text{ cm}^{-1}$, and $49\ 661.6\text{ cm}^{-1}$, which were assigned as $4f^{13}5d^26s\ ^3D_3$, $4f^{13}5d^26s\ ^1F_3$, and $4f^{13}5d^26s\ ^3G_3$ states, respectively (see Tab. S21). The laser spectroscopic data was modeled by a five-channel MQDT model, which was optimized for states in the range $9 \leq n \leq 20$ and does not

include the perturbing state observed in by Aymar et al. [26]. Lehec [31] performed high-precision microwave spectroscopy of new $6snf\ ^{1,3}F_3$ states for $47 \leq n \leq 75$, with 500 kHz accuracy.

In this work, we extend the coverage of microwave spectroscopy to lower principal quantum numbers, reporting measurements of $6snf\ ^{1,3}F_3$ states in the range $30 \leq n \leq 50$ with 100 kHz accuracy. These results bridge the gap between the earlier laser [26, 30] and microwave [31] spectroscopy, and provide more accurate benchmark data for MQDT modeling. The $6snf\ ^{1,3}F_3$ states reported in this work are probed by a single-photon microwave transition from $6snf'd\ ^{1,3}D_2$ Rydberg states (see Tab. S19) or by a two-photon microwave transition from another $6snf'f\ ^3F_3$ state (see Tab. S20).

Based on the previous [26, 30, 31] and new spectroscopic data, we develop a new seven-channel MQDT model. This model combines the previously developed MQDT models [26, 30] into a single model for all $6snf$ states with $n \geq 9$. The MQDT model consists of the two $6snf\ ^1F_3$ and $6snf\ ^3F_3$ series, as well as five channels converging to the weighted average of the $4f^{13}(2F_{7/2})5d6s\ ^{1,3}D$ ionization thresholds at $83\ 967.70\text{ cm}^{-1}$. Four of the channels correspond to the perturbers observed in Refs. [26, 30]. To capture the energy dependence of the quantum defect of the $6snf\ ^{1,3}F_3$ Rydberg states, we found it necessary to include a fifth perturbing state with an energy above the lowest ionization threshold.

The parameters of the $6snf\ ^{1,3}F_3$ MQDT models obtained from the global fit routine (see Sec. II B) are tabulated in Tab. S7. The resulting model is presented as a Lu-Fano-type plot of the quantum defects and fit residuals in Fig. 2.

We observe excellent agreement between the observed and predicted state energies in the range of $30 \leq \nu_{6s} \leq 65$, with a maximum fit residual of less than 500 kHz. We note that the microwave data with $\nu > 65$ from Ref. [31] exhibits large scattering and is thus excluded from the fit. Additionally, we shift the laser spectroscopy data of Ref. [26] by 2.4 GHz to align with our microwave data in the range where they overlap. This is within the quoted 3 GHz uncertainty in Ref. [26].

We note that despite the inclusion of additional perturbing states, the energy dependence of the $6snf\ ^1F_3$ eigenchannel quantum defect $\mu_{^1F_3}$ is unusually large. Together with the significant deviations between the MQDT model predictions and the experimentally determined term values at low effective principal quantum number, this could indicate additional unaccounted perturbing states.

The singlet-triplet mixing for $6snf\ ^{1,3}F_3$ states is too small to measure from g -factors. We extract a mixing angle of $\theta(\nu) = -0.02084(4) + 0.239(2)/\nu^2$ from the hyperfine structure [13, 39, 40] of $6snf$ states in ^{171}Yb (see Sec. IV), yielding a 1F_3 admixture of $\sim 0.04\%$ in the 3F_3 states. Curiously, this is significantly smaller than the singlet-triplet mixing in high- n $6snP$ ($\sim 4\%$) and

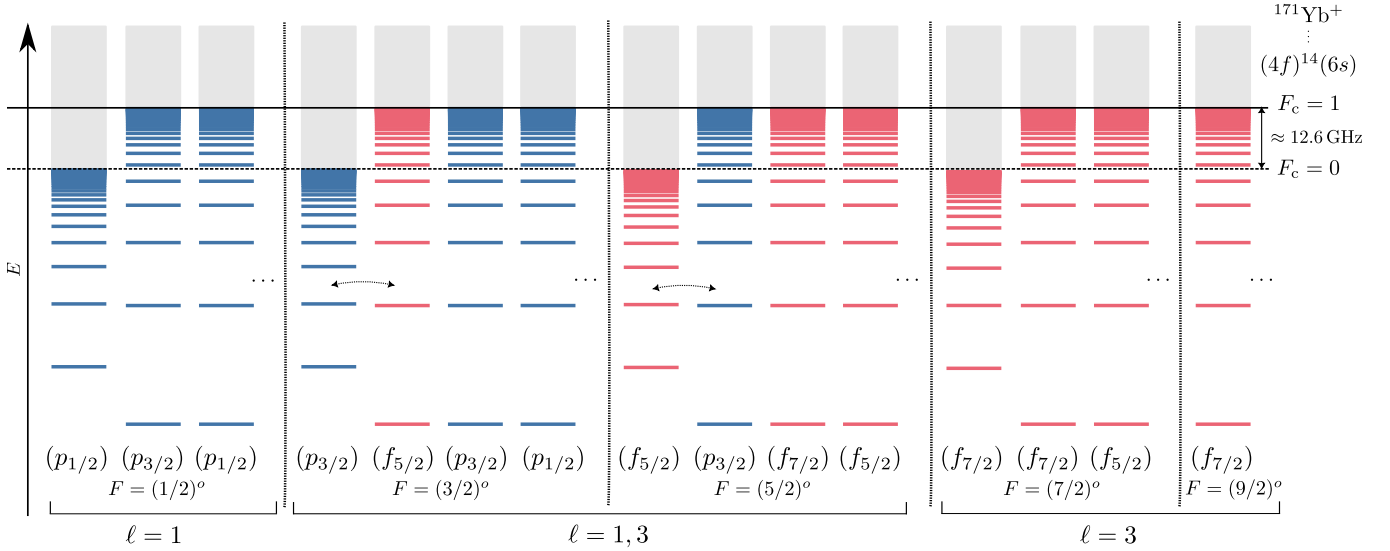


Figure 3. Schematic energy level diagram of the odd-parity $6snp$ (blue) and $6snf$ (red) Rydberg states of ^{171}Yb . Rydberg series with the same parity and total angular momentum F can mix. Arrows indicate mixing between the $6snp$ and $6snf$ series. Channels converging to ion-core-excited states are omitted, but are included in the MQDT models. The series are labeled by F and the quantum numbers of the Rydberg electron.

$6snd D$ ($\sim 15\%$) states of ytterbium [13]. We tentatively attribute this to the large singlet-triplet splitting between the $6snf\,{}^1,{}^3F_3$ states.

B. 3F_2 and 3F_4

Low-lying $6snf\,{}^3F_2$ and 3F_4 states ($5 \leq n \leq 14$) were previously assigned based on discharge-tube spectra recorded on a grating spectrometer [38]. Here, we present the results of microwave spectroscopy of the $6snf\,{}^3F_2$ and $6snf\,{}^3F_4$ series in the ranges $27 < \nu_{6s} < 47$ and $44 < \nu_{6s} < 53$, respectively. The $6snf\,{}^3F_2$ states are probed by microwave transitions from $6sn'd\,{}^1,{}^3D_2$ states (see Tab. S22) or two-photon microwave transitions from $6snf\,{}^3F_2$ or 3F_3 states (see Tab. S23). For $6snf\,{}^3F_4$ states, we record single-photon transitions from $6sn'd\,{}^3D_3$ states, which we populate by a preceding two-photon microwave transition from a $6sn''d\,{}^3D_2$ state (see Tab. S24).

We restrict the theoretical modeling of the $6snf\,{}^3F_2$ and $6snf\,{}^3F_4$ series to the microwave spectroscopic data reported in this work. Over the limited energy range of states recorded in this work, the $6snf\,{}^3F_2$ and $6snf\,{}^3F_4$ series are well described by a single-channel quantum defect model using energy-dependent quantum defects μ_α

$$\mu_\alpha(\nu_{6s}) = \mu_\alpha^{(0)} + \frac{\mu_\alpha^{(2)}}{\nu_{6s}^2} + \frac{\mu_\alpha^{(4)}}{\nu_{6s}^4} \dots, \quad (1)$$

where ν_{6s} is the effective principal quantum number with respect to the lowest ionization limit [13, 22]. The single-channel quantum defects for $6snf\,{}^3F_2$ and $6snf\,{}^3F_4$ are presented in Tab. S1.

A more comprehensive MQDT model of the $6snf\,{}^3F_2$ and $6snf\,{}^3F_4$ Rydberg series would require additional spectroscopic data, particularly of lower lying states [38].

IV. ODD-PARITY RYDBERG STATES OF ${}^{171}\text{YB}$

Hyperfine coupling with the $I = 1/2$ nucleus doubles the number of Rydberg series in ${}^{171}\text{Yb}$, compared to ${}^{174}\text{Yb}$. There are eight $6snf$ series, which in LS coupling are described as 3F_2 ($F = \{3/2, 5/2\}$), 1F_3 ($F = \{5/2, 7/2\}$), 3F_3 ($F = \{5/2, 7/2\}$), and 3F_4 ($F = \{7/2, 9/2\}$). However, certain $6snf$ series are mixed with $6snp$ series with the same F by a configuration interaction, which is allowed since both series have odd parity (see Fig. 3). Therefore, our model also includes the seven $6snp$ series, which in LS coupling are described as 3P_0 ($F = \{1/2\}$), 1P_1 ($F = \{1/2, 3/2\}$), 3P_1 ($F = \{1/2, 3/2\}$), and 3P_2 ($F = \{3/2, 5/2\}$) [13].

Spectroscopy of the $6snp$ Rydberg states of ${}^{171}\text{Yb}$ has been reported previously in Refs. [13, 27]. In Ref. [13], the spectroscopic data were modeled by introducing hyperfine interaction through a frame transformation [36, 41], with mostly good agreement particularly for higher lying ($\nu_{F_c=1} > 30$) Rydberg states. However, the energy of certain $6snp$ ($F = 3/2$) Rydberg states obtained by precision microwave spectroscopy deviated significantly from the theoretical predictions obtained from the presented MQDT model [13], with the fit residuals resembling a dispersion-like feature, implying the existence of an unaccounted channel interaction.

The observed discrepancies can be attributed to configuration interaction between Rydberg series with different orbital angular momenta. In multichannel systems

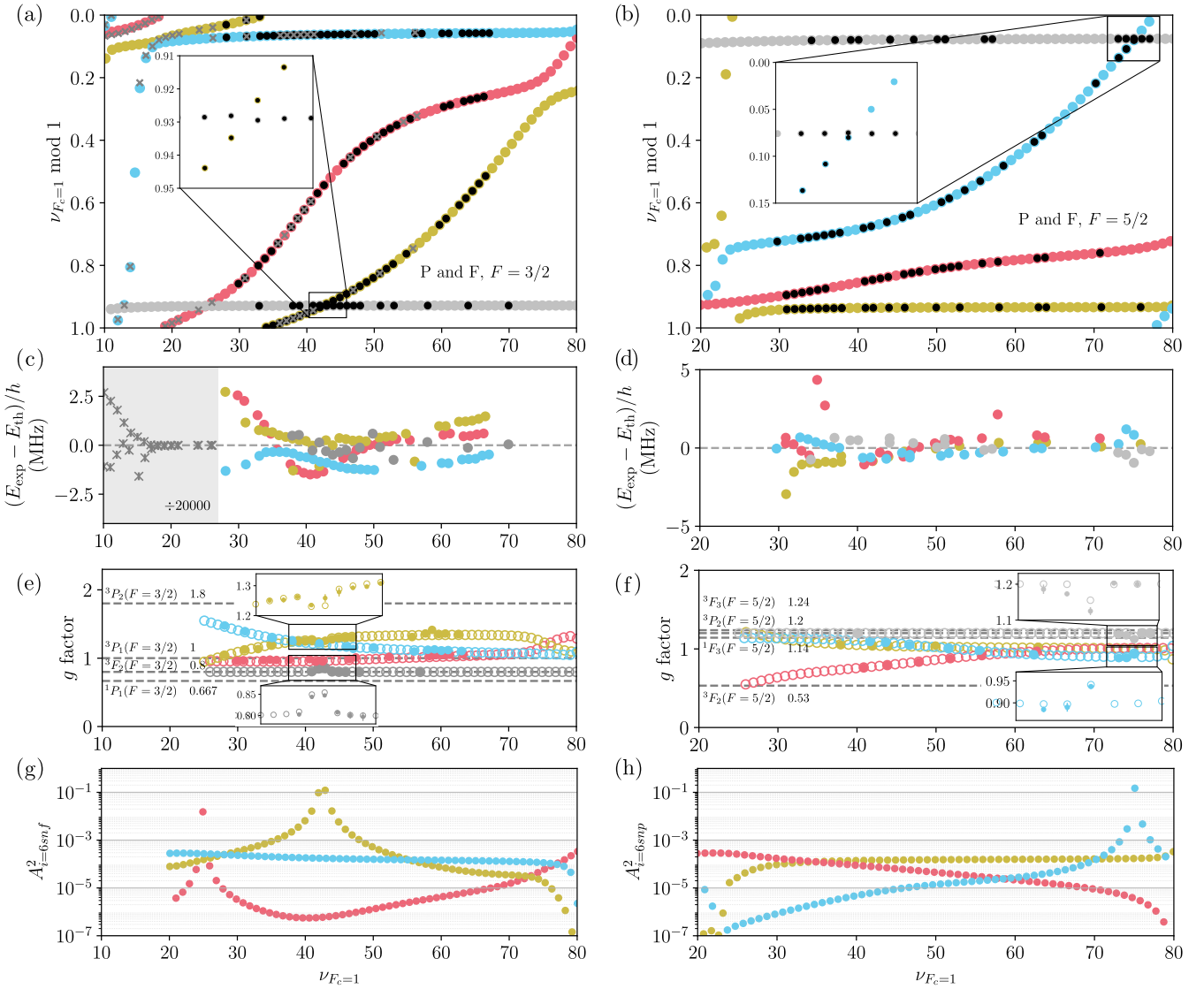


Figure 4. MQDT models for ^{171}Yb odd-parity Rydberg series. (a) Lu-Fano-type plots of the $F = 3/2$ and (b) $F = 5/2$ series, respectively. The black points are microwave spectroscopy data measured in this work and in Ref. [13]. The gray crosses are laser spectroscopic data reported in Ref. [27] and compiled in Ref. [13]. In (a), the gray colored series is of dominantly $\ell = 3$ character and the rest are dominantly $\ell = 1$. In (b), the gray colored series is of dominantly $\ell = 1$ character and the rest are dominantly $\ell = 3$. The insets are zoomed in near the avoided crossing between the $\ell = 1$ and $\ell = 3$ series. (c),(d) Deviation between experimental energies and the MQDT model bound state energies. (e),(f) Measured (filled points) and predicted (open circles) g -factors. The insets are zoomed in near the avoided crossing, where we observe admixture in the g -factors. The gray dashed lines indicate the analytical g -factors in LS coupling. (g) $6snf$ channel fraction of the dominantly $6snf$ series for $F = 3/2$. (h) $6snp$ channel fraction of the dominantly $6snp$ series for $F = 5/2$.

like ytterbium, such interactions play a central role in shaping both the energy spectrum and the character of the Rydberg wavefunctions. Although total parity and total angular momentum F remain conserved, coupling between channels with different orbital angular momentum ℓ —notably with $\Delta\ell = 2$ —can occur through effective quadrupole interactions in the ionic core [42]. This mechanism has been observed as p – f mixing in molecular hydrogen [43] and as s – d mixing in noble gases [44, 45]. While such mixing can occur even in the absence of hy-

perfine structure, the dense level structure of ^{171}Yb creates near-degeneracies between series of different ℓ , significantly enhancing sensitivity to these interactions [44].

In order to probe the p – f mixing in ytterbium, we record microwave spectra of previously unobserved $6snp$ and $6snf$ states. These states are excited via single photons from $6snd$ $F = 3/2$ and $F = 5/2$ states, which are populated by a two-photon laser transition from the ground state via the $6s6p\,{}^1P_1$ intermediate state. With this scheme, odd-parity Rydberg series with

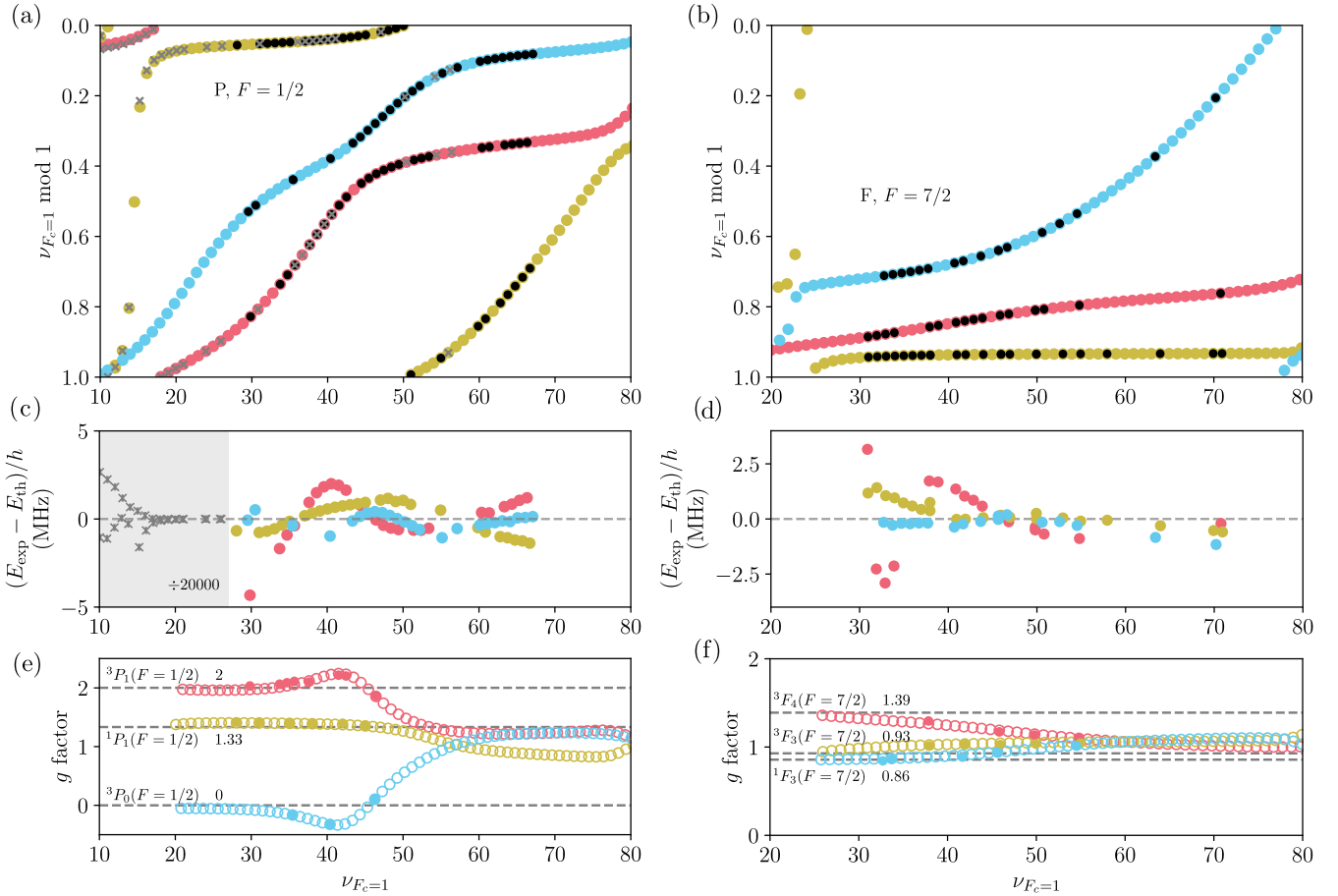


Figure 5. MQDT models for the ^{171}Yb 6snp ($F = 1/2$) and 6snf ($F = 7/2$) Rydberg series. (a),(b) Lu-Fano-type plots. The black points correspond to microwave spectroscopic data, and colored points are MQDT bound state energy predictions. The gray crosses are three-photon laser spectroscopic data reported in Ref. [27]. (c),(d) Deviation between experimental energies and the MQDT model bound state energies. (e),(f) Measured (filled circles) and predicted (open circles) g-factors. The gray dashed lines indicate the analytical g-factors in LS coupling.

$F = \{1/2, 3/2, 5/2, 7/2\}$ are accessible. The newly observed experimental transition frequencies are reported in Tabs. S32, S34 and S36 for $F = 3/2, 5/2$, and $7/2$, respectively.

The multi-channel models for odd-parity states with $F = 3/2$ and $F = 5/2$ include contributions from both the 6snp and 6snf Rydberg series (see Fig. 3), making them susceptible to p - f mixing. To account for this, we construct a combined MQDT model for the 6snp and 6snf states based on the spectroscopic data presented here and in previous studies [13, 27]. We find that a single mixing angle between the $6s_{1/2}np_{3/2}$ and $6s_{1/2}nf_{5/2}$ series is sufficient to capture the observed structure. In LS coupling, this corresponds to a mixing between the 6snp 3P_2 and 6snf 3F_2 channels.

On the other hand, the single- and multi-channel models for odd-parity states with $F = 1/2$, $F = 7/2$ and $F = 9/2$ only contain contributions from either 6snp or 6snf Rydberg series. Thus, these series do not exhibit p - f series mixing.

Starting from an initial guess based on the ^{174}Yb

MQDT parameters of the 6snp and 6snf state models, we optimize the ^{171}Yb MQDT parameters in a global fit of all $\ell \leq 4$ spectroscopic data. The resulting MQDT models are presented in App. B 2.

The experimental and theoretical energies are presented in Fig. 4(a) and (b) for $F = \{3/2, 5/2\}$ and Fig. 5(a) and (b) for $F = \{1/2, 7/2\}$. Generally, we observe good agreement between the experimental energies and the MQDT predictions, particularly resolving the dispersion-like feature observed in Ref. [13] (see Fig. 6(a)), with an RMS deviation of 0.91 MHz for all 6snp and 6snf states measured via microwave transitions.

We additionally probe the accuracy of the MQDT wavefunctions by measuring Landé g -factors and comparing to the theoretical predictions (Fig. 4(e) and (f) for $F = \{3/2, 5/2\}$ and Fig. 5(e) and (f) for $F = \{1/2, 7/2\}$). The experimentally observed g -factors are reproduced by the MQDT predictions accurately, and both experimental and theory g -factors are tabulated in Tabs. S33, S35 and S37.

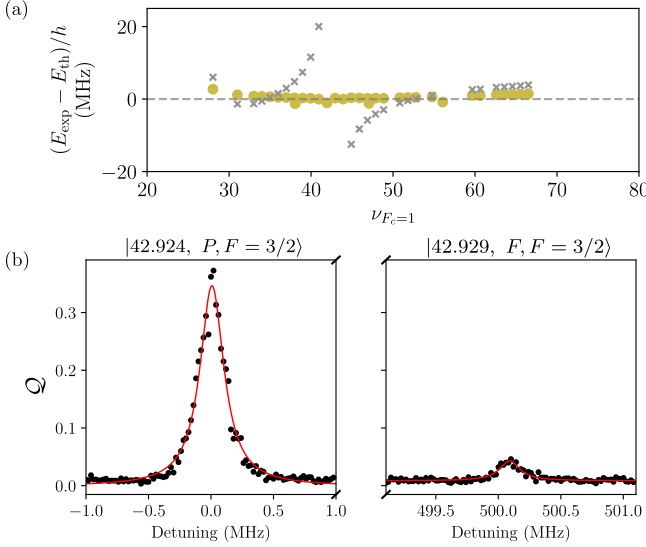


Figure 6. (a) Deviation between experimental energies and MQDT model bound state energies before (gray crosses) [13] and after (yellow points) the introduction of the p - f mixing angle in the MQDT model. (b) Microwave excitation spectrum from the $|\nu_{F_c=1} = 41.703, S, F = 1/2\rangle$ state to the $|\nu_{F_c=1} = 42.924, P, F = 3/2\rangle$ and $|\nu_{F_c=1} = 42.929, F, F = 3/2\rangle$ states, respectively. The experimentally measured ratio between the transition strengths was 11.9(9), which is comparable with the MQDT model prediction of 8.0. We note that this deviation may arise from potentially frequency dependent microwave intensity at the atoms between the two transitions. Q denotes the fraction of the microwave signal with respect to the original Rydberg laser signal.

As part of our fitting of the MQDT model to spectroscopic data, we extract a p - f mixing angle of $\theta_{pf} = 1.842(8) \times 10^{-2}$, which governs the strength of coupling between the $6snp$ and $6snf$ channels. The states with predominantly p character therefore have a $\mathcal{O}(\theta_{pf}^2) \approx 10^{-4}$ admixture of f states population, and the predominantly f states have a similar p character (see Fig. 4(g) and (h)). Near degeneracies between $6snp$ and $6snf$ series with the same F , the states are more strongly mixed, reaching an admixture of $> 10\%$. An avoided-crossing feature is observed in the energies for $F = 3/2$ and $F = 5/2$ (see insets in Fig. 4(a) and (b)), and the g -factors are also affected (see insets in Fig. 4(e) and (f)). To further demonstrate the mixed wavefunctions, we drive a single-photon microwave transition from $|\nu_{F_c=1} = 41.703, S, F = 1/2\rangle$ to $|\nu_{F_c=1} = 42.929, F, F = 3/2\rangle$ (see Fig. 6(b)).

The singlet-triplet mixing angle of the $6snf$ states, fitted to ^{171}Yb spectroscopic data as $\theta(\nu) = -0.02084(4) + 0.239(2)/\nu^2$, yields a small 1F_3 admixture of $\sim 0.04\%$ in the 3F_3 states. We apply this same mixing angle to the $6snf$ $^1,^3F_3$ states of ^{174}Yb . In addition, p - f mixing between the $6snp$ 3P_2 and $6snf$ 3F_2 series is also expected in ^{174}Yb , but the admixture remains inherently small—on

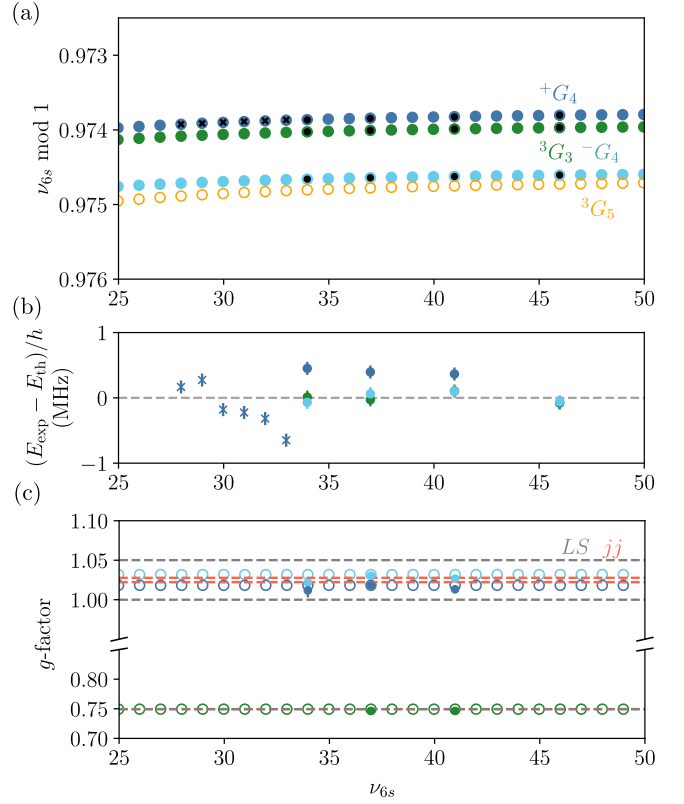


Figure 7. (a) Lu-Fano-type plot of ^{174}Yb $\ell = 4$ Rydberg states: $^+G_4$ (dark blue), $^-G_4$ (light blue), 3G_3 (green), and 3G_5 (orange). The $J = 4$ series are fit to a single MQDT channel described in jj coupling. The 3G_5 MQDT parameters are inferred from the ^{171}Yb model, as described in the text. The black points and crosses correspond to experimentally observed states by microwave spectroscopy reported in this work and in Ref. [33], respectively. (b) Deviation between experimental energies and the MQDT bound state energies. Markers as in panel (a). (c) Measured (filled points) and predicted (open circles) g -factors. The gray dashed lines correspond to the theoretical g -factors for purely LS coupling, while the orange dashed lines correspond to theoretical g -factors for jj coupling.

the order of $\sin^2(\theta_{pf}) \sim 10^{-4}$ —due to the absence of near-degeneracies, despite a similar mixing angle θ_{pf} as ^{171}Yb .

V. ^{174}YB $6sng$ STATES

In ^{174}Yb , there are four distinct $6sng$ Rydberg series, which in LS coupling are labeled as 1G_4 , 3G_4 , 3G_3 , and 3G_5 . Only the 1G_4 Rydberg series has been previously observed, using microwave spectroscopy [33].

Here, we present new spectroscopic data and MQDT models of $6sng$ Rydberg states in ^{174}Yb , which we measure by laser excitation to $6sn''d$ states followed by sequential two-photon excitations via $6sn'f$ 3F_3 states. The observed transition frequencies are reported in

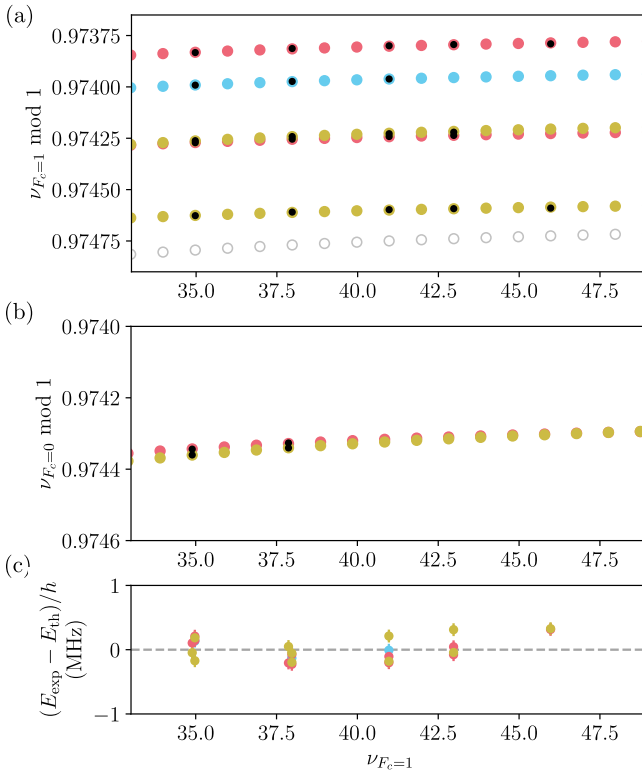


Figure 8. (a),(b) Lu-Fano-type plots of the G $F = 5/2$ (yellow), $F = 7/2$ (blue), $F = 9/2$ (pink), and $F = 11/2$ (light gray) series in ^{171}Yb , converging to the $F_c = 1$ and $F_c = 0$ hyperfine thresholds, respectively. The black points correspond to experimentally observed states by microwave spectroscopy reported in this work. (c) Deviation between the experimental energies and predicted MQDT bound state energies, with all energies plotted with respect to the $F_c = 1$ hyperfine threshold.

Tabs. S25 and S27. An overview of the observed $6sng$ states is presented in Fig. 7.

For the $6sng$ ($J = 4$) states, we observe two distinct series with small quantum defects of approximately 0.026, one of which aligns with the previously reported 1G_4 states from Ref. [33], while the other represents a newly observed $6sng$ ($J = 4$) series. The small quantum defects indicate that these high- ℓ states are close to the hydrogenic limit, where the centrifugal barrier strongly suppresses penetration of the Rydberg electron into the Yb^+ ion-core. As a result, the spin-orbit interaction (favoring jj -coupling) becomes stronger relative to the exchange interaction (favoring LS -coupling), and the states are more accurately described in the jj -coupled basis. Such behavior has been observed in other alkaline-earth-like atoms including helium, barium, and strontium [46–48].

The precise nature of the ^{174}Yb $6sng$ ($J = 4$) series is probed by measuring the Landé g -factors (see Fig. 7(c), Tab. S28). When treating the two series in terms of LS -coupled ${}^1,{}^3G_4$, the extracted singlet-triplet mixing angle between the two series is $\theta^{LS} = 0.66(4)$. This is close to the full singlet-triplet mixing of $\theta^{LS} = 0.73$, given by

the analytic expression $\arctan\left(\sqrt{\ell}/(\ell+1)\right)$, obtained by expressing the LS - jj frame transformation [49] in terms of a rotation matrix. Instead, when describing the two series in jj coupling, the mixing angle evaluates to $\theta^{jj} = -0.06(3)$. This indicates that the two series are more accurately described in jj coupling. We therefore denote these two series as $6sng^{\pm} G_4$, corresponding to the state labels $(1/2, \ell \pm 1/2)_4$. The two-channel MQDT model is presented in Tab. S8). An overview of the microwave spectroscopic data and MQDT predictions are shown in a Lu-Fano-type plot (Fig. 7(a)). The deviations between the experimental and MQDT bound state energies are shown in Fig. 7(b).

For the $6sng$ 3G_3 series, we record energies of four states and model the quantum defects of this series with a single-channel quantum defect model (see Tab. S1). Over the limited energy range of observed states, the quantum defects of $6sng$ 3G_3 series are well described by the series expansion given in Eq. 1. The deviations between the experimentally observed and predicted energies are shown in Fig. 7(b). To check the assignment of the observed states, we record g -factors, which align with the analytical expression for $6sng$ 3G_3 states of $g_J = 0.75$ (see Fig. 7(c), Tab. S26).

The $6sng$ 3G_5 states are not accessible via a single photon transition from the $6snf$ 3F_3 intermediate state. However, we observe 3G_5 Rydberg states in ^{171}Yb , as presented in Sec. VI. Thus, we present a single-channel quantum defect model of ^{174}Yb $6sng$ 3G_5 in Tab. S1 using the corresponding parameters in ^{171}Yb .

VI. ^{171}YB $6sng$ STATES

There are eight $6sng$ series in ^{171}Yb , which can be expressed as 3G_3 ($F = \{5/2, 7/2\}$), ${}^+G_4$ ($F = \{7/2, 9/2\}$), ${}^-G_4$ ($F = \{7/2, 9/2\}$), and 3G_5 ($F = \{9/2, 11/2\}$). To our knowledge, no prior spectroscopic data have been reported for the $\ell = 4$ states of ^{171}Yb .

Here, we report spectroscopic data on the $6sng$ $F = 5/2$, $7/2$, and $9/2$ series by two-step microwave transitions starting from laser excited $6sn''d$ states, followed by $6sn'f$ ($F = 7/2$) states. Transitions from $6snf$ $F = 3/2$ and $F = 5/2$ states were used to verify the assignment of states based on selection rules. Six of the series (including $6sng(F = 11/2)$) converge to the $F_c = 1$ hyperfine threshold (Fig. 8(a)), while two converge to the $F_c = 0$ hyperfine threshold (Fig. 8(b)). The measurement range is limited to $\nu = 35$ to 46 by the available microwave sources and difficulties in state-selective field ionization. The recorded transition frequencies are presented in Tabs. S38 to S40.

We observe small quantum defects for each of these series, which are consistent with the $6sng$ quantum defects observed in ^{174}Yb . Also similarly to ^{174}Yb , we describe these series in jj coupling, using a frame transformation matrix to achieve this effect in our MQDT model. The

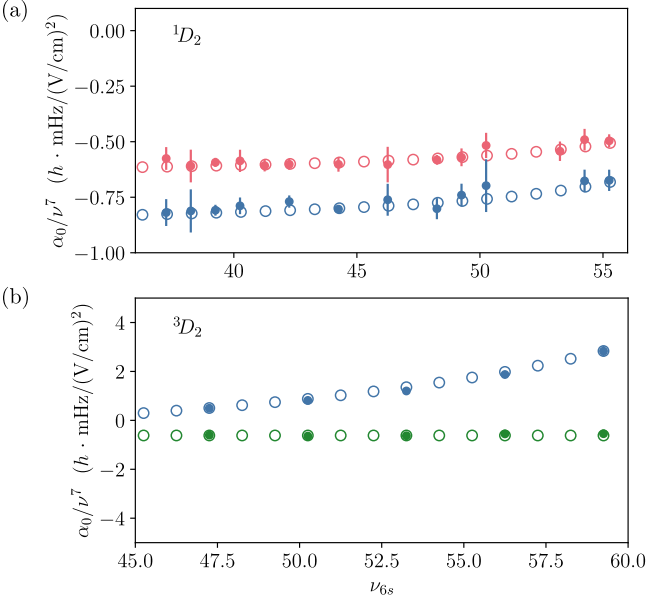


Figure 9. Measured (filled circles) and predicted (open circles) static dipole polarizabilities of (a) $6snd\ ^1D_2$ and (b) $6snd\ ^3D_2$ states in ^{174}Yb , scaled by ν_{6s}^7 . The blue, red, and green points correspond to $m_J = 0, 1$, and 2 sublevels, respectively.

MQDT model parameters are fitted in a global optimization as described in Sec. II B. The resultant model parameters are tabulated in Tabs. S16 to S18. In particular, the mixing angle between the $\pm G_4$ states is determined to be $\theta^{jj} = -0.082(6)$, which is consistent with the inferred mixing angle from the ^{174}Yb g -factors. The sign of the mixing angle cannot be determined from state energies, but is inferred from the ^{174}Yb g -factor measurements.

We have not directly measured states of the $6sng$ ($F = 11/2$) series, but can predict their location using parameters obtained from the 3G_5 ($F = 9/2$) channel.

VII. DC STARK SHIFTS OF $6snd$ RYDBERG STATES OF ^{174}YB AND ^{171}YB

Knowledge of the $6sns$, $6snp$, $6snd$, $6snf$ and $6sng$ Rydberg state energies and wavefunctions allow us to make accurate predictions on the static dipole polarizabilities of $6snd$ Rydberg states. Here, we test the predictions by measuring energy shifts for a range of $6snd$ states as a function of the static electric field, for both ^{174}Yb and ^{171}Yb .

Experimentally, we measure the Stark shift ΔE_{Stark} over a range of electric fields F chosen so that the maximum Stark shifts are on the order of tens of MHz. We extract the static dipole polarizability α_0 by a fit to the quadratic region:

$$\Delta E_{\text{Stark}}(\mathbf{F}) = -\frac{1}{2}\alpha_0\mathbf{F}^2 \quad (2)$$

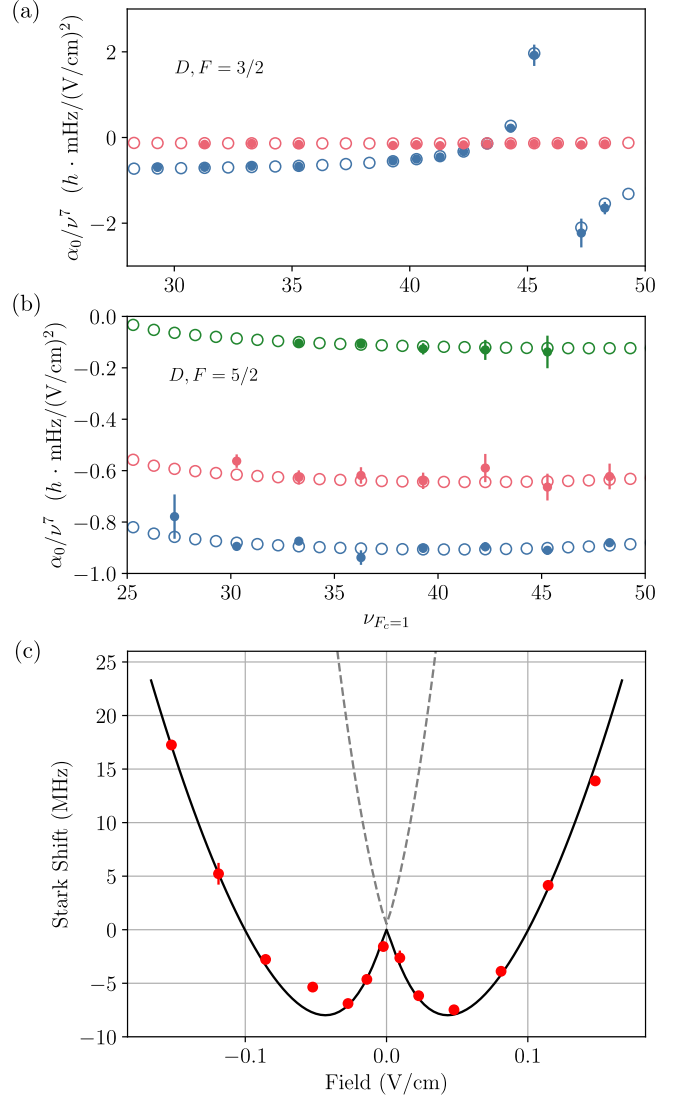


Figure 10. (a),(b) Measured (filled circles) and predicted (open circles) static dipole polarizabilities of (a) $|\nu, D, F = 3/2\rangle$ and (b) $|\nu, D, F = 5/2\rangle$ states of dominantly 1D_2 character in ^{171}Yb , scaled by $\nu_{F_c=1}^7$. The blue, red, and green points correspond to $m_F = 1/2, 3/2$, and $5/2$, respectively. (c) Experimental (red dots) and theoretical (solid black line) Stark shifts of the $|\nu_{F_c=1} = 62.28, D, F = 5/2\rangle$ state near a degeneracy with a $|\nu_{F_c=1} = 62.28, P, F = 3/2\rangle$ state. The Stark shifts of the $|\nu_{F_c=1} = 62.28, P, F = 3/2\rangle$ state are plotted as the dashed gray line.

For ^{174}Yb we measure polarizabilities of 1D_2 and 3D_2 Rydberg states (see Fig. 9). For ^{171}Yb , we measure $|\nu, D, F = 3/2\rangle$ and $|\nu, D, F = 5/2\rangle$ states of dominantly 1D_2 character (see Fig. 10). We observe excellent agreement between the experimentally measured polarizabilities and theoretical predictions. The observed and predicted polarizabilities are presented in Tabs. S30, S31, S41 and S42. Predicted static dipole polarizabilities of additional $6snd$ Rydberg series in both isotopes are presented in App. A.

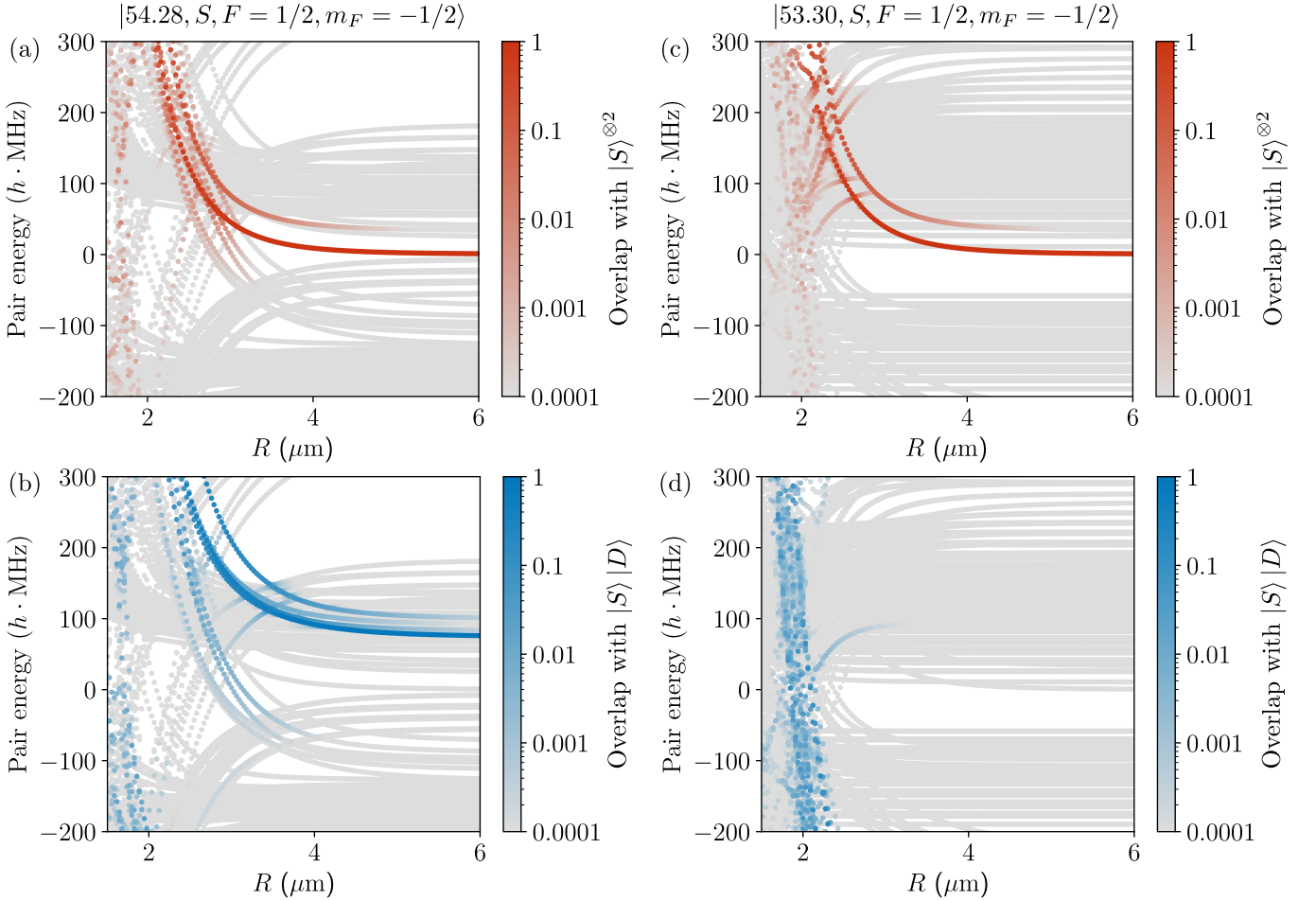


Figure 11. Predicted ^{171}Yb pair-interaction potentials for target Rydberg states $|S\rangle = |\nu, L = 0, F = 1/2, m_F = -1/2\rangle$ at a magnetic field strength of 5 G perpendicular to the interatomic axis, shown for (a),(b) $\nu = 54.28$ and (c),(d) $\nu = 53.30$. Each pair of panels is referenced to the corresponding $|S\rangle^{\otimes 2}$ asymptote. The color of each curve indicates the overlap with product states of $|S\rangle$ and $|D\rangle = |\nu, L = 2, F = 3/2, m_F = -1/2\rangle$ atoms, with $\nu = 54.29$ in (a),(b) and $\nu = 53.29$ in (c),(d). Panels (a),(c) highlight states with dominant $|S\rangle^{\otimes 2}$ character, while panels (b),(d) show those with dominant $|S\rangle|D\rangle$ character.

When these $6snd$ states are near-degenerate with opposite parity states, their dc Stark shifts can be non-quadratic even for small fields. In particular, the divergent feature of the $|\nu, D, F = 3/2, m_F = 1/2\rangle$ polarizability from the expected $\nu_{F_c=1}^7$ scaling near $\nu_{F_c=1} \approx 46$ is caused by a near-degeneracy with $P, F = 1/2$ states. More generally, most of the $D, F = \{3/2, 5/2\}$ states in the range $\nu_{F_c=1} > 40$ experience a series of near degeneracies with dipole-coupled states, resulting in non-quadratic Stark shifts even for small fields.

In Fig. 10(c), we present measurements of dc Stark shifts of the $|\nu_{F_c=1} = 62.28, D, F = 5/2\rangle$ state, which is near-degenerate with the $|\nu_{F_c=1} = 62.28, P, F = 3/2\rangle$ state. The energy separation between the two states is approximately one MHz, which causes a deviation from a quadratic Stark shift, and we observe a double-well-type Stark shift.

VIII. 6snd RYDBERG-RYDBERG INTERACTION POTENTIALS

Entangling gates in ^{171}Yb have been implemented via laser excitation to $6sns$ Rydberg states, using single-photon excitation from the metastable qubit state $6s6p^3P_0$ [2, 3, 5, 13]. These gate protocols rely on the Rydberg blockade mechanism, in which strong dipole–dipole interactions between nearby Rydberg atoms prevent simultaneous excitation, enabling conditional logic operations between qubits [50].

Extensive laser and microwave spectroscopy and modeling of $\ell \leq 2$ Rydberg series of ^{171}Yb Rydberg states in Ref. [13] enabled the accurate prediction of static dipole polarizabilities and interaction potentials of $6sns$ Rydberg states. This revealed the presence of Förster resonances in the interaction of $6sns$ ($F = 3/2$) Rydberg states, previously used for implementing two-qubit gates [2]. The Förster resonances result in a dense manifold of weakly

interacting pair states near zero energy at short separations, which can be unintentionally populated within the blockade radius, thereby reducing the fidelity of Rydberg-mediated gates. Recognizing this limitation led to the adoption of a $6sns$ ($F = 1/2$) state, whose interaction spectrum is free of Förster resonances and thus more favorable for high-fidelity entangling operations.

Another potential source of blockade violations comes from $6snd$ Rydberg states, which are also accessible by a single-photon transition from $6s6p\ ^3P_0$. In particular, interactions can shift SD pair states into resonance with the driving laser at particular short atom separations. Accurate predictions of the interactions involving $6snd$ states requires precise models of the $6snf$ state energies and wavefunctions, which are developed in this work.

As an example, in Fig. 11(a) and (b) we present predicted Rydberg-Rydberg interaction potentials near the $|S\rangle^{\otimes 2} = |54.28, L=0, F=1/2, m_F=-1/2\rangle^{\otimes 2}$ pair state used for entangling gates in our tweezer setup [13]. The $|S\rangle$ state is detuned from $|D\rangle = |54.29, L=2, F=3/2\rangle$ by only 70 MHz at zero magnetic field. In this case, the Rydberg blockade remains strong, because the $|S\rangle|D\rangle$ state lies energetically above the $|S\rangle^{\otimes 2}$ state, and both the $|S\rangle^{\otimes 2}$ and $|S\rangle|D\rangle$ pair states exhibit large repulsive interaction shifts.

In contrast, the Rydberg-Rydberg interaction potentials near the $|S'\rangle^{\otimes 2} = |53.30, L=0, F=1/2, m_F=-1/2\rangle^{\otimes 2}$ asymptote are presented in Fig. 11(c) and (d). In this case, the corresponding $|D'\rangle = |53.29, L=2, F=3/2\rangle$ state lies 600 MHz below the $|S'\rangle$ state. Naively, this large detuning of the $|S'|D'\rangle$ state should reduce the impact of a Rydberg blockade violation. However, the $|S'|D'\rangle$ pair state exhibits a strong repulsive interaction, shifting the $|S'|D'\rangle$ into resonance of the laser at a tweezer separation of $\sim 2 \mu\text{m}$ (see Fig. 11(d)).

These two examples illustrate that a detailed analysis is required for specific experimental conditions, including the effects of magnetic field and orientation.

IX. DISCUSSION AND OUTLOOK

The precision microwave spectroscopy presented in this work enabled the development of accurate MQDT models for the $6snp$, $6snf$, and $6sng$ Rydberg series of both ^{174}Yb and ^{171}Yb . Particularly, in ^{171}Yb we identified mixing between $6snp$ and $6snf$ states with total angular momentum $F = 3/2$ and $F = 5/2$, which leads to significant variations in energies and wavefunctions near accidental degeneracies. Incorporating this effect into combined-channel MQDT models resolves previously unexplained deviations in the $6snp$ ($F = 3/2$) series [13]. In addition, we characterized several previously unobserved $\ell = 4$ Rydberg series and demonstrated that they are better described in a jj -coupling framework—unlike the lower- ℓ states, which follow LS coupling. Finally, we validated the MQDT models through

static polarizability measurements of $6snd$ states, finding excellent agreement with predictions derived from the fitted energies and wavefunctions. These models enable quantitative predictions of atomic properties relevant for quantum computing and precision metrology, including Rydberg–Rydberg interactions, polarizabilities, and g -factors, and are made available through an open-source software package `rydcalc` [51]. However, several important challenges remain unresolved.

First, while existing MQDT models are constrained primarily by high- n spectroscopic data ($n \gtrsim 20$), the accuracy at low- n remains limited. In some cases, low- n data exist but lack precision; in others, data are missing entirely. Moreover, the large number of accurate high- n measurements skews the fits toward this regime, often at the expense of the model accuracy at low- n . Discrepancies at low n may thus arise from either limitations in the available data or missing additional core-excited perturbing channels in the MQDT model. Improved spectroscopy in the low- n regime is therefore essential for refining the models and capturing perturbations from nearby core-excited states, which are critical for calculating matrix elements and state lifetimes.

Second, while energy levels are now predicted to within a few MHz, modeling Rydberg state lifetimes remains challenging due to contributions from core-excited perturber channels [52]. The resulting perturbing states are effectively low- n members of Rydberg series converging to higher ionization thresholds, and their short lifetimes arise from rapid decay within the core-excited configuration. Since the relevant dipole matrix elements of the ionic core are poorly known and cannot be calculated within a single-electron approximation, their impact on Rydberg lifetimes is difficult to predict. Lifetime measurements across a range of n are therefore essential to constrain these contributions and guide improved modeling. Such insights are essential for quantifying leakage pathways from $6sns$ Rydberg states and improving the erasure fraction and overall fidelity of Rydberg-based quantum gates.

Finally, further work is needed in the characterization of doubly excited Rydberg series, many of which remain poorly understood. In current MQDT models, several phenomenological channels are included to reproduce experimental spectra, but their physical identities are unknown. These states belong to Rydberg series converging to core-excited ionization thresholds. Members of these series can couple strongly to the continuum of lower lying ionization limits, resulting in rapid autoionization. Among them, the $6p_{1/2}nl$ states are of particular interest, as they can be used for high-fidelity Rydberg-state detection [53, 54], coherent control of population transfer [55, 56], and erasure-based quantum error correction [9].

ACKNOWLEDGMENTS

We wish to acknowledge helpful conversations with Yiyi Li, Yicheng Bao, and Chenyuan Li. This work was supported by the Army Research Office (W911NF-24-10358), the Office of Naval Research (N00014-20-1-2426), the National Science Foundation (QLCI grant OMA-2120757, and NSF CAREER PHY-2047620), the Sloan

Foundation, and the Gordon and Betty Moore Foundation (Grant DOI 10.37807/gbmfl2253). R.K. acknowledges Princeton University's Office of Undergraduate Research OURSIP Program through the Hewlett Foundation. V.M.H. acknowledges Princeton University's Office of Undergraduate Research OURSIP Program through the Class of 1952 Fund for Undergraduate Independent Work.

-
- [1] A. Jenkins, J. W. Lis, A. Senoo, W. F. McGrew, and A. M. Kaufman, Ytterbium Nuclear-Spin Qubits in an Optical Tweezer Array, *Phys. Rev. X* **12**, 021027 (2022).
 - [2] S. Ma, G. Liu, P. Peng, B. Zhang, S. Jandura, J. Claes, A. P. Burgers, G. Pupillo, S. Puri, and J. D. Thompson, High-fidelity gates and mid-circuit erasure conversion in an atomic qubit, *Nature* **622**, 279 (2023).
 - [3] J. A. Muniz, M. Stone, D. T. Stack, M. Jaffe, J. M. Kindem, L. Wadleigh, E. Zalys-Geller, X. Zhang, C.-A. Chen, M. A. Norcia, J. Epstein, E. Halperin, F. Hummel, T. Wilkason, M. Li, K. Barnes, P. Battaglino, T. C. Bohdanowicz, G. Booth, A. Brown, M. O. Brown, W. B. Cairncross, K. Cassella, R. Coxe, D. Crow, M. Feldkamp, C. Griger, A. Heinz, A. M. W. Jones, H. Kim, J. King, K. Kotru, J. Lauigan, J. Marjanovic, E. Megidish, M. Meredith, M. McDonald, R. Morshed, S. Narayanaswami, C. Nishiguchi, T. Paule, K. A. Pawlak, K. L. Pudenz, D. Rodríguez Pérez, A. Ryou, J. Simon, A. Smull, M. Urbanek, R. J. M. van de Veerdonk, Z. Vendeiro, T.-Y. Wu, X. Xie, and B. J. Bloom, High-Fidelity Universal Gates in the ^{171}Yb Ground-State Nuclear-Spin Qubit, *PRX Quantum* **6**, 020334 (2025).
 - [4] Y. Nakamura, T. Kusano, R. Yokoyama, K. Saito, K. Higashi, N. Ozawa, T. Takano, Y. Takasu, and Y. Takahashi, Hybrid Atom Tweezer Array of Nuclear Spin and Optical Clock Qubits, *Phys. Rev. X* **14**, 041062 (2024).
 - [5] A. Senoo, A. Baumgärtner, J. W. Lis, G. M. Vaidya, Z. Zeng, G. Giudici, H. Pichler, and A. M. Kaufman, High-fidelity entanglement and coherent multi-qubit mapping in an atom array (2025), arXiv:2506.13632 [quant-ph].
 - [6] Boulder Atomic Clock Optical Network (BACON) Collaboration, Frequency ratio measurements at 18-digit accuracy using an optical clock network, *Nature* **591**, 564 (2021).
 - [7] T. Bothwell, B. D. Hunt, J. L. Siegel, Y. S. Hassan, T. Grogan, T. Kobayashi, K. Gibble, S. G. Porosev, M. S. Safranova, R. C. Brown, K. Beloy, and A. D. Ludlow, Lattice Light Shift Evaluations in a Dual-Ensemble Yb Optical Lattice Clock, *Phys. Rev. Lett.* **134**, 033201 (2025).
 - [8] P. Niroula, J. Dolde, X. Zheng, J. Bringewatt, A. Ehrenberg, K. C. Cox, J. Thompson, M. J. Gullans, S. Kolkowitz, and A. V. Gorshkov, Quantum sensing with erasure qubits, *Phys. Rev. Lett.* **133**, 080801 (2024).
 - [9] Y. Wu, S. Kolkowitz, S. Puri, and J. D. Thompson, Erasure conversion for fault-tolerant quantum computing in alkaline earth Rydberg atom arrays, *Nat. Commun.* **13**, 4657 (2022).
 - [10] J. W. Lis, A. Senoo, W. F. McGrew, F. Rönchen, A. Jenkins, and A. M. Kaufman, Midcircuit Operations Using the *omg* Architecture in Neutral Atom Arrays, *Phys. Rev. X* **13**, 041035 (2023).
 - [11] B. Zhang, G. Liu, G. Bornet, S. P. Horvath, P. Peng, S. Ma, S. Huang, S. Puri, and J. D. Thompson, Leveraging erasure errors in logical qubits with metastable ^{171}Yb atoms (2025), arXiv:2506.13724 [quant-ph].
 - [12] Y. Li, Y. Bao, M. Peper, C. Li, and J. D. Thompson, Fast, continuous and coherent atom replacement in a neutral atom qubit array (2025), arXiv:2506.15633 [quant-ph].
 - [13] M. Peper, Y. Li, D. Y. Knapp, M. Bileska, S. Ma, G. Liu, P. Peng, B. Zhang, S. P. Horvath, A. P. Burgers, and J. D. Thompson, Spectroscopy and modeling of ^{171}Yb Rydberg states for high-fidelity two-qubit gates, *Phys. Rev. X* **15**, 011009 (2025).
 - [14] J. A. Armstrong, P. Esherick, and J. J. Wynne, Bound even-parity $J = 0$ and 2 spectra of Ca: A multichannel quantum-defect theory analysis, *Phys. Rev. A* **15**, 180 (1977).
 - [15] P. Esherick, Bound, even-parity $J = 0$ and $J = 2$ spectra of Sr, *Phys. Rev. A* **15**, 1920 (1977).
 - [16] M. Aymar, P. Camus, M. Dieulin, and C. Morillon, Two-photon spectroscopy of neutral barium: Observations of the highly excited even levels and theoretical analysis of the $J = 0$ spectrum, *Phys. Rev. A* **18**, 2173 (1978).
 - [17] H. Rinneberg and J. Neukammer, Resonance in Singlet-Triplet Mixing in Two-Electron Systems Caused by Perturbing Configurations, *Phys. Rev. Lett.* **49**, 124 (1982).
 - [18] H. Rinneberg and J. Neukammer, Hyperfine structure and three-channel quantum-defect theory of $6s\text{nd}^1D_2$ Rydberg states of Ba, *Phys. Rev. A* **27**, 1779 (1983).
 - [19] R. Beigang, W. Makat, A. Timmermann, and P. J. West, Hyperfine-Induced n Mixing in High Rydberg States of ^{87}Sr , *Phys. Rev. Lett.* **51**, 771 (1983).
 - [20] M. J. Seaton, Quantum defect theory I. General formulation, *Proc. Phys. Soc. (London)* **88**, 801 (1966).
 - [21] U. Fano, Quantum Defect Theory of l Uncoupling in H_2 as an Example of Channel-Interaction Treatment, *Phys. Rev. A* **2**, 353 (1970).
 - [22] C.-M. Lee and K. T. Lu, Spectroscopy and Collision Theory. II. the Ar Absorption Spectrum, *Phys. Rev. A* **8**, 1241 (1973).
 - [23] W. E. Cooke and C. L. Cromer, Multichannel quantum-defect theory and an equivalent N-level system, *Phys. Rev. A* **32**, 2725 (1985).
 - [24] P. Camus and F. S. Tomkins, Spectre d'absorption de Yb I, *J. Physique* **30**, 545 (1969).
 - [25] M. Aymar, A. Débarre, and O. Robaux, Highly excited levels of neutral ytterbium. II. Multichannel quantum defect analysis of odd- and even-parity spectra, *J. Phys. B:*

- At. Mol. Phys. **13**, 1089 (1980).
- [26] M. Aymar, R. J. Champeau, C. Delsart, and O. Robaux, Three-step laser spectroscopy and multichannel quantum defect analysis of odd-parity Rydberg states of neutral ytterbium, J. Phys. B: At. Mol. Phys. **17**, 3645 (1984).
- [27] U. Majewski, "Hochauflösende Laserspektroskopie von Ytterbium-Rydbergzuständen", Diploma thesis, Freie Universität Berlin (1985).
- [28] W. Bi-ru, Z. You-feng, X. Yun-fei, P. Li-gang, L. Ji, and Z. Jian-wei, The $6snp\ ^3P_{0,2}$ Rydberg series of neutral ytterbium, J. Phys. B: At., Mol. Opt. Phys. **24**, 49 (1991).
- [29] H. Maeda, Y. Matsuo, M. Takami, and A. Suzuki, Optical-microwave double-resonance spectroscopy of highly excited Rydberg states of ytterbium, Phys. Rev. A **45**, 1732 (1992).
- [30] R. Ali, M. Yaseen, A. Nadeem, S. A. Bhatti, and M. A. Baig, Two-colour three-photon excitation of the $6snf\ ^1,^3F_3$ and $6snp\ ^1P_1, ^3P_{1,2}$ Rydberg levels of Yb I, J. Phys. B: At., Mol. Opt. Phys. **32**, 953 (1999).
- [31] H. Lehec, *Spectroscopie Rydberg et excitation du cœur isolé d'atomes d'ytterbium ultra-froids*, Ph.D. thesis, Université Paris Saclay (COMUE) (2017).
- [32] H. Lehec, A. Zuliani, W. Maineult, E. Luc-Koenig, P. Pillet, P. Cheinet, F. Niyaz, and T. F. Gallagher, Laser and microwave spectroscopy of even-parity Rydberg states of neutral ytterbium and multichannel-quantum-defect-theory analysis, Phys. Rev. A **98**, 062506 (2018).
- [33] F. Niyaz, J. Nunkaew, and T. F. Gallagher, Microwave spectroscopy of the Yb $6s(n+3)d \rightarrow 6sng, 6snh$, and $6sni$ transitions, Phys. Rev. A **99**, 042507 (2019).
- [34] T. F. Gallagher, *Rydberg Atoms*, Cambridge Monographs on Atomic, Molecular and Chemical Physics (Cambridge University Press, 1994).
- [35] J.-Q. Sun and K. T. Lu, Hyperfine structure of extremely high Rydberg $msns\ ^1S_0$ and $msns\ ^3S_1$ series in odd alkaline-earth isotopes, J. Phys. B: At., Mol. Opt. Phys. **21**, 1957 (1988).
- [36] F. Robicheaux, D. W. Booth, and M. Saffman, Theory of long-range interactions for Rydberg states attached to hyperfine-split cores, Phys. Rev. A **97**, 022508 (2018).
- [37] W. F. Meggers and J. L. Tech, The First Spectrum of Ytterbium (Yb I), J. Res. NBS **83**, 13 (1977).
- [38] J.-F. Wyart and P. Camus, Extended Analysis of the Emission Spectrum of Neutral Ytterbium (Yb I), Phys. Scr. **20**, 43 (1979).
- [39] M. Aymar, Rydberg series of alkaline-earth atoms Ca through Ba. the interplay of laser spectroscopy and multichannel quantum defect analysis, Phys. Rep. **110**, 163 (1984).
- [40] G. Clausen and F. Merkt, Ionization Energy of Metastable 3He ($2\ ^3S_1$) and the Alpha- and Helion-Particle Charge-Radius Difference from Precision Spectroscopy of the np Rydberg Series, Phys. Rev. Lett. **134**, 223001 (2025).
- [41] J.-Q. Sun, K. T. Lu, and R. Beigang, Hyperfine structure of extremely high Rydberg $msnd\ ^1D_2, ^3D_1, ^3D_2$ and 3D_3 series in odd alkaline-earth isotopes, J. Phys. B: At., Mol. Opt. Phys. **22**, 2887 (1989).
- [42] C. M. Lee, Spectroscopy and collision theory. III. Atomic eigenchannel calculation by a Hartree-Fock-Roothaan method, Phys. Rev. A **10**, 584 (1974).
- [43] A. Osterwalder, A. Wüst, F. Merkt, and C. Jungen, High-resolution millimeter wave spectroscopy and multichannel quantum defect theory of the hyperfine struc-
- ture in high Rydberg states of molecular hydrogen H_2 , J. Chem. Phys. **121**, 11810 (2004).
- [44] H. J. Wörner, U. Hollenstein, and F. Merkt, Multichannel quantum defect theory and high-resolution spectroscopy of the hyperfine structure of high Rydberg states of ^{83}Kr , Phys. Rev. A **68**, 032510 (2003).
- [45] M. Schäfer and F. Merkt, Millimeter-wave spectroscopy and multichannel quantum-defect-theory analysis of high Rydberg states of krypton: The hyperfine structure of $^{83}Kr^+$, Phys. Rev. A **74**, 062506 (2006).
- [46] T. F. Gallagher, R. Kachru, and N. H. Tran, Radio frequency resonance measurements of the Ba $6sng-6snh-6sni-6snk$ intervals: An investigation of the nonadiabatic effects in core polarization, Phys. Rev. A **26**, 2611 (1982).
- [47] E. L. Snow, R. A. Komara, M. A. Gearba, and S. R. Lundeen, Indirect spin-orbit interaction in high- l Rydberg states with $^2S_{1/2}$ cores, Phys. Rev. A **68**, 022510 (2003).
- [48] G. Fields, R. Brienza, F. B. Dunning, S. Yoshida, and J. Burgdörfer, High- n limit of quantum defects for high- ℓ strontium Rydberg states, Phys. Rev. A **104**, 032817 (2021).
- [49] A. R. Edmonds, *Angular momentum in quantum mechanics*, 4th ed. (Princeton University Press, Princeton, 1996).
- [50] M. Saffman, T. G. Walker, and K. Mølmer, Quantum information with Rydberg atoms, Rev. Mod. Phys. **82**, 2313 (2010).
- [51] rydcalc, <https://github.com/ThompsonLabPrinceton/rydcalc>.
- [52] C. L. Vaillant, M. P. A. Jones, and R. M. Potvliege, Multichannel quantum defect theory of strontium bound Rydberg states, J. Phys. B: At., Mol. Opt. Phys. **47**, 155001 (2014).
- [53] G. Lochead, D. Boddy, D. P. Sadler, C. S. Adams, and M. P. A. Jones, Number-resolved imaging of excited-state atoms using a scanning autoionization microscope, Phys. Rev. A **87**, 053409 (2013).
- [54] I. S. Madjarov, J. P. Covey, A. L. Shaw, J. Choi, A. Kale, A. Cooper, H. Pichler, V. Schkolnik, J. R. Williams, and M. Endres, High-fidelity entanglement and detection of alkaline-earth Rydberg atoms, Nat. Phys **16**, 857 (2020).
- [55] A. P. Burgers, S. Ma, S. Saskin, J. Wilson, M. A. Alarcón, C. H. Greene, and J. D. Thompson, Controlling Rydberg Excitations Using Ion-Core Transitions in Alkaline-Earth Atom-Tweezer Arrays, PRX Quantum **3**, 020326 (2022).
- [56] K.-L. Pham, T. F. Gallagher, P. Pillet, S. Lepoutre, and P. Cheinet, Coherent Light Shift on Alkaline-Earth Rydberg Atoms from Isolated Core Excitation without Autoionization, PRX Quantum **3**, 020327 (2022).
- [57] W. C. Martin, R. Zalubas, and L. Hagan, Atomic Energy Levels: The Rare Earth Elements, Nat. Stand. Ref. Data Ser., NSRDS-NBS **60**, 10.6028/NBS.NSRDS.60 (1978).
- [58] M. L. Zimmerman, M. G. Littman, M. M. Kash, and D. Kleppner, Stark structure of the Rydberg states of alkali-metal atoms, Phys. Rev. A **20**, 2251 (1979).

Appendix A: Polarizability Trends in $6s\text{nd}$ Rydberg States

In Fig. 12 and Fig. 13, we present predicted static dipole polarizabilities of the $6s\text{nd}$ Rydberg series in ^{174}Yb and ^{171}Yb , respectively. In ^{174}Yb , the $6s\text{nd}^1D_2$ static dipole polarizabilities exhibits a divergent feature near $\nu \approx 64$, due to energy crossings with the $6snp^3P_1$ series. For $6s\text{nd}^3D_2$, the MQDT model predicts small static dipole polarizabilities near $\nu \approx 43$, giving Rydberg states that are highly insensitive to electric fields. For ^{171}Yb , we present the predicted polarizabilities for the three $6s\text{nd}$ ($F = 3/2$) and the three $6s\text{nd}$ ($F = 5/2$) series. We note that these polarizabilities exhibit much more complex behavior due to energy crossings with multiple dipole-coupled series.

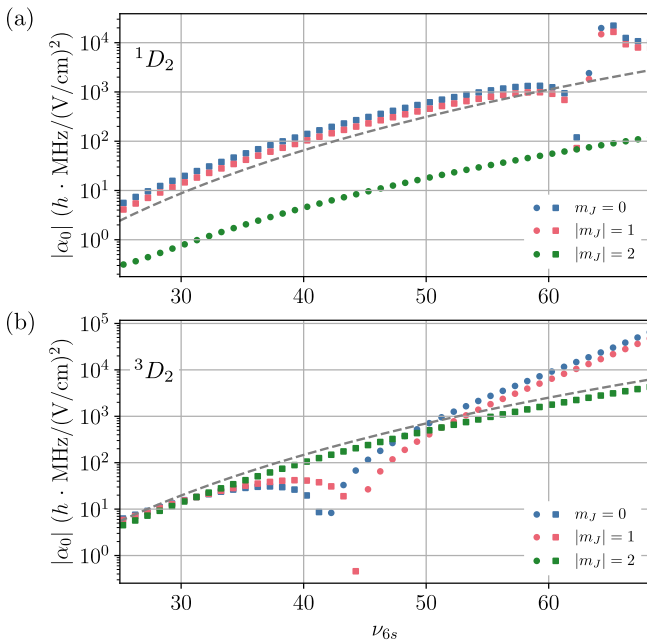


Figure 12. Predicted absolute static dipole polarizabilities of (a) $6s\text{nd}^1D_2$ and (b) $6s\text{nd}^3D_2$ states in ^{174}Yb . The blue, red, and green points correspond to $m_J = 0, 1$, and 2 sublevels, respectively. Circles indicate positive values of α_0 , while squares indicate negative values. The gray dashed lines show ν_{6s}^7 scaling as a guide to the eye.

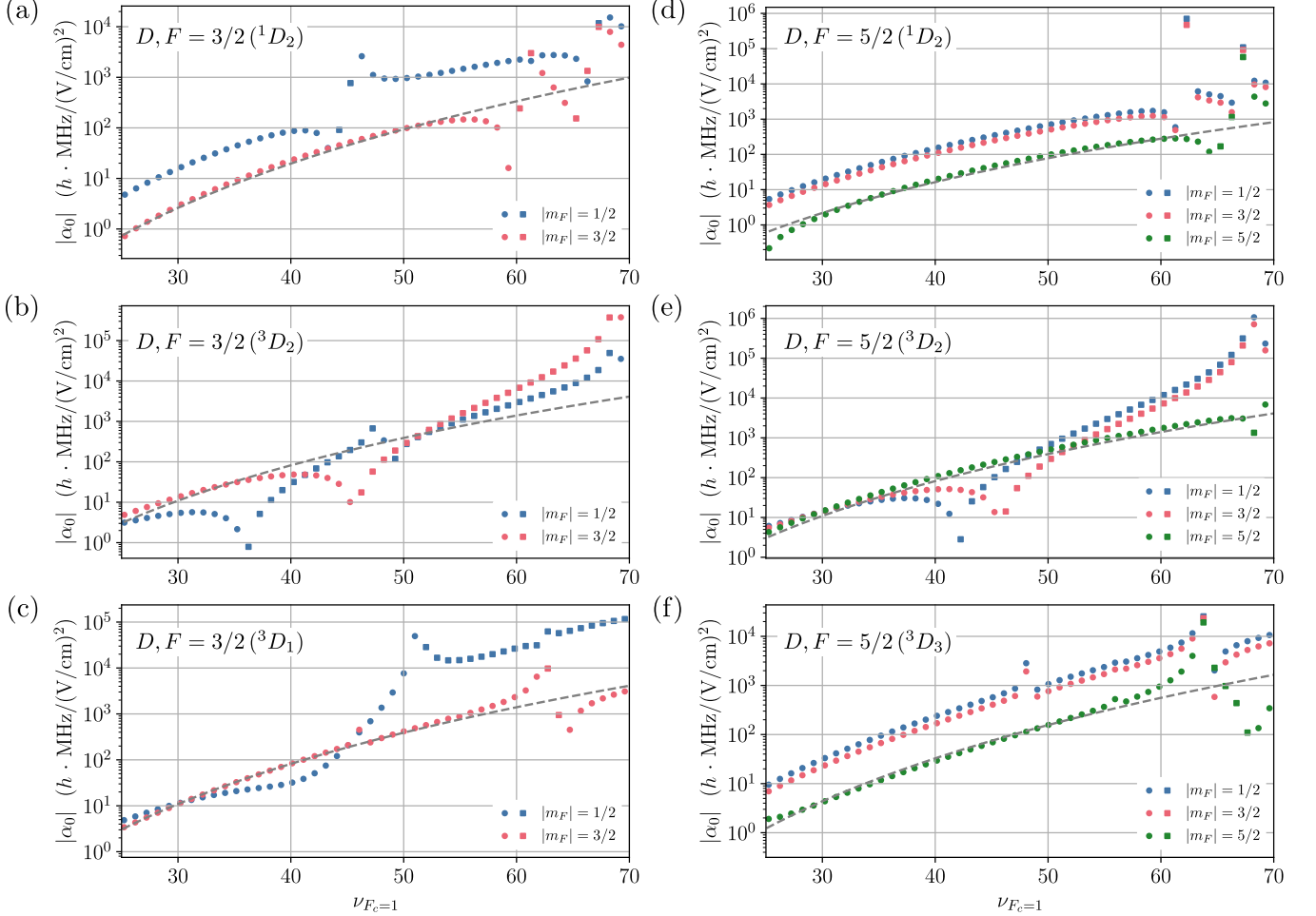


Figure 13. Predicted absolute static dipole polarizabilities of (a),(b),(c) $|D, F = 3/2\rangle$ (series of dominantly 1D_2 , 3D_2 , 3D_1 character, respectively) and (d),(e),(f) $|D, F = 5/2\rangle$ (series of dominantly 1D_2 , 3D_2 , 3D_3 character, respectively) states in ^{171}Yb . The blue, red, and green points correspond to $m_F = 1/2, 3/2$, and $5/2$ sublevels, respectively. Circles indicate positive values of α_0 , while squares indicate negative values. The gray dashed lines show $\nu_{F_c=1}^7$ scaling as a guide to the eye.

Appendix B: MQDT Model Parameters

1. ^{174}Yb

Table S1. Single-channel model parameters for the $6snd\,{}^3D_3$, $6snf\,{}^3F_2$, $6snf\,{}^3F_4$, $6sng\,{}^3G_3$, and $6sng\,{}^3G_5$ series of ^{174}Yb described by Eq. (1), obtained from fit to spectroscopic data presented in Tabs. S22, S24, S25 and S29. † The $6sng\,{}^3G_5$ parameters are obtained from a fit to the ^{171}Yb $6sng$ ($F = 9/2$) spectroscopic data.

	$6snd\,{}^3D_3$	$6snf\,{}^3F_2$	$6snf\,{}^3F_4$	$6sng\,{}^3G_3$	$6sng\,{}^3G_5$
$\mu_\alpha^{(0)}$	0.72902016	0.0718252326	0.0839027969	0.0260964574	0.02529201 †
$\mu_\alpha^{(2)}$	-0.705328923	-1.00091963	-2.91009023	-0.14139526	-0.11588052 †
$\mu_\alpha^{(4)}$	829.238844	-106.291066			

Table S2. Six-channel MQDT model parameters for the $6sns\,{}^1S_0$ series of ^{174}Yb , obtained by fitting to spectroscopic data reported in Refs. [25, 29, 32]. The electronic configuration of the perturbing Rydberg channels $4f^{13}5d6snp$ is abbreviated as $5d$. The rotations $\mathcal{R}(\theta_{ij})$ are applied in the order $\mathcal{R}(\theta_{12})\mathcal{R}(\theta_{13})\mathcal{R}(\theta_{14})\mathcal{R}(\theta_{34})\mathcal{R}(\theta_{35})\mathcal{R}(\theta_{16})$.

$i, \bar{\alpha}, \alpha$	1	2	3	4	5	6
$ i\rangle$	$(6s_{1/2})(ns_{1/2})$	$5d \mathbf{a}$	$(6p_{3/2})(np_{3/2})$	$5d \mathbf{b}$	$(6p_{1/2})(np_{1/2})$	$5d \mathbf{c}$
$I_i \text{ (cm}^{-1}\text{)}$	50 443.070393	83 967.7	80 835.39	83 967.7	77 504.98	83 967.7
$ \bar{\alpha}\rangle$	$6sns\,{}^1S_0$	$5d \mathbf{a}$	$6pnp\,{}^1S_0$	$5d \mathbf{b}$	$6pnp\,{}^3P_0$	$5d \mathbf{c}$
$\mu_\alpha^{(0)}$	0.355101645	0.204537535	0.116393648	0.295439966	0.257664798	0.155797119
$\mu_\alpha^{(2)}$	0.277673956	0.0	0.0	0.0	0.0	0.0
$V_{\bar{\alpha}\alpha}$	$\theta_{12} = 0.126557575$	$\theta_{13} = 0.300103593$	$\theta_{14} = 0.056987912$	$\theta_{34} = 0.114312578$	$\theta_{35} = 0.0986363362$	$\theta_{16} = 0.142498543$
$U_{i\bar{\alpha}}$	1	0	0	0	0	0
	0	1	0	0	0	0
	0	0	$\sqrt{2/3}$	0	$-\sqrt{1/3}$	0
	0	0	0	1	0	0
	0	0	$\sqrt{1/3}$	0	$\sqrt{2/3}$	0
	0	0	0	0	0	1

Table S3. Two-channel MQDT model parameters for the $6snp\,{}^3P_0$ series of ^{174}Yb , obtained by fitting to spectroscopic data reported in Refs. [13, 26]. Following Refs. [13, 26], we include a perturbing channel of character $4f^{13}5d6snp\,{}^3P_0$ (labeled Q) with an ionization limit of $83 967.7 \text{ cm}^{-1}$.

$i, \bar{\alpha}, \alpha$	1	2
$ i\rangle$	$(6s_{1/2})(np_{1/2})$	$4f^{13}5d6snp\,{}^3P_0$
$I_i \text{ (cm}^{-1}\text{)}$	50 443.070393	83 967.7
$ \bar{\alpha}\rangle$	$6snp\,{}^3P_0$	Q
$\mu_\alpha^{(0)}$	0.953661478	0.198460766
$\mu_\alpha^{(2)}$	-0.287531374	0.0
$V_{\bar{\alpha}\alpha}$	$\theta_{12} = 0.163343232$	
$U_{i\bar{\alpha}}$	1	0
	0	1

Table S4. Six-channel MQDT model parameters for the $6snp\,{}^{1,3}P_1$ series of ${}^{174}\text{Yb}$, obtained by fitting to spectroscopic data reported in Refs. [13, 24, 26, 31]. The electronic configuration of the perturbing Rydberg channels $4f^{13}5d6snd$ is abbreviated as $5d$. The rotations $\mathcal{R}(\theta_{ij})$ are applied in the order $\mathcal{R}(\theta_{12}(\varepsilon))\mathcal{R}(\theta_{13})\mathcal{R}(\theta_{14})\mathcal{R}(\theta_{15})\mathcal{R}(\theta_{16})\mathcal{R}(\theta_{23})\mathcal{R}(\theta_{24})\mathcal{R}(\theta_{25})\mathcal{R}(\theta_{26})$.

$i, \bar{\alpha}, \alpha$	1	2	3	4	5	6
$ i\rangle$	$(6s_{1/2})(np_{3/2})$	$(6s_{1/2})(np_{1/2})$	$5d \mathbf{a}$	$5d \mathbf{b}$	$5d \mathbf{c}$	$5d \mathbf{d}$
I_i (cm $^{-1}$)	50 443.070393	50 443.070393	83 967.7	83 967.7	83 967.7	83 967.7
$ \bar{\alpha}\rangle$	$6snp\,{}^1P_1$	$6snp\,{}^3P_1$	$5d \mathbf{a}$	$5d \mathbf{b}$	$5d \mathbf{c}$	$5d \mathbf{d}$
$\mu_\alpha^{(0)}$	0.922709076	0.982084772	0.228518316	0.206081775	0.193527605	0.181533031
$\mu_\alpha^{(2)}$	2.60055203	-5.45063476	0.0	0.0	0.0	0.0
$V_{\bar{\alpha}\alpha}$	$\theta_{12}^{(0)} = -0.08410871$ $\theta_{16} = -0.10452109$	$\theta_{12}^{(2)} = 120.37555$ $\theta_{23} = 0.02477464$	$\theta_{12}^{(4)} = -9.314.23$ $\theta_{24} = 0.05763934$	$\theta_{13} = -0.07317986$ $\theta_{25} = 0.0860644$	$\theta_{14} = -0.06651879$ $\theta_{26} = 0.04993818$	$\theta_{15} = -0.02212194$
$U_{i\bar{\alpha}}$	$\begin{matrix} \sqrt{2/3} \\ -\sqrt{1/3} \\ 0 \\ 0 \\ 0 \\ 0 \end{matrix}$	$\begin{matrix} \sqrt{1/3} \\ \sqrt{2/3} \\ 0 \\ 0 \\ 0 \\ 0 \end{matrix}$	$\begin{matrix} 0 \\ 0 \\ 1 \\ 0 \\ 0 \\ 0 \end{matrix}$	$\begin{matrix} 0 \\ 0 \\ 0 \\ 1 \\ 0 \\ 0 \end{matrix}$	$\begin{matrix} 0 \\ 0 \\ 0 \\ 0 \\ 1 \\ 0 \end{matrix}$	$\begin{matrix} 0 \\ 0 \\ 0 \\ 0 \\ 0 \\ 1 \end{matrix}$

Table S5. Four-channel MQDT model parameters for the $6snp\,{}^3P_2$ series of ${}^{174}\text{Yb}$, obtained by fitting to spectroscopic data reported in Refs. [26, 28, 30, 31, 38, 57]. The electronic configuration of the perturbing Rydberg channels $4f^{13}5d6snd$ is abbreviated as $5d$. The rotations $\mathcal{R}(\theta_{ij})$ are applied in the order $\mathcal{R}(\theta_{12})\mathcal{R}(\theta_{13})\mathcal{R}(\theta_{14})$.

$i, \bar{\alpha}, \alpha$	1	2	3	4
$ i\rangle$	$(6s_{1/2})(np_{3/2})$	$5d \mathbf{a}$	$5d \mathbf{b}$	$5d \mathbf{c}$
I_i (cm $^{-1}$)	50 443.070393	83 967.7	83 967.7	83 967.7
$ \bar{\alpha}\rangle$	$6snp\,{}^3P_2$	$5d \mathbf{a}$	$5d \mathbf{b}$	$5d \mathbf{c}$
$\mu_\alpha^{(0)}$	0.925150932	0.230028034	0.209224174	0.186236574
$\mu_\alpha^{(2)}$	-2.69197178	0.0	0.0	0.0
$\mu_\alpha^{(4)}$	66.7159709	0.0	0.0	0.0
$V_{\bar{\alpha}\alpha}$	$\theta_{12} = 0.0706189664$	$\theta_{13} = 0.0231221428$	$\theta_{14} = -0.0291730345$	
$U_{i\bar{\alpha}}$	$\begin{matrix} 1 \\ 0 \\ 0 \\ 0 \end{matrix}$	$\begin{matrix} 0 \\ 1 \\ 0 \\ 0 \end{matrix}$	$\begin{matrix} 0 \\ 0 \\ 1 \\ 0 \end{matrix}$	$\begin{matrix} 0 \\ 0 \\ 0 \\ 1 \end{matrix}$

Table S6. Five-channel MQDT model parameters for the $6s\text{nd}^{1,3}D_2$ series of ^{174}Yb , obtained by fitting to spectroscopic data reported in Refs. [26, 29, 32]. The electronic configuration of the perturbing Rydberg channels $4f^{13}5d6snp$ is abbreviated as $5d$. The rotations $\mathcal{R}(\theta_{ij})$ are applied in the order $\mathcal{R}(\theta_{12}(\varepsilon))\mathcal{R}(\theta_{13})\mathcal{R}(\theta_{14})\mathcal{R}(\theta_{24})\mathcal{R}(\theta_{15})\mathcal{R}(\theta_{25})$. The channel- g -factors g^* are as given in Ref. [13].

$i, \bar{\alpha}, \alpha$	1	2	3	4	5
$ i\rangle$	$(6s_{1/2})(nd_{5/2})$	$(6s_{1/2})(nd_{3/2})$	5d a	5d b	$(6p)(np)$
I_i (cm^{-1})	50 443.070393	50 443.070393	83 967.7	83 967.7	79 725.35
$ \bar{\alpha}\rangle$	$6s\text{nd}^1D_2$	$6s\text{nd}^3D_2$	5d a	5d b	$6pnp^1D_2$
$\mu_\alpha^{(0)}$	0.729513646	0.752292223	0.19612036	0.233752026	0.152911249
$\mu_\alpha^{(2)}$	-0.0377841183	0.104072325	0.0	0.0	0.0
$V_{\bar{\alpha}\alpha}$	$\theta_{12}^{(0)} = 0.21157531$ $\theta_{12}^{(2)} = -15.3844$	$\theta_{13} = 0.00521559431$ $\theta_{25} = 0.0721660042$	$\theta_{14} = 0.0398131577$	$\theta_{24} = -0.0071658109$	$\theta_{15} = 0.10481227$
g^*	1	1.1670	1.1846	0.9390	1.2376
$U_{i\bar{\alpha}}$	$\sqrt{3/5}$ $-\sqrt{2/5}$ 0 0 0	$\sqrt{2/5}$ $\sqrt{3/5}$ 0 0 0	0 0 1 0 0	0 0 0 1 0	0 0 0 0 1

Table S7. Seven-channel MQDT model parameters for the $6snf\ ^{1,3}F_3$ series of ^{174}Yb , obtained by fitting to spectroscopic data presented in Tabs. S19 to S21. The electronic configuration of the perturbing Rydberg channels $4f^{13}5d6s$ nd is abbreviated as $5d$. The rotations $\mathcal{R}(\theta_{ij})$ are applied in the order $\mathcal{R}(\theta_{12}(\varepsilon))\mathcal{R}(\theta_{13})\mathcal{R}(\theta_{14})\mathcal{R}(\theta_{15})\mathcal{R}(\theta_{16})\mathcal{R}(\theta_{17})\mathcal{R}(\theta_{23})\mathcal{R}(\theta_{24})\mathcal{R}(\theta_{25})\mathcal{R}(\theta_{26})\mathcal{R}(\theta_{27})$.

$i, \bar{\alpha}, \alpha$	1	2	3	4	5	6	7
$ i\rangle$	$(6s_{1/2})(n7/2)$	$(6s_{1/2})(n5/2)$	$5d \mathbf{a}$	$5d \mathbf{b}$	$5d \mathbf{c}$	$5d \mathbf{d}$	$5d \mathbf{e}$
$I_i \text{ (cm}^{-1}\text{)}$	50 443.070393	50 443.070393	83 967.7	83 967.7	83 967.7	83 967.7	83 967.7
$ \bar{\alpha}\rangle$	$6snf\ ^1F_3$	$6snf\ ^3F_3$	$5d \mathbf{a}$	$5d \mathbf{b}$	$5d \mathbf{c}$	$5d \mathbf{d}$	$5d \mathbf{e}$
$\mu_\alpha^{(0)}$	0.276158949	0.0715123712	0.239015576	0.226770354	0.175354845	0.196660618	0.21069642
$\mu_\alpha^{(2)}$	-12.7258012	-0.768462937	0.0	0.0	0.0	0.0	0.0
$V_{\bar{\alpha}\alpha}$	$\theta_{12}^{(0)}$	$\theta_{12}^{(2)}$	θ_{13}	θ_{14}	θ_{15}	θ_{16}	
	-0.0208481417	0.239045493	-0.00411835457	-0.0962784945	0.132826901	-0.0439244317	
	θ_{17}	θ_{23}	θ_{24}	θ_{25}	θ_{26}	θ_{27}	
	0.0508460294	-0.0376574252	0.026944623	-0.0148474857	-0.0521244126	0.0349516329	
$U_{i\bar{\alpha}}$	$\sqrt{4/7}$	$\sqrt{3/7}$	0	0	0	0	0
	$-\sqrt{3/7}$	$\sqrt{4/7}$	0	0	0	0	0
	0	0	1	0	0	0	0
	0	0	0	1	0	0	0
	0	0	0	0	1	0	0
	0	0	0	0	0	1	0
	0	0	0	0	0	0	1

Table S8. Two-channel MQDT model parameters for the $6sng^{\pm}G_4$ series of ^{174}Yb , obtained by fitting to spectroscopic data presented in Tab. S27.

$i, \bar{\alpha}, \alpha$	1	2
$ i\rangle$	$(6s_{1/2})(ng_{9/2})$	$(6s_{1/2})(ng_{7/2})$
I_i (cm^{-1})	50 443.070393	50 443.070393
$ \bar{\alpha}\rangle$	$6sng^+G_4$	$6sng^-G_4$
$\mu_{\alpha}^{(0)}$	0.0262659964	-0.148808463
$\mu_{\alpha}^{(2)}$	0.0254568575	-0.134219071
$V_{\bar{\alpha}\alpha}$	$\theta_{12}^{(0)} = -0.08222676$	
$U_{i\bar{\alpha}}$	1 0	0 1

2. ^{171}Yb

Table S9. Seven-channel MQDT model parameters for the $|\nu, L=0, F=1/2\rangle$ series of ^{171}Yb , obtained by fitting to spectroscopic data reported in Ref. [13]. The electronic configuration of the perturbing Rydberg channels $4f^35d6snp$ is abbreviated as $5d$. The rotations $\mathcal{R}(\theta_{ij})$ are applied in the order $\mathcal{R}(\theta_{12})\mathcal{R}(\theta_{13})\mathcal{R}(\theta_{14})\mathcal{R}(\theta_{34})\mathcal{R}(\theta_{35})\mathcal{R}(\theta_{16})$.

$i, \bar{\alpha}, \alpha$	$1 (F_c = 0)$	2	3	4	5	6	$7 (F_c = 1)$
$ i_F\rangle$	$(6s_{1/2})(7s_{1/2})$	$5d \mathbf{a}$	$(6p_{3/2})(np_{3/2})$	$5d \mathbf{b}$	$(6p_{1/2})(np_{1/2})$	$5d \mathbf{c}$	$(6s_{1/2})(ns_{1/2})$
$I_i (\text{cm}^{-1})$	50 442.795744	83 967.7	80 835.39	83 967.7	77 504.98	83 967.7	50 443.217463
$ \bar{\alpha}\rangle$	$6sns^1S_0$	$5d \mathbf{a}$	$6pnp^1S_0$	$5d \mathbf{b}$	$6pmp^3P_0$	$5d \mathbf{c}$	$6sns^3S_1$
$\mu_\alpha^{(0)}$	0.357488757	0.203917828	0.116813499	0.287210377	0.247550262	0.148686263	$\mu_{3S_1}^{rr}$
$\mu_\alpha^{(2)}$	0.163255076	0.0	0.0	0.0	0.0	0.0	
$\mu_{3S_1}^{rr}$	$\mu_{3S_1}^{(0)} = 0.438803844$	$\mu_{3S_1}^{(2)} = 3.54561559$	$\mu_{3S_1}^{(4)} = -10673.2496$	$\mu_{3S_1}^{(6)} = 7702824.55$	$\mu_{3S_1}^{(8)} = -2255973430$		
$V_{\bar{\alpha}\alpha}$	$\theta_{12} = 0.13179534$	$\theta_{13} = 0.29748039$	$\theta_{14} = 0.0553920359$	$\theta_{34} = 0.100843905$	$\theta_{35} = 0.10317753$	$\theta_{16} = 0.137709223$	
$U_{i\bar{\alpha}}$	$1/2$	0	0	0	0	0	$\sqrt{3}/2$
	0	1	0	0	0	0	0
	0	0	$\sqrt{2}/3$	0	$-\sqrt{1/3}$	0	0
	0	0	0	1	0	0	0
	0	0	$\sqrt{1/3}$	0	$\sqrt{2/3}$	0	0
	0	0	0	0	0	1	0
	$\sqrt{3}/2$	0	0	0	0	0	$-1/2$

Eight-channel MQDT model parameters for the $|v, \ell = 1, F = 1/2\rangle$ series of ^{171}Yb , obtained by fitting to spectroscopic data reported in Refs. [13, 27]. The electronic configuration of the perturbing Rydberg channels $4f^{13}5d6snd$ is abbreviated as $5d$. The rotations $\mathcal{R}(\theta_{ij})$ are applied in the order $\mathcal{R}(\theta_{12}(\varepsilon))\mathcal{R}(\theta_{27})\mathcal{R}(\theta_{13})\mathcal{R}(\theta_{14})\mathcal{R}(\theta_{15})\mathcal{R}(\theta_{16})\mathcal{R}(\theta_{23})\mathcal{R}(\theta_{24})\mathcal{R}(\theta_{25})\mathcal{R}(\theta_{26})\mathcal{R}(\theta_{78})$.

Table S11. Eight-channel MQDT model parameters for the $|\nu, \ell = 3, F = 7/2\rangle$ series of ^{171}Yb , obtained by fitting to spectroscopic data presented in Tab. S36. The electronic configuration of the perturbing Rydberg channels $4f_{13}^3 5d 6s n d$ is abbreviated as $5d$. The rotations $\mathcal{R}(\theta_{ij})$ are applied in the order $\mathcal{R}(\theta_{12}(\varepsilon))\mathcal{R}(\theta_{13})\mathcal{R}(\theta_{14})\mathcal{R}(\theta_{15})\mathcal{R}(\theta_{16})\mathcal{R}(\theta_{23})\mathcal{R}(\theta_{24})\mathcal{R}(\theta_{25})\mathcal{R}(\theta_{26})\mathcal{R}(\theta_{27})$.

$i, \bar{\alpha}, \alpha$	1 ($F_c = 1$)	2 ($F_c = 1$)	3	4	5	6	7	8 ($F_c = 0$)
$ i\rangle$	$(6s_{1/2})(nf_{7/2})$	$(6s_{1/2})(nf_{5/2})$	$5d \mathbf{a}$	$5d \mathbf{b}$	$5d \mathbf{c}$	$5d \mathbf{d}$	$5d \mathbf{e}$	$(6s_{1/2})(nf_{7/2})$
I_i (cm $^{-1}$)	50 443.217463	50 443.217463	83 967.7	83 967.7	83 967.7	83 967.7	83 967.7	50 442.795744
$ \bar{\alpha}\rangle$	$6snf^1 F_3$	$6snf^3 F_3$	$5d \mathbf{a}$	$5d \mathbf{b}$	$5d \mathbf{c}$	$5d \mathbf{d}$	$5d \mathbf{e}$	$6snf^3 F_4$
$\mu_\alpha^{(0)}$	0.27707535	0.0719827367	0.250829254	0.227042016	0.17576256	0.19654694	0.214351625	$\mu_{3F_4}^{rr}$
$\mu_\alpha^{(2)}$	-13.2829133	-0.741492064						
$\mu_{3F_4}^{(0)}$	$\mu_{3F_4}^{(2)} = 0.0834066138$	$\mu_{3F_4}^{(4)} = -1.11349283$	$\mu_{3F_4}^{(4)} = -1539.63739$					
$V_{\bar{\alpha}\alpha}$	$\theta_{12}^{(0)}$	$\theta_{12}^{(2)}$	θ_{13}	θ_{14}	θ_{15}	θ_{16}	θ_{17}	
	-0.0208481417	0.239045493	-0.0593782568	-0.0755947274	0.1122678758	-0.040418576	0.0646373252	
	θ_{23}	θ_{24}	θ_{25}	θ_{26}	θ_{27}			
	-0.0684538786	0.0352130279	-0.0326572035	-0.050215299	0.0453892695			
$U_{i\bar{\alpha}}$	$3/(2\sqrt{7})$	$3\sqrt{3}/(4\sqrt{7})$	0	0	0	0	0	$-\sqrt{7}/4$
	$-\sqrt{3/7}$	$\sqrt{2/7}$	0	0	0	0	0	0
	0	0	1	0	0	0	0	0
	0	0	0	1	0	0	0	0
	0	0	0	0	1	0	0	0
	0	0	0	0	0	1	0	0
	0	0	0	0	0	0	1	0
	$\sqrt{3}/4$					0	0	0
	1/2					0	0	0

Table S12. Six-channel MQDT model parameters for the $|\nu, L = 2, F = 3/2\rangle$ series of ^{171}Yb , obtained by fitting to spectroscopic data presented in Ref. [13]. The electronic configuration of the perturbing Rydberg channels $4f^35d6snp$ is abbreviated as $5d$. The rotations $\mathcal{R}(\theta_{ij})$ are applied in the order $\mathcal{R}(\theta_{12})\mathcal{R}(\theta_{13})\mathcal{R}(\theta_{14})\mathcal{R}(\theta_{24})\mathcal{R}(\theta_{15})\mathcal{R}(\theta_{25})$.

$i, \bar{\alpha}, \alpha$	1 ($F_c = 1$)	2 ($F_c = 1$)	3	4	5	6 ($F_c = 0$)
$ i\rangle$	$(6s_{1/2})(nd_{5/2})$	$(6s_{1/2})(nd_{3/2})$	$5d \mathbf{a}$	$5d \mathbf{b}$	$(6p)(np)$	$(6s_{1/2})(nd_{3/2})$
I_i (cm $^{-1}$)	50 443.217463	50 443.217463	83 967.7	83 967.7	79 725.35	50 442.795744
$ \bar{\alpha}\rangle$	$6snpd^1D_2$	$6snpd^3D_2$	$5d \mathbf{a}$	$5d \mathbf{b}$	$6pnp^1D_2$	$6snpd^3D_1$
$\mu_\alpha^{(0)}$	0.730541589	0.751542685	0.195864083	0.235944408	0.147483609	$\mu_{3D_1}^{rr}$
$\mu_\alpha^{(2)}$	-0.0967938662	0.000038836127	0.0	0.0	0.0	$\mu_{3D_1}^{rr}$
$\mu_{3D_1}^{rr}$	$\mu_{3D_1}^{(0)} = 0.75334159$	$\mu_{3D_1}^{(2)} = -1.80187083$	$\mu_{3D_1}^{(4)} = 986.918851$			
$V_{\bar{\alpha}\alpha}$	$\theta_{12}^{(0)} = 0.220048245$	$\theta_{13} = 0.00427599$	$\theta_{14} = 0.0381563093$	$\theta_{24} = -0.00700797918$	$\theta_{15} = 0.109380331$	$\theta_{25} = 0.0635544456$
	$\theta_{12}^{(2)} = -14.9486$					
$U_{i\bar{\alpha}}$	$\frac{-\sqrt{3/5}}{\sqrt{3/5}/2}$	$\frac{-\sqrt{2/5}}{-3/(2\sqrt{10})}$	0	0	0	0
	0	0	1	0	0	$\sqrt{5/2}/2$
	0	0	0	1	0	0
	0	0	0	0	1	0
	-1/2	$\sqrt{3/2}/2$	0	0	0	$\sqrt{3/2}/2$

Table S13. Six-channel MQDT model parameters for the $|v, L=2, F=5/2\rangle$ series of ^{171}Yb , obtained by fitting to spectroscopic data reported in Ref. [3]. The electronic configuration of the perturbing Rydberg channels $4f^15d6snp$ is abbreviated as $5d$. The rotations $\mathcal{R}(\theta_{ij})$ are applied in the order $\mathcal{R}(\theta_{12})\mathcal{R}(\theta_{13})\mathcal{R}(\theta_{14})\mathcal{R}(\theta_{24})\mathcal{R}(\theta_{15})\mathcal{R}(\theta_{25})$.

$i, \bar{\alpha}, \alpha$	1 ($F_c = 1$)	2 ($F_c = 1$)	3	4	5	6 ($F_c = 0$)
$ i\rangle$	$(6s_{1/2})(nd_{3/2})$	$5d \mathbf{a}$		$5d \mathbf{b}$	$(6p)(np)$	$(6s_{1/2})(nd_{5/2})$
I_i (cm $^{-1}$)	$50\,443\,217463$	$83\,967.7$		$83\,967.7$	$79\,725.35$	$50\,442.795744$
$ \bar{\alpha}\rangle$	$6snd^3D_2$	$5d \mathbf{a}$		$5d \mathbf{b}$	$6pnp^1D_2$	$6snd^3D_3$
$\mu_\alpha^{(0)}$	0.730541589	0.195864083		0.235944408	0.147483609	μ_α^{rr}
$\mu_\alpha^{(2)}$	-0.0967938662	0.00038836127	0.0	0.0	0.0	$\mu_{3D_3}^{rr}$
$\mu_{3D_3}^{rr}$	$\mu_{3D_3}^{(0)} = 0.72865616$	$\mu_{3D_3}^{(2)} = 0.793185994$	$\mu_{3D_3}^{(4)} = -523.858959$			
$V_{\bar{\alpha}\alpha}$	$\theta_{12}^{(0)} = 0.220048245$	$\theta_{13} = 0.00427599$	$\theta_{14} = 0.0381563093$	$\theta_{24} = -0.00700797918$	$\theta_{15} = 0.109380331$	$\theta_{25} = 0.063554456$
	$\theta_{12}^{(2)} = -14.9486$					
$U_{i\bar{\alpha}}$	$\sqrt{7/5}/2$	$\sqrt{7/30}$	0	0	0	$-\sqrt{5/3}/2$
	$-\sqrt{2/5}$	$\sqrt{3/5}$	0	0	0	0
	0	0	1	0	0	0
	0	0	0	1	0	0
	0	0	0	0	1	0
	$1/2$	$\sqrt{1/6}$	0	0	0	$\sqrt{7/3}/2$

Table S14. 11-channel MQDT model parameters for the odd-parity $F = 3/2$ series of ^{171}Yb , obtained by spectroscopic data presented in Tab. S32. The electronic configuration of the perturbing Rydberg channels $4f^{13}5d6snp$ is abbreviated as $5d$. The rotations $\mathcal{R}(\theta_{ij})$ are applied in the order $\mathcal{R}(\theta_{12}(\varepsilon))\mathcal{R}(\theta_{13})\mathcal{R}(\theta_{14})\mathcal{R}(\theta_{15})\mathcal{R}(\theta_{16})\mathcal{R}(\theta_{23})\mathcal{R}(\theta_{24})\mathcal{R}(\theta_{25})\mathcal{R}(\theta_{26})\mathcal{R}(\theta_{78})\mathcal{R}(\theta_{79})\mathcal{R}(\theta_{7,10})\mathcal{R}(\theta_{pf})$.

$i, \bar{\alpha}, \alpha$	1 ($F_c = 1$)	2 ($F_c = 1$)	3	4	5	6
$ i\rangle$	$(6s_{1/2})(np_{3/2})$	$(6s_{1/2})(np_{1/2})$	5d a	5d b	5d c	5d d
I_i (cm $^{-1}$)	50 443.217463	50 443.217463	83 967.7	83 967.7	83 967.7	83 967.7
$ \bar{\alpha}\rangle$	$6sn p^1 P_1$	$6sn p^3 P_1$	5d a	5d b	5d c	5d d
$\mu_\alpha^{(0)}$	0.922046003	0.981076381	0.229019212	0.205999445	0.19352756	0.181271472
$\mu_\alpha^{(2)}$	2.17932092	-4.48995034	0.0	0.0	0.0	0.0
$V_{\bar{\alpha}\alpha}$	$\theta_{12}^{(0)}$ -0.100292816	$\theta_{12}^{(2)}$ 149.140925	$\theta_{12}^{(4)}$ -13487.7692	θ_{13} -0.0727917308	θ_{14} -0.0669120237	θ_{15} -0.0221321759
	θ_{16} -0.107302569	θ_{23} 0.0396527798	θ_{24} 0.0596597186	θ_{25} 0.0861416497	θ_{26} 0.0565415641	...
$U_{i\bar{\alpha}}$	$\sqrt{5/3}/2$ -1/ $\sqrt{3}$ 0 0 0 0 1/2 0 0 0 0 0	$\sqrt{5/6}/2$ $\sqrt{2}/3$ 0 0 0 0 0 0 0 0 0	0 0 1 0 0 0 0 0 0 0 0	0 0 0 1 0 0 0 0 0 0 0	0 0 0 0 1 0 0 0 0 0 0	0 0 0 0 0 1 0 0 0 0 0

Table S14 (*continued*)

$i, \bar{\alpha}, \alpha$	7 ($F_c = 0$)	8	9	10	11 ($F_c = 0$)
$ i\rangle$	$(6s_{1/2})(np_{3/2})$	$5d\ e$	$5d\ f$	$5d\ g$	$(6s_{1/2})(n_{f_{5/2}})$
I_i (cm^{-1})	50 442.795744	83 967.7	83 967.7	83 967.7	50 443.217463
$ \bar{\alpha}\rangle$	$6snp\ ^3P_2$	$5d\ e$	$5d\ f$	$5d\ g$	$6snf\ ^3F_2$
$\mu_{\alpha}^{(0)}$	$\mu_{^3P_2}$	0.223859222	0.240057861	0.184824687	$\mu_{^3F_2}^{rr}$
$\mu_{\alpha}^{(2)}$		0.0	0.0	0.0	
$\mu_{^3P_2}$	$\mu_{^3P_2}^{(0)} = 0.926908753$	$\mu_{^3P_2}^{(2)} = -4.6228148$	$\mu_{^3P_2}^{(4)} = 453.565911$		
$\mu_{^3F_2}^{rr}$	$\mu_{^3F_2}^{(0)} = 0.0718810048$	$\mu_{^3F_2}^{(2)} = -1.08216233$	$\mu_{^3F_2}^{(4)} = -38.2507093$		
$V_{\bar{\alpha}\alpha}$		θ_{78} 0.0657620037	θ_{79} 0.0215995148	$\theta_{7,10}$ -0.028252844	θ_{pf} 0.0184267375
<hr/>					
...					
$U_{i\bar{\alpha}}$	$-\sqrt{3/2}/2$	0	0	0	0
	0	0	0	0	0
	0	0	0	0	0
	0	0	0	0	0
	0	0	0	0	0
$U_{i\bar{\alpha}}$	0	0	0	0	0
	$\sqrt{5/2}/2$	0	0	0	0
	0	1	0	0	0
	0	0	1	0	0
	0	0	0	1	0
$U_{i\bar{\alpha}}$	0	0	0	0	-1

Table S15. 12-channel MQDT model parameters for the odd-parity $F = 5/2$ series of ^{171}Yb , obtained by fitting to spectroscopic data presented in Tab. S34. The electronic configuration of the perturbing Rydberg channels $4f^{13}5d6snp$ is abbreviated as $5d$. The rotations $\mathcal{R}(\theta_{ij})$ are applied in the order $\mathcal{R}(\theta_{12})\mathcal{R}(\theta_{13})\mathcal{R}(\theta_{14})\mathcal{R}(\theta_{15})\mathcal{R}(\theta_{16})\mathcal{R}(\theta_{17})\mathcal{R}(\theta_{23})\mathcal{R}(\theta_{24})\mathcal{R}(\theta_{25})\mathcal{R}(\theta_{26})\mathcal{R}(\theta_{27})\mathcal{R}(\theta_{89})\mathcal{R}(\theta_{8,10})\mathcal{R}(\theta_{8,11})\mathcal{R}(\theta_{pf})$.

$i, \bar{\alpha}, \alpha$	1 ($F_c = 1$)	2 ($F_c = 1$)	3	4	5	6
$I_i (\text{cm}^{-1})$	$ i\rangle (6s_{1/2})(nf_{7/2})$	$(6s_{1/2})(nf_{5/2})$	$5d \mathbf{a}$	$5d \mathbf{b}$	$5d \mathbf{c}$	$5d \mathbf{d}$
	50 443.217463	50 443.217463	83 967.7	83 967.7	83 967.7	83 967.7
	$ \bar{\alpha}\rangle 6snf^1F_3$	$6snf^3F_3$	$5d \mathbf{a}$	$5d \mathbf{b}$	$5d \mathbf{c}$	$5d \mathbf{d}$
	$\mu_\alpha^{(0)} 0.27707535$	0.0719827367	0.250829254	0.227042016	0.17576256	0.19654694
$V_{\bar{\alpha}\alpha}$	$\mu_\alpha^{(2)} -13.2829133$	-0.741492064	0.0	0.0	0.0	0.0
	$\theta_{12}^{(0)}$	$\theta_{12}^{(2)}$	θ_{13}	θ_{14}	θ_{15}	θ_{16}
	-0.0208481417	0.239045493	-0.0593782568	-0.0755947274	0.122678758	-0.0400418576
	θ_{17}	θ_{23}	θ_{24}	θ_{25}	θ_{26}	θ_{27}
$U_{i\bar{\alpha}}$	0.0646373252	-0.0684538786	0.0352130279	-0.0326572035	-0.050215299	0.0453892695
	$-2/\sqrt{7}$	$-\sqrt{3}/7$	0	0	0	0
	$\sqrt{5}/7/2$	$-\sqrt{5}/21$	0	0	0	0
	0	0	1	0	0	0
	0	0	0	1	0	0
	0	0	0	0	1	0
	0	0	0	0	0	1
	0	0	0	0	0	0
	0	0	0	0	0	0
	0	0	0	0	0	0
$V_{\bar{\alpha}\alpha}$	-1/2	$1/\sqrt{3}$	0	0	0	0

Table S15 (continued)

$i, \bar{\alpha}, \alpha$	7	8 ($F_c = 1$)	9	10	11	12 ($F_c = 0$)
$I_i (\text{cm}^{-1})$	$5d \mathbf{e}$	$(6s_{1/2})(np_{3/2})$	$5d \mathbf{f}$	$5d \mathbf{g}$	$5d \mathbf{h}$	$(6s_{1/2})(nf_{5/2})$
	83 967.7	50 443.217463	83 967.7	83 967.7	83 967.7	50 442.795744
	$5d \mathbf{e}$	$6snp^3P_2$	$5d \mathbf{f}$	$5d \mathbf{g}$	$5d \mathbf{h}$	$6snf^3F_2$
	$\mu_\alpha^{(0)} 0.214351625$	μ_{3P_2}	0.223859222	0.240057861	0.184824687	$\mu_{3F_2}^{rr}$
$V_{\bar{\alpha}\alpha}$	$\mu_{3P_2}^{(0)} = 0.926908753$	$\mu_{3P_2}^{(2)} = -4.6228148$	$\mu_{3P_2}^{(4)} = 453.565911$			
	$\mu_{3F_2}^{(0)} = 0.0718810048$	$\mu_{3F_2}^{(2)} = -1.08216233$	$\mu_{3F_2}^{(4)} = -38.2507093$			
		θ_{89}	$\theta_{8,10}$	$\theta_{8,11}$		θ_{pf}
		0.0657620037	0.0215995148	-0.028252844		0.0184267375
$U_{i\bar{\alpha}}$	0	0	0	0	0	0
	0	0	0	0	0	$\sqrt{7/3}/2$
	0	0	0	0	0	0
	0	0	0	0	0	0
	0	0	0	0	0	0
	0	0	0	0	0	0
	0	0	0	0	0	0
	0	0	0	0	0	0
	0	0	1	0	0	0
	0	0	0	1	0	0
$V_{\bar{\alpha}\alpha}$	0	0	0	0	1	0
	0	0	0	0	0	$\sqrt{5}/12$

Table S16. Single-channel model parameters for the $6sng\ ^3G_3(F = 5/2)$ series of ^{171}Yb described by Eq. (1), obtained by fitting to spectroscopic data presented in Tab. S26.

$\mu_\alpha^{(0)}$	0.02611627
$\mu_\alpha^{(2)}$	-0.13079392

Table S17. Three-channel MQDT model parameters for the $|\nu, \ell = 4, F = 7/2\rangle$ series of ^{171}Yb , obtained by fitting to spectroscopic data presented in Tab. S39.

$i, \bar{\alpha}, \alpha$	1 ($F_c = 1$)	2 ($F_c = 1$)	3 ($F_c = 0$)
$ i\rangle$	$(6s_{1/2})(ng_{9/2})$	$(6s_{1/2})(ng_{7/2})$	$(6s_{1/2})(ng_{7/2})$
I_i (cm^{-1})	50 443.217463	50 443.217463	50 442.795744
$ \bar{\alpha}\rangle$	$6sng^+G_4$	$6sng^-G_4$	$6sng^3G_3$
$\mu_\alpha^{(0)}$	0.02627822	0.02536987	0.02611627
$\mu_\alpha^{(2)}$	-0.13288481	-0.11668088	-0.13079392
$V_{\bar{\alpha}\alpha}$	$\theta_{12} = -0.08222676$		
$U_{i\bar{\alpha}}$	-1 0 0	0 $-\sqrt{7}/4$ $3/4$	0 $3/4$ $\sqrt{7}/4$

Table S18. Three-channel MQDT model parameters for the $|\nu, \ell = 4, F = 9/2\rangle$ series of ^{171}Yb , obtained by fitting to spectroscopic data presented in Tab. S40.

$i, \bar{\alpha}, \alpha$	1 ($F_c = 1$)	2 ($F_c = 1$)	3 ($F_c = 0$)
$ i\rangle$	$(6s_{1/2})(ng_{9/2})$	$(6s_{1/2})(ng_{7/2})$	$(6s_{1/2})(ng_{9/2})$
I_i (cm^{-1})	50 443.217463	50 443.217463	50 442.795744
$ \bar{\alpha}\rangle$	$6sng^+G_4$	$6sng^-G_4$	$6sng^3G_5$
$\mu_\alpha^{(0)}$	0.02627822	0.02547095	0.02536987
$\mu_\alpha^{(2)}$	-0.13288481	-0.11668088	-0.2007948
$V_{\bar{\alpha}\alpha}$	$\theta_{12} = -0.08222676$		
$U_{i\bar{\alpha}}$	$\sqrt{11/20}$ 0 $\sqrt{9/20}$	0 1 0	$-\sqrt{9/20}$ 0 $\sqrt{11/20}$

Appendix C: Spectroscopy Data

1. ^{174}Yb ${}^1,{}^3F_3$

Table S19: Spectroscopic data of $6snf\,{}^1,{}^3F_3 \leftrightarrow 6sn'd\,{}^1,{}^3D_2$ Rydberg-Rydberg transitions obtained by microwave spectroscopy in an atomic beam setup described in Sec. II A and from Ref. [31].

<i>f</i>	<i>i</i>	$\nu_{f \leftarrow i}$ (MHz)	$\tilde{\nu}_{\text{exp.}}$ (cm^{-1})	$\tilde{\nu}_{\text{th.}}$ (cm^{-1})	$E_{\text{exp.}} - E_{\text{th.}}$ ($\text{h} \cdot \text{MHz}$)	Ref.
$6s29f\,{}^1F_3$	$6s31d\,{}^1D_2$	-164 206.72(10)	50 300.470 140	50 300.470 142	-0.05	This work
$6s29f\,{}^3F_3$	$6s31d\,{}^1D_2$	-99 421.74(10)	50 302.631 134	50 302.631 134	0.00	This work
$6s31f\,{}^3F_3$	$6s33d\,{}^3D_2$	-73 096.89(10)	50 320.720 998	50 320.720 996	0.06	This work
$6s31f\,{}^1F_3$	$6s33d\,{}^1D_2$	-134 171.16(10)	50 318.978 603	50 318.978 607	-0.12	This work
$6s31f\,{}^3F_3$	$6s33d\,{}^1D_2$	-81 935.64(10)	50 320.720 992	50 320.720 996	-0.12	This work
$6s32f\,{}^1F_3$	$6s34d\,{}^1D_2$	-121 856.46(10)	50 326.911 906	50 326.911 903	0.07	This work
$6s32f\,{}^3F_3$	$6s34d\,{}^1D_2$	-74 583.66(10)	50 328.488 756	50 328.488 757	-0.03	This work
$6s33f\,{}^1F_3$	$6s35d\,{}^1D_2$	-110 995.57(10)	50 334.108 980	50 334.108 975	0.16	This work
$6s33f\,{}^3F_3$	$6s35d\,{}^1D_2$	-68 041.70(10)	50 335.541 767	50 335.541 766	0.03	This work
$6s36f\,{}^1F_3$	$6s38d\,{}^1D_2$	-85 230.75(10)	50 352.103 009	50 352.103 004	0.17	This work
$6s36f\,{}^3F_3$	$6s38d\,{}^1D_2$	-52 372.02(10)	50 353.199 059	50 353.199 055	0.11	This work
$6s37f\,{}^1F_3$	$6s39d\,{}^3D_2$	-73 381.29(10)	50 357.119 634	50 357.119 621	0.38	This work
$6s37f\,{}^1F_3$	$6s39d\,{}^1D_2$	-78 426.33(10)	50 357.119 626	50 357.119 621	0.13	This work
$6s38f\,{}^1F_3$	$6s40d\,{}^1D_2$	-72 324.79(10)	50 361.732 705	50 361.732 701	0.12	This work
$6s38f\,{}^3F_3$	$6s40d\,{}^1D_2$	-44 469.84(10)	50 362.661 846	50 362.661 845	0.05	This work
$6s39f\,{}^1F_3$	$6s41d\,{}^1D_2$	-66 838.02(10)	50 365.984 358	50 365.984 354	0.11	This work
$6s39f\,{}^3F_3$	$6s41d\,{}^1D_2$	-41 103.48(10)	50 366.842 770	50 366.842 773	-0.11	This work
$6s40f\,{}^1F_3$	$6s42d\,{}^1D_2$	-61 890.86(10)	50 369.911 346	50 369.911 345	0.03	This work
$6s40f\,{}^3F_3$	$6s43d\,{}^1D_2$	-142 553.73(10)	50 370.706 082	50 370.706 085	-0.09	This work
$6s41f\,{}^1F_3$	$6s43d\,{}^1D_2$	-57 418.65(10)	50 373.545 883	50 373.545 883	-0.01	This work
$6s41f\,{}^3F_3$	$6s44d\,{}^1D_2$	-132 306.30(10)	50 374.283 119	50 374.283 122	-0.09	This work
$6s42f\,{}^1F_3$	$6s42d\,{}^1D_2$	148 111.99(10)	50 376.916 287	50 376.916 286	0.02	This work
$6s42f\,{}^3F_3$	$6s42d\,{}^1D_2$	168 652.95(10)	50 377.601 459	50 377.601 457	0.05	This work
$6s43f\,{}^1F_3$	$6s43d\,{}^1D_2$	137 495.71(10)	50 380.047 526	50 380.047 526	0.02	This work
$6s43f\,{}^3F_3$	$6s43d\,{}^1D_2$	156 619.68(10)	50 380.685 433	50 380.685 432	0.05	This work
$6s44f\,{}^3F_3$	$6s44d\,{}^1D_2$	145 705.65(10)	50 383.556 599	50 383.556 591	0.22	This work
$6s45f\,{}^1F_3$	$6s47d\,{}^1D_2$	-43 276.85(10)	50 385.678 386	50 385.678 392	-0.18	This work
$6s45f\,{}^3F_3$	$6s45d\,{}^1D_2$	135 783.12(10)	50 386.234 069	50 386.234 065	0.14	This work
$6s46f\,{}^1F_3$	$6s48d\,{}^1D_2$	-40 482.28(10)	50 388.215 052	50 388.215 057	-0.15	This work
$6s46f\,{}^3F_3$	$6s46d\,{}^1D_2$	126 742.21(10)	50 388.734 887	50 388.734 881	0.16	This work
$6s46f\,{}^3F_3$	$6s48d\,{}^1D_2$	-24 898.28(10)	50 388.734 878	50 388.734 881	-0.10	This work
$6s47f\,{}^1F_3$	$6s49d\,{}^1D_2$	-37 922.75(10)	50 390.587 240	50 390.587 246	-0.18	This work
$6s47f\,{}^1F_3$	$6s47d\,{}^1D_2$	103 887.00(50)	50 390.587 244	50 390.587 246	-0.06	[31]
$6s47f\,{}^3F_3$	$6s47d\,{}^1D_2$	118 486.92(10)	50 391.074 245	50 391.074 240	0.14	This work
$6s47f\,{}^3F_3$	$6s49d\,{}^1D_2$	-23 322.93(10)	50 391.074 237	50 391.074 240	-0.08	This work
$6s48f\,{}^1F_3$	$6s50d\,{}^1D_2$	-35 574.03(10)	50 392.808 865	50 392.808 870	-0.16	This work
$6s48f\,{}^1F_3$	$6s48d\,{}^1D_2$	97 236.90(50)	50 392.808 869	50 392.808 870	-0.03	[31]
$6s48f\,{}^3F_3$	$6s48d\,{}^1D_2$	110 933.77(10)	50 393.265 747	50 393.265 741	0.20	This work
$6s49f\,{}^1F_3$	$6s49d\,{}^1D_2$	91 142.82(10)	50 394.892 404	50 394.892 403	0.01	This work
$6s49f\,{}^1F_3$	$6s49d\,{}^1D_2$	91 142.70(50)	50 394.892 400	50 394.892 403	-0.11	[31]
$6s49f\,{}^3F_3$	$6s49d\,{}^1D_2$	104 009.38(10)	50 395.321 586	50 395.321 583	0.09	This work
$6s50f\,{}^1F_3$	$6s50d\,{}^1D_2$	85 547.74(10)	50 396.849 052	50 396.849 053	-0.01	This work
$6s50f\,{}^1F_3$	$6s50d\,{}^1D_2$	85 547.80(50)	50 396.849 054	50 396.849 053	0.05	[31]
$6s50f\,{}^3F_3$	$6s50d\,{}^1D_2$	97 649.88(10)	50 397.252 736	50 397.252 733	0.10	This work
$6s50f\,{}^3F_3$	$6s50d\,{}^1D_2$	97 649.50(50)	50 397.252 724	50 397.252 733	-0.28	[31]
$6s51f\,{}^1F_3$	$6s51d\,{}^1D_2$	80 401.70(50)	50 398.688 913	50 398.688 912	0.03	[31]
$6s51f\,{}^3F_3$	$6s51d\,{}^1D_2$	91 798.60(50)	50 399.069 073	50 399.069 072	0.02	[31]
$6s52f\,{}^1F_3$	$6s52d\,{}^1D_2$	75 660.40(50)	50 400.421 092	50 400.421 092	-0.01	[31]
$6s52f\,{}^3F_3$	$6s52d\,{}^1D_2$	86 405.90(50)	50 400.779 523	50 400.779 522	0.04	[31]
$6s53f\,{}^1F_3$	$6s53d\,{}^1D_2$	71 284.90(50)	50 402.053 831	50 402.053 831	-0.01	[31]

Table S19 (*continued*)

<i>f</i>	<i>i</i>	$\nu_{f \leftarrow i}$ (MHz)	$\tilde{\nu}_{\text{exp.}}$ (cm $^{-1}$)	$\tilde{\nu}_{\text{th.}}$ (cm $^{-1}$)	$E_{\text{exp.}} - E_{\text{th.}}$ (h · MHz)	Ref.
$6s53f^3F_3$	$6s53d^1D_2$	81 427.60(50)	50 402.392 155	50 402.392 154	0.04	[31]
$6s54f^1F_3$	$6s54d^1D_2$	67 240.40(50)	50 403.594 592	50 403.594 597	-0.15	[31]
$6s54f^3F_3$	$6s54d^1D_2$	76 824.60(50)	50 403.914 286	50 403.914 286	-0.01	[31]
$6s55f^1F_3$	$6s55d^1D_2$	63 496.60(50)	50 405.050 167	50 405.050 166	0.01	[31]
$6s55f^3F_3$	$6s55d^1D_2$	72 562.20(50)	50 405.352 563	50 405.352 565	-0.07	[31]
$6s56f^1F_3$	$6s56d^1D_2$	60 025.60(50)	50 406.426 705	50 406.426 706	-0.03	[31]
$6s56f^3F_3$	$6s56d^1D_2$	68 609.60(50)	50 406.713 037	50 406.713 037	0.00	[31]
$6s57f^1F_3$	$6s56d^1D_2$	99 092.50(50)	50 407.729 837	50 407.729 834	0.08	[31]
$6s57f^3F_3$	$6s57d^1D_2$	64 938.50(50)	50 408.001 198	50 408.001 213	-0.46	[31]
$6s58f^1F_3$	$6s57d^1D_2$	93 822.90(50)	50 408.964 678	50 408.964 678	0.00	[31]
$6s58f^3F_3$	$6s57d^1D_2$	101 541.10(50)	50 409.222 129	50 409.222 128	0.06	[31]
$6s59f^1F_3$	$6s58d^1D_2$	88 920.70(50)	50 410.135 928	50 410.135 925	0.09	[31]
$6s59f^3F_3$	$6s58d^1D_2$	96 249.30(50)	50 410.380 384	50 410.380 381	0.10	[31]
$6s60f^1F_3$	$6s59d^1D_2$	84 354.30(50)	50 411.247 876	50 411.247 869	0.21	[31]
$6s60f^3F_3$	$6s59d^1D_2$	91 319.00(50)	50 411.480 193	50 411.480 189	0.12	[31]
$6s61f^1F_3$	$6s60d^1D_2$	80 095.20(50)	50 412.304 448	50 412.304 444	0.12	[31]
$6s61f^3F_3$	$6s60d^1D_2$	86 719.80(50)	50 412.525 421	50 412.525 418	0.09	[31]
$6s62f^1F_3$	$6s61d^1D_2$	76 118.30(50)	50 413.309 274	50 413.309 267	0.19	[31]
$6s62f^3F_3$	$6s61d^1D_2$	82 424.40(50)	50 413.519 622	50 413.519 621	0.06	[31]
$6s63f^1F_3$	$6s62d^1D_2$	72 400.40(50)	50 414.265 669	50 414.265 663	0.19	[31]
$6s63f^3F_3$	$6s62d^1D_2$	78 408.20(50)	50 414.466 068	50 414.466 064	0.10	[31]
$6s64f^1F_3$	$6s63d^1D_2$	68 920.70(50)	50 415.176 695	50 415.176 693	0.07	[31]
$6s64f^3F_3$	$6s63d^1D_2$	74 648.70(50)	50 415.367 761	50 415.367 759	0.04	[31]
$6s65f^1F_3$	$6s64d^1D_2$	65 660.70(50)	50 416.045 186	50 416.045 181	0.15	[31]
$6s65f^3F_3$	$6s64d^1D_2$	71 125.90(50)	50 416.227 486	50 416.227 483	0.07	[31]
$6s66f^1F_3$	$6s65d^1D_2$	62 603.00(50)	50 416.873 738	50 416.873 736	0.06	[31]
$6s66f^3F_3$	$6s65d^1D_2$	67 821.20(50)	50 417.047 798	50 417.047 800	-0.07	[31]
$6s67f^1F_3$	$6s66d^1D_2$	59 732.50(50)	50 417.664 773	50 417.664 767	0.18	[31]
$6s67f^3F_3$	$6s66d^1D_2$	64 717.50(50)	50 417.831 055	50 417.831 083	-0.82	[31]
$6s68f^1F_3$	$6s67d^1D_2$	57 034.80(50)	50 418.420 514	50 418.420 508	0.20	[31]
$6s68f^3F_3$	$6s67d^1D_2$	61 801.80(50)	50 418.579 524	50 418.579 526	-0.06	[31]
$6s69f^1F_3$	$6s68d^1D_2$	54 496.50(50)	50 419.143 010	50 419.143 025	-0.47	[31]
$6s69f^3F_3$	$6s68d^1D_2$	59 057.40(50)	50 419.295 145	50 419.295 167	-0.66	[31]
$6s70f^1F_3$	$6s69d^1D_2$	52 107.80(50)	50 419.834 242	50 419.834 239	0.10	[31]
$6s70f^3F_3$	$6s69d^1D_2$	56 474.20(50)	50 419.979 889	50 419.979 894	-0.14	[31]
$6s71f^1F_3$	$6s70d^1D_2$	49 855.70(50)	50 420.495 916	50 420.495 930	-0.42	[31]
$6s71f^3F_3$	$6s70d^1D_2$	54 037.50(50)	50 420.635 406	50 420.635 462	-1.68	[31]
$6s72f^1F_3$	$6s71d^1D_2$	47 732.00(50)	50 421.129 742	50 421.129 757	-0.45	[31]
$6s72f^3F_3$	$6s71d^1D_2$	51 740.00(50)	50 421.263 435	50 421.263 504	-2.07	[31]
$6s73f^1F_3$	$6s72d^1D_2$	45 728.00(50)	50 421.737 272	50 421.737 263	0.27	[31]
$6s73f^3F_3$	$6s72d^1D_2$	49 572.00(50)	50 421.865 494	50 421.865 539	-1.35	[31]
$6s74f^1F_3$	$6s73d^1D_2$	43 834.00(50)	50 422.319 893	50 422.319 884	0.26	[31]
$6s74f^3F_3$	$6s73d^1D_2$	47 524.00(50)	50 422.442 978	50 422.442 984	-0.17	[31]
$6s75f^1F_3$	$6s74d^1D_2$	42 042.00(50)	50 422.878 930	50 422.878 962	-0.94	[31]
$6s75f^3F_3$	$6s74d^1D_2$	45 584.00(50)	50 422.997 079	50 422.997 159	-2.42	[31]

Table S20: Spectroscopic data of $6snf^3F_3 \leftrightarrow 6sn'f^3F_3$ Rydberg-Rydberg transitions obtained by two-photon microwave spectroscopy in an atomic beam setup described in Sec. II A.

<i>f</i>	<i>i</i>	$\nu_{f \leftarrow i}$ (MHz)	$\tilde{\nu}_{\text{exp.}}$ (cm $^{-1}$)	$\tilde{\nu}_{\text{th.}}$ (cm $^{-1}$)	$E_{\text{exp.}} - E_{\text{th.}}$ (h · MHz)	Ref.
$6s35f^3F_3$	$6s35d^3F_3$	-160 978.75(10)	50 347.829 382	50 347.829 377	0.14	This work
$6s37f^3F_3$	$6s37d^3F_3$	-135 934.43(10)	50 358.127 560	50 358.127 566	-0.17	This work

Table S21: Laser spectroscopic data of the $6snp^{1,3}F_3$ Rydberg series included in the determination of the MQDT model. The state energies and respective uncertainties are taken from Refs. [26, 30].

State label	$\tilde{\nu}_{\text{exp.}} \text{ (cm}^{-1}\text{)}$	$\tilde{\nu}_{\text{th.}} \text{ (cm}^{-1}\text{)}$	$E_{\text{exp.}} - E_{\text{th.}}$ ($\text{h} \cdot \text{MHz}$)	Ref.
$4f^{13}5d^26s^3D_3$	48 584.1(5)	48 584.114 897	-447	[30]
$6s9f^1F_3$	48 669.2(5)	48 685.533 000	-489 651	[30]
$6s9f^3F_3$	48 702.0(5)	48 706.677 201	-140 219	[30]
$6s10f^1F_3$	49 032.2(5)	49 033.291 629	-32 726	[30]
$6s10f^3F_3$	49 063.7(5)	49 066.998 105	-98 875	[30]
$4f^{13}5d^26s^1F_3$	49 122.4(5)	49 121.830 010	17 088	[30]
$6s11f^1F_3$	49 308.2(5)	49 314.602 047	-191 929	[30]
$6s11f^3F_3$	49 339.1(5)	49 331.711 343	221 506	[30]
$6s12f^1F_3$	49 503.9(5)	49 508.000 851	-122 940	[30]
$6s12f^3F_3$	49 525.2(5)	49 524.509 732	20 694	[30]
$6s13f^1F_3$	49 653.6(5)	49 656.805 108	-96 087	[30]
$4f^{13}5d^26s^3G_3$	49 661.6(5)	49 702.733 221	143 747	[30]
$6s13f^3F_3$	49 669.6(5)	49 668.862 937	22 097	[30]
$6s14f^1F_3$	49 772.6(5)	49 773.490 091	-26 684	[30]
$6s14f^3F_3$	49 789.6(5)	49 787.740 667	55 741	[30]
$6s15f^1F_3$	49 865.6(5)	49 866.060 843	-13 816	[30]
$6s15f^3F_3$	49 878.2(5)	49 877.843 312	10 693	[30]
$6s16f^1F_3$	49 940.2(5)	49 940.833 994	-19 007	[30]
$6s16f^1F_3$	49 940.54(10)	49 940.833 994	-8938	[26]
$6s16f^3F_3$	49 950.9(5)	49 950.795 043	3147	[30]
$6s16f^3F_3$	49 951.24(10)	49 950.795 043	13 437	[26]
$6s17f^1F_3$	50 001.9(5)	50 002.046 151	-4381	[30]
$6s17f^1F_3$	50 001.74(10)	50 002.046 151	-9032	[26]
$6s17f^3F_3$	50 010.9(5)	50 010.512 221	11 625	[30]
$6s17f^3F_3$	50 010.82(10)	50 010.512 221	9162	[26]
$6s18f^1F_3$	50 052.9(5)	50 052.764 874	4051	[30]
$6s18f^1F_3$	50 052.61(10)	50 052.764 874	-4541	[26]
$6s18f^3F_3$	50 060.3(5)	50 059.980 373	9582	[30]
$6s18f^3F_3$	50 060.35(10)	50 059.980 373	11 144	[26]
$6s19f^1F_3$	50 095.5(5)	50 095.243 412	7692	[30]
$6s19f^1F_3$	50 095.18(10)	50 095.243 412	-2016	[26]
$6s19f^3F_3$	50 101.5(5)	50 101.399 173	3023	[30]
$6s19f^3F_3$	50 101.78(10)	50 101.399 173	11 439	[26]
$6s20f^1F_3$	50 131.1(5)	50 131.163 165	-1894	[30]
$6s20f^1F_3$	50 131.03(10)	50 131.163 165	-3863	[26]
$6s20f^3F_3$	50 136.6(5)	50 136.402 844	5911	[30]
$6s20f^3F_3$	50 136.40(10)	50 136.402 844	56	[26]
$6s21f^1F_3$	50 161.7(5)	50 161.795 284	-2857	[30]
$6s21f^1F_3$	50 161.69(10)	50 161.795 284	-3191	[26]
$6s21f^3F_3$	50 166.23(10)	50 166.210 695	439	[26]
$6s21f^3F_3$	50 166.6(5)	50 166.210 695	11 671	[30]
$6s22f^1F_3$	50 188.04(10)	50 188.102 878	-1872	[26]
$6s22f^3F_3$	50 191.78(10)	50 191.702 033	2228	[26]
$6s23f^1F_3$	50 210.69(10)	50 210.730 948	-1245	[26]
$6s23f^3F_3$	50 213.42(10)	50 213.310 551	3421	[26]
$4f^{13}5d^26s \text{ (}J = 3\text{)}$	50 228.00(10)	50 227.660 774	10 212	[26]
$6s24f^1F_3$	50 231.47(10)	50 231.438 180	968	[26]
$6s26f^3F_3$	50 238.21(10)	50 238.037 593	5122	[26]
$6s25f^1F_3$	50 248.55(10)	50 248.580 288	-940	[26]
$6s25f^3F_3$	50 252.69(10)	50 252.643 079	1261	[26]
$6s26f^1F_3$	50 263.89(10)	50 263.899 769	-206	[26]
$6s27f^3F_3$	50 267.16(10)	50 267.149 825	360	[26]
$6s27f^1F_3$	50 277.47(10)	50 277.505 462	-1094	[26]
$6s28f^3F_3$	50 280.30(10)	50 280.283 178	632	[26]
$6s28f^1F_3$	50 289.61(10)	50 289.627 606	-507	[26]
$6s29f^3F_3$	50 292.05(10)	50 292.061 713	-480	[26]

Table S21 (*continued*)

State label	$\tilde{\nu}_{\text{exp.}} \text{ (cm}^{-1}\text{)}$	$\tilde{\nu}_{\text{th.}} \text{ (cm}^{-1}\text{)}$	$E_{\text{exp.}} - E_{\text{th.}}$ ($h \cdot \text{MHz}$)	Ref.
$6s29f^1F_3$	50 300.48(10)	50 300.470 142	442	[26]

2. ^{174}Yb 3F_2

Table S22: Spectroscopic data of $6snf\ ^3F_2 \leftrightarrow 6sn'd\ ^1,^3D_2$ Rydberg-Rydberg transitions obtained by microwave spectroscopy in an atomic beam setup described in Sec. II A.

f	i	$\nu_{f \leftarrow i}$ (MHz)	$\tilde{\nu}_{\text{exp.}}$ (cm^{-1})	$\tilde{\nu}_{\text{th.}}$ (cm^{-1})	$E_{\text{exp.}} - E_{\text{th.}}$ ($\text{h} \cdot \text{MHz}$)
$6s29f\ ^3F_2$	$6s31d\ ^1D_2$	-106 543.58(10)	50 302.393 575	50 302.393 583	-0.22
$6s31f\ ^3F_2$	$6s33d\ ^3D_2$	-77 781.96(10)	50 320.564 722	50 320.564 713	0.24
$6s31f\ ^3F_2$	$6s33d\ ^1D_2$	-86 620.74(10)	50 320.564 714	50 320.564 713	0.02
$6s32f\ ^3F_2$	$6s34d\ ^1D_2$	-78 514.61(10)	50 328.357 634	50 328.357 632	0.06
$6s33f\ ^3F_2$	$6s35d\ ^1D_2$	-71 392.41(10)	50 335.429 999	50 335.429 997	0.06
$6s34f\ ^3F_2$	$6s36d\ ^1D_2$	-65 108.14(10)	50 341.867 973	50 341.867 970	0.09
$6s36f\ ^3F_2$	$6s38d\ ^1D_2$	-54 592.62(10)	50 353.124 987	50 353.124 984	0.11
$6s38f\ ^3F_2$	$6s41d\ ^1D_2$	-168 201.53(10)	50 362.603 235	50 362.603 234	0.04
$6s39f\ ^3F_2$	$6s42d\ ^1D_2$	-155 461.45(10)	50 366.790 166	50 366.790 168	-0.05
$6s39f\ ^3F_2$	$6s41d\ ^1D_2$	-42 680.44(10)	50 366.790 168	50 366.790 168	0.00
$6s40f\ ^3F_2$	$6s43d\ ^1D_2$	-143 976.38(10)	50 370.658 628	50 370.658 632	-0.12
$6s41f\ ^3F_2$	$6s44d\ ^1D_2$	-133 595.46(10)	50 374.240 117	50 374.240 122	-0.16
$6s42f\ ^3F_2$	$6s42d\ ^1D_2$	167 479.86(10)	50 377.562 329	50 377.562 335	-0.19
$6s43f\ ^3F_2$	$6s43d\ ^1D_2$	155 548.62(10)	50 380.649 707	50 380.649 706	0.01
$6s44f\ ^3F_2$	$6s44d\ ^3D_2$	148 123.37(10)	50 383.523 862	50 383.523 858	0.11
$6s44f\ ^3F_2$	$6s44d\ ^1D_2$	144 724.15(10)	50 383.523 860	50 383.523 858	0.04
$6s45f\ ^3F_2$	$6s45d\ ^3D_2$	138 041.33(10)	50 386.203 985	50 386.203 981	0.12
$6s45f\ ^3F_2$	$6s45d\ ^1D_2$	134 881.05(10)	50 386.203 980	50 386.203 981	-0.05
$6s46f\ ^3F_2$	$6s46d\ ^1D_2$	125 910.68(10)	50 388.707 150	50 388.707 154	-0.14
$6s47f\ ^3F_2$	$6s47d\ ^1D_2$	117 718.50(10)	50 391.048 613	50 391.048 618	-0.16
$6s48f\ ^3F_2$	$6s48d\ ^1D_2$	110 221.93(10)	50 393.242 003	50 393.242 007	-0.12

Table S23: Spectroscopic data of $6snf\ ^3F_2 \leftrightarrow 6sn'f\ ^3F_2$ Rydberg-Rydberg transitions obtained by two-photon microwave spectroscopy in an atomic beam setup described in Sec. II A.

f	i	$\nu_{f \leftarrow i}$ (MHz)	$\tilde{\nu}_{\text{exp.}}$ (cm^{-1})	$\tilde{\nu}_{\text{th.}}$ (cm^{-1})	$E_{\text{exp.}} - E_{\text{th.}}$ ($\text{h} \cdot \text{MHz}$)
$6s35f\ ^3F_2$	$6s35f\ ^3F_2$	-161 281.47(10)	50 347.745 213	50 347.745 208	0.15
$6s37f\ ^3F_2$	$6s37f\ ^3F_3$	-137 903.16(10)	50 358.061 891	50 358.061 891	0.00
$6s38f\ ^3F_2$	$6s38f\ ^3F_2$	-125 521.25(10)	50 362.603 230	50 362.603 234	-0.12

3. ^{174}Yb 3F_4

Table S24: Spectroscopic data of $6snf\,{}^3F_4 \leftrightarrow 6sn'd\,{}^3D_3$ Rydberg-Rydberg transitions obtained by microwave spectroscopy in an atomic beam setup described in Sec. II A.

f	i	$\nu_{f \leftarrow i}$ (MHz)	$\tilde{\nu}_{\text{exp.}}$ (cm^{-1})	$\tilde{\nu}_{\text{th.}}$ (cm^{-1})	$E_{\text{exp.}} - E_{\text{th.}}$ ($\hbar \cdot \text{MHz}$)
$6s46f\,{}^3F_4$	$6s46d\,{}^3D_3$	126 444.06(10)	50 388.680 141	50 388.680 145	-0.09
$6s47f\,{}^3F_4$	$6s47d\,{}^3D_3$	118 209.09(10)	50 391.023 243	50 391.023 247	-0.13
$6s48f\,{}^3F_4$	$6s48d\,{}^3D_3$	110 674.37(10)	50 393.218 148	50 393.218 147	0.05
$6s49f\,{}^3F_4$	$6s49d\,{}^3D_3$	103 766.85(10)	50 395.277 090	50 395.277 083	0.23
$6s50f\,{}^3F_4$	$6s50d\,{}^3D_3$	97 422.14(10)	50 397.211 055	50 397.211 056	-0.03
$6s51f\,{}^3F_4$	$6s51d\,{}^3D_3$	91 584.75(10)	50 399.029 981	50 399.029 979	0.07
$6s52f\,{}^3F_4$	$6s52d\,{}^3D_3$	86 204.42(10)	50 400.742 794	50 400.742 797	-0.11
$6s53f\,{}^3F_4$	$6s53d\,{}^3D_3$	134 615.34(10)	50 402.357 608	50 402.357 607	0.05
$6s54f\,{}^3F_4$	$6s53d\,{}^3D_3$	126 930.25(10)	50 403.881 744	50 403.881 744	0.02

4. ^{174}Yb 3G_3

Table S25: Spectroscopic data of $6sng\ ^3G_3 \leftrightarrow 6sn'd\ ^{1,3}D_2$ Rydberg-Rydberg transitions. The transitions are obtained by two-step microwave spectroscopy via an intermediate $6sn''f\ ^3F_3$ state in an atomic beam setup described in Sec. II A.

f	i	$\nu_{f \leftarrow i}$ (MHz)	$\tilde{\nu}_{\text{exp.}}$ (cm^{-1})	$\tilde{\nu}_{\text{th.}}$ (cm^{-1})	$E_{\text{exp.}} - E_{\text{th.}}$ ($\hbar \cdot \text{MHz}$)
$6s34g\ ^3G_3$	$6s38d\ ^1D_2$	-208 325.48(10)	50 347.997 011	50 347.997 013	-0.07
$6s37g\ ^3G_3$	$6s41d\ ^1D_2$	-162 327.74(10)	50 362.799 164	50 362.799 162	0.06
$6s41g\ ^3G_3$	$6s45d\ ^1D_2$	-119 860.50(10)	50 377.706 716	50 377.706 713	0.10
$6s46g\ ^3G_3$	$6s51d\ ^1D_2$	-145 576.92(10)	50 391.151 078	50 391.151 080	-0.06

Table S26: Predicted g_{th} and experimental g_{exp} factors of the $6sng\ ^3G_3$ Rydberg states obtained from microwave spectroscopy in an atomic beam setup described in Sec. II A.

State Label	g_{exp}	g_{th}
$6s37g\ ^3G_3$	0.746(4)	0.75
$6s41g\ ^3G_3$	0.746(3)	0.75

5. $^{174}\text{Yb}^{\pm G_4}$

Table S27: Spectroscopic data of $6sng^{\pm}G_4 \leftrightarrow 6sn'd^{1,3}D_2$ Rydberg-Rydberg transitions. These transitions are obtained by two-step microwave spectroscopy via an intermediate $6sn''f^3F_3$ state in an atomic beam setup described in Sec. II A.

f	i	$\nu_{f \leftarrow i}$ (MHz)	$\tilde{\nu}_{\text{exp.}}$ (cm^{-1})	$\tilde{\nu}_{\text{th.}}$ (cm^{-1})	$E_{\text{exp.}} - E_{\text{th.}}$ ($h \cdot \text{MHz}$)	Ref.
$6s28g^+G_4$	$6s31d^1D_2$	-93 198.90(10)	50 302.838 706	50 302.838 700	0.17	[33]
$6s29g^+G_4$	$6s32d^1D_2$	-83 854.12(10)	50 312.351 404	50 312.351 395	0.27	[33]
$6s30g^+G_4$	$6s33d^1D_2$	-75 730.23(10)	50 320.927 982	50 320.927 988	-0.18	[33]
$6s31g^+G_4$	$6s34d^1D_2$	-68 628.92(10)	50 328.687 385	50 328.687 393	-0.22	[33]
$6s32g^+G_4$	$6s35d^1D_2$	-62 392.36(10)	50 335.730 209	50 335.730 219	-0.32	[33]
$6s33g^+G_4$	$6s36d^1D_2$	-56 891.84(10)	50 342.142 039	50 342.142 061	-0.65	[33]
$6s34g^+G_4$	$6s38d^1D_2$	-208 352.33(10)	50 347.996 116	50 347.996 100	0.45	This work
$6s34g^-G_4$	$6s38d^1D_2$	-208 219.13(10)	50 348.000 559	50 348.000 558	0.01	This work
$6s37g^+G_4$	$6s41d^1D_2$	-162 348.77(10)	50 362.798 462	50 362.798 449	0.40	This work
$6s37g^-G_4$	$6s41d^1D_2$	-162 245.26(10)	50 362.801 915	50 362.801 916	-0.03	This work
$6s41g^+G_4$	$6s45d^1D_2$	-119 876.03(10)	50 377.706 198	50 377.706 186	0.37	This work
$6s41g^-G_4$	$6s45d^1D_2$	-119 799.73(10)	50 377.708 743	50 377.708 740	0.10	This work
$6s46g^+G_4$	$6s51d^1D_2$	-145 588.17(10)	50 391.150 703	50 391.150 705	-0.07	This work
$6s46g^-G_4$	$6s51d^1D_2$	-145 533.86(10)	50 391.152 514	50 391.152 517	-0.08	This work

Table S28: Predicted g_{th} and experimental g_{exp} factors of the $6sng^{\pm}G_4$ Rydberg states obtained from microwave spectroscopy in an atomic beam setup described in Sec. II A.

State Label	g_{exp}	g_{th}
$6s34g^-G_4$	1.021(4)	1.0327
$6s37g^-G_4$	1.031(4)	1.0327
$6s41g^-G_4$	1.027(5)	1.0327
$6s34g^+G_4$	1.012(9)	1.0174
$6s37g^+G_4$	1.018(4)	1.0174
$6s41g^+G_4$	1.013(4)	1.0174

6. ^{174}Yb 3D_3

Table S29: Spectroscopic data of $6sn\,{}^3D_3 \leftrightarrow 6sn'\,{}^3D_2$ Rydberg-Rydberg transitions obtained by two-photon microwave spectroscopy in an atomic beam setup described in Sec. II A.

f	i	$\nu_{f \leftarrow i}$ (MHz)	$\tilde{\nu}_{\text{exp.}}$ (cm^{-1})	$\tilde{\nu}_{\text{th.}}$ (cm^{-1})	$E_{\text{exp.}} - E_{\text{th.}}$ ($\hbar \cdot \text{MHz}$)
$6s46d\,{}^3D_3$	$6s45d\,{}^3D_2$	85 831.61(10)	50 384.462 457	50 384.462 422	1.05
$6s47d\,{}^3D_3$	$6s46d\,{}^3D_2$	80 078.09(10)	50 387.080 168	50 387.080 212	-1.32
$6s48d\,{}^3D_3$	$6s47d\,{}^3D_2$	74 831.41(10)	50 389.526 471	50 389.526 449	0.66
$6s49d\,{}^3D_3$	$6s48d\,{}^3D_2$	70 028.11(10)	50 391.815 708	50 391.815 801	-2.79
$6s50d\,{}^3D_3$	$6s49d\,{}^3D_2$	65 632.47(10)	50 393.961 388	50 393.961 403	-0.44
$6s52d\,{}^3D_3$	$6s51d\,{}^3D_2$	57 884.10(10)	50 397.867 372	50 397.867 324	1.44

7. ^{174}Yb ${}^1\text{D}_2$

Table S30: Experimental ($\alpha_{0,\text{exp.}}$) and predicted ($\alpha_{0,\text{theo.}}$) static dipole polarizabilities of $6snd\,{}^1D_2$ Rydberg states of ^{174}Yb for $m_J = 0, 1$, scaled by ν_{6s}^7 . The experimental values for $\alpha_{0,\text{exp.}}$ are obtained by measurement of quadratic Stark shifts. Prediction for the static dipole polarizability $\alpha_{0,\text{theo.}}$ are obtained from a non-perturbative diagonalization of the atomic Hamiltonian including electric fields [58].

State label	$m_J = 0$		$m_J = 1$	
	$\alpha_{0,\text{exp.}}/\nu_{6s}^7$ ($h \cdot \text{mHz}/(\text{V/cm})^2$)	$\alpha_{0,\text{theo.}}/\nu_{6s}^7$ ($h \cdot \text{mHz}/(\text{V/cm})^2$)	$\alpha_{0,\text{exp.}}/\nu_{6s}^7$ ($h \cdot \text{mHz}/(\text{V/cm})^2$)	$\alpha_{0,\text{theo.}}/\nu_{6s}^7$ ($h \cdot \text{mHz}/(\text{V/cm})^2$)
$6s40d\,{}^1D_2$	-0.82(6)	-0.826	-0.58(5)	-0.612
$6s41d\,{}^1D_2$	-0.81(10)	-0.823	-0.61(7)	-0.610
$6s42d\,{}^1D_2$	-0.81(2)	-0.820	-0.59(2)	-0.608
$6s43d\,{}^1D_2$	-0.79(4)	-0.816	-0.59(5)	-0.605
$6s44d\,{}^1D_2$	—	—	-0.61(3)	-0.603
$6s45d\,{}^1D_2$	-0.77(3)	-0.809	-0.60(2)	-0.600
$6s47d\,{}^1D_2$	-0.80(1)	-0.799	-0.60(3)	-0.593
$6s49d\,{}^1D_2$	-0.76(7)	-0.789	-0.60(8)	-0.585
$6s51d\,{}^1D_2$	-0.80(5)	-0.775	-0.58(2)	-0.575
$6s52d\,{}^1D_2$	-0.74(5)	-0.767	-0.57(4)	-0.569
$6s53d\,{}^1D_2$	-0.70(12)	-0.758	-0.52(6)	-0.563
$6s56d\,{}^1D_2$	—	—	-0.54(4)	-0.535
$6s57d\,{}^1D_2$	-0.68(5)	-0.703	-0.49(5)	-0.522
$6s58d\,{}^1D_2$	-0.67(5)	-0.681	-0.50(3)	-0.506

Table S31: Experimental ($\alpha_{0,\text{exp.}}$) and predicted ($\alpha_{0,\text{theo.}}$) static dipole polarizabilities of $6snd\,{}^3D_2$ Rydberg states of ^{174}Yb for $m_J = 0, 2$, scaled by ν_{6s}^7 . The experimental values for $\alpha_{0,\text{exp.}}$ are obtained by measurement of quadratic Stark shifts. Prediction for the static dipole polarizability $\alpha_{0,\text{theo.}}$ are obtained from a non-perturbative diagonalization of the atomic Hamiltonian including electric fields [58].

State label	$m_J = 0$		$m_J = 2$	
	$\alpha_{0,\text{exp.}}/\nu_{6s}^7$ ($h \cdot \text{mHz}/(\text{V/cm})^2$)	$\alpha_{0,\text{theo.}}/\nu_{6s}^7$ ($h \cdot \text{mHz}/(\text{V/cm})^2$)	$\alpha_{0,\text{exp.}}/\nu_{6s}^7$ ($h \cdot \text{mHz}/(\text{V/cm})^2$)	$\alpha_{0,\text{theo.}}/\nu_{6s}^7$ ($h \cdot \text{mHz}/(\text{V/cm})^2$)
$6s50d\,{}^3D_2$	0.50(2)	0.505	-0.60(2)	-0.617
$6s53d\,{}^3D_2$	0.82(1)	0.879	-0.64(9)	-0.618
$6s56d\,{}^3D_2$	1.20(12)	1.356	-0.63(6)	-0.618
$6s59d\,{}^3D_2$	1.87(10)	1.981	-0.55(3)	-0.618
$6s62d\,{}^3D_2$	2.83(21)	2.836	-0.54(3)	-0.618

8. ^{171}Yb P and F , $F = 3/2$

Table S32: Spectroscopic data of the odd-parity $F = 3/2$ Rydberg series obtained from microwave spectroscopy in an atomic beam setup described in Sec. II A and from Ref. [13]. The transitions are from $i = |\nu, S, F = 1/2\rangle$ (^a) and $i = |\nu, D, F = 5/2\rangle$ (^b).

$\nu_{F_c=1}^f$	$\nu_{F_c=1}^i$	$\nu_{f \leftarrow i}$ (MHz)	$\tilde{\nu}_{\text{exp.}}$ (cm ⁻¹)	$\tilde{\nu}_{\text{th.}}$ (cm ⁻¹)	$E_{\text{exp.}} - E_{\text{th.}}$ ($h \cdot \text{MHz}$)	Ref.
28.030 820 8	27.720 660 0 ^a	94 221.66(10)	50 303.554 600	50 303.554 509	2.73	[13]
28.071 220 1	27.720 660 0 ^a	106 260.55(10)	50 303.956 173	50 303.956 217	-1.31	[13]
29.858 590 3	29.717 920 8 ^a	35 019.09(10)	50 320.129 965	50 320.129 880	2.55	[13]
30.840 632 3	30.716 600 5 ^a	27 991.62(10)	50 327.843 979	50 327.843 904	2.26	[13]
31.015 842 1	30.716 600 5 ^a	66 958.10(10)	50 329.143 761	50 329.143 722	1.16	[13]
31.068 424 0	30.716 600 5 ^a	78 522.04(10)	50 329.529 492	50 329.529 525	-0.98	[13]
32.800 505 7	33.712 781 1 ^a	-163 250.19(10)	50 341.219 493	50 341.219 442	1.54	[13]
33.004 377 3	32.714 033 5 ^a	53 847.84(10)	50 342.475 682	50 342.475 656	0.77	[13]
33.066 926 4	32.714 033 5 ^a	65 261.55(10)	50 342.856 402	50 342.856 421	-0.54	[13]
33.778 293 1	34.711 547 2 ^a	-152 958.42(10)	50 347.039 127	50 347.039 092	1.05	[13]
33.998 147 4	33.712 781 1 ^a	48 388.47(10)	50 348.278 999	50 348.278 975	0.71	[13]
34.066 266 8	33.712 781 1 ^a	59 758.58(10)	50 348.658 265	50 348.658 277	-0.35	[13]
34.754 702 3	35.710 331 2 ^a	-143 820.20(10)	50 352.367 329	50 352.367 310	0.59	[13]
34.991 564 5	34.711 547 2 ^a	43 525.38(10)	50 353.593 121	50 353.593 099	0.67	[13]
35.065 658 8	34.711 547 2 ^a	54 867.19(10)	50 353.971 443	50 353.971 455	-0.34	[13]
35.729 854 2	34.711 547 2 ^a	153 415.52(10)	50 357.258 661	50 357.258 669	-0.22	[13]
35.984 613 3	35.710 331 2 ^a	39 178.15(10)	50 358.471 497	50 358.471 480	0.51	[13]
36.065 097 2	35.710 331 2 ^a	50 504.09(10)	50 358.849 290	50 358.849 301	-0.34	[13]
36.977 279 3	36.709 132 5 ^a	35 279.35(10)	50 362.960 484	50 362.960 470	0.42	[13]
37.064 577 4	36.709 132 5 ^a	46 599.12(10)	50 363.338 071	50 363.338 083	-0.36	[13]
37.677 229 1	36.709 132 5 ^a	123 844.31(10)	50 365.914 693	50 365.914 725	-0.97	[13]
37.928 821 4	39.281 782 8 ^b	-154 815.18(10)	50 366.936 881	50 366.936 865	0.49	This work
37.969 548 9	37.707 951 4 ^a	31 771.80(10)	50 367.100 431	50 367.100 420	0.34	[13]
38.064 095 2	39.281 782 8 ^b	-138 591.74(10)	50 367.478 037	50 367.478 080	-1.29	This work
38.064 095 2	37.707 951 4 ^a	43 093.02(10)	50 367.478 066	50 367.478 080	-0.42	[13]
38.650 038 8	37.707 951 4 ^a	111 416.29(10)	50 369.757 085	50 369.757 127	-1.26	[13]
38.928 757 6	40.281 707 2 ^b	-143 376.97(10)	50 370.805 289	50 370.805 272	0.53	This work
38.961 410 7	38.706 787 7 ^a	28 607.17(10)	50 370.926 605	50 370.926 597	0.27	[13]
39.063 647 0	38.706 787 7 ^a	39 935.50(10)	50 371.304 478	50 371.304 497	-0.57	[13]
39.622 732 7	38.706 787 7 ^a	100 345.82(10)	50 373.319 549	50 373.319 596	-1.41	[13]
39.952 859 6	39.705 641 9 ^a	25 744.76(10)	50 374.469 951	50 374.469 944	0.22	[13]
40.063 229 6	39.705 641 9 ^a	37 083.96(10)	50 374.848 186	50 374.848 207	-0.61	[13]
40.595 683 2	39.705 641 9 ^a	90 497.21(10)	50 376.629 861	50 376.629 910	-1.49	[13]
40.928 549 0	39.281 782 8 ^b	168 112.56(10)	50 377.708 591	50 377.708 600	-0.26	This work
40.943 915 2	40.704 514 0 ^a	23 151.73(10)	50 377.757 761	50 377.757 761	-0.02	[13]
41.062 840 1	40.704 514 0 ^a	34 501.65(10)	50 378.136 353	50 378.136 377	-0.72	[13]
41.569 243 8	40.704 514 0 ^a	81 748.21(10)	50 379.712 329	50 379.712 377	-1.46	[13]
41.928 131 1	40.281 707 2 ^b	156 103.54(10)	50 380.794 884	50 380.794 879	0.14	This work
41.934 801 1	40.281 707 2 ^b	156 697.60(10)	50 380.814 699	50 380.814 735	-1.07	This work
42.062 475 9	41.703 404 2 ^a	32 157.17(10)	50 381.192 961	50 381.192 990	-0.84	[13]
42.543 722 8	41.703 404 2 ^a	73 986.21(10)	50 382.588 228	50 382.588 273	-1.34	[13]
42.923 452 3	41.281 638 8 ^b	144 854.98(10)	50 383.656 270	50 383.656 261	0.26	This work
42.929 475 5	41.252 322 8 ^b	148 100.17(10)	50 383.672 963	50 383.672 973	-0.30	This work
43.062 134 6	42.702 312 6 ^a	30 023.54(10)	50 384.039 250	50 384.039 279	-0.89	[13]
43.913 466 9	42.281 576 7 ^b	134 229.83(10)	50 386.311 565	50 386.311 565	0.00	This work
43.928 970 1	42.281 576 7 ^b	135 433.28(10)	50 386.351 707	50 386.351 724	-0.49	This work
44.061 814 4	43.701 238 9 ^a	28 077.18(10)	50 386.694 068	50 386.694 102	-1.02	[13]
44.902 607 5	43.701 238 9 ^a	90 943.91(10)	50 388.791 076	50 388.791 064	0.37	[13]
44.928 839 0	43.281 520 2 ^b	126 419.56(10)	50 388.854 587	50 388.854 599	-0.35	This work
45.061 513 3	44.700 182 9 ^a	26 297.88(10)	50 389.174 211	50 389.174 248	-1.11	[13]
45.474 768 0	44.700 182 9 ^a	55 611.41(10)	50 390.152 005	50 390.152 027	-0.66	[13]
45.891 173 6	44.700 182 9 ^a	84 351.63(10)	50 391.110 676	50 391.110 665	0.31	[13]
45.928 769 7	44.281 468 5 ^b	118 191.96(10)	50 391.195 929	50 391.195 937	-0.25	This work

Table S32 (*continued*)

$\nu_{F_c=1}^f$	$\nu_{F_c=1}^i$	$\nu_{f \leftarrow i}$ (MHz)	$\tilde{\nu}_{\text{exp.}}$ (cm $^{-1}$)	$\tilde{\nu}_{\text{th.}}$ (cm $^{-1}$)	$E_{\text{exp.}} - E_{\text{th.}}$ ($h \cdot \text{MHz}$)	Ref.
46.061 229 8	45.699 144 1 ^a	24 667.90(10)	50 391.494 668	50 391.494 707	-1.19	[13]
46.454 674 2	45.699 144 1 ^a	50 822.88(10)	50 392.367 104	50 392.367 122	-0.53	[13]
46.879 193 2	45.699 144 1 ^a	78 308.34(10)	50 393.283 921	50 393.283 913	0.24	[13]
46.928 722 2	49.281 264 7 ^b	-139 216.97(10)	50 393.389 236	50 393.389 258	-0.66	This work
47.060 962 2	45.281 421 0 ^b	119 046.51(10)	50 393.668 856	50 393.668 896	-1.21	This work
47.060 962 2	45.699 144 1 ^a	89 848.41(10)	50 393.668 856	50 393.668 896	-1.21	[13]
47.436 056 3	46.698 121 6 ^a	46 571.54(10)	50 394.449 387	50 394.449 396	-0.25	[13]
47.928 685 3	46.281 377 3 ^b	103 762.80(10)	50 395.446 753	50 395.446 757	-0.12	This work
48.060 709 4	46.698 121 6 ^a	84 328.11(10)	50 395.708 811	50 395.708 851	-1.23	[13]
48.418 868 7	47.697 114 5 ^a	42 790.10(10)	50 396.409 099	50 396.409 104	-0.18	[13]
47.866 665 5	46.698 121 6 ^a	72 758.62(10)	50 395.322 894	50 395.322 886	0.25	[13]
48.853 583 6	47.697 114 5 ^a	67 653.05(10)	50 397.238 437	50 397.238 430	0.21	[13]
49.060 470 1	47.697 114 5 ^a	79 252.57(10)	50 397.625 355	50 397.625 397	-1.25	[13]
49.403 040 3	48.696 121 5 ^a	39 419.62(10)	50 398.255 494	50 398.255 494	0.01	[13]
49.839 938 9	48.281 299 5 ^b	86 890.51(10)	50 399.040 335	50 399.040 315	0.59	This work
50.060 243 1	51.693 211 6 ^a	-81 630.86(10)	50 399.428 246	50 399.428 288	-1.26	[13]
50.388 484 2	48.696 121 5 ^a	91 626.72(10)	50 399.996 935	50 399.996 934	0.04	[13]
50.825 722 1	52.692 257 8 ^a	-88 626.40(10)	50 400.737 374	50 400.737 361	0.39	[13]
50.928 604 4	48.281 299 5 ^b	142 906.15(10)	50 400.908 816	50 400.908 819	-0.09	This work
51.375 105 8	50.694 172 0 ^a	33 709.67(10)	50 401.641 039	50 401.641 033	0.19	[13]
51.810 924 1	50.694 172 0 ^a	54 590.95(10)	50 402.337 563	50 402.337 549	0.44	[13]
52.362 808 4	50.694 172 0 ^a	80 288.24(10)	50 403.194 733	50 403.194 726	0.20	[13]
52.795 535 8	51.693 211 6 ^a	50 873.91(10)	50 403.848 129	50 403.848 114	0.47	[13]
52.928 563 7	50.281 232 2 ^b	126 913.64(10)	50 404.045 738	50 404.045 763	-0.75	This work
53.351 496 8	51.693 211 6 ^a	75 343.99(10)	50 404.664 363	50 404.664 353	0.31	[13]
54.762 954 0	53.691 308 0 ^a	44 227.83(10)	50 406.626 094	50 406.626 075	0.59	[13]
55.331 473 1	53.691 308 0 ^a	66 654.24(10)	50 407.374 159	50 407.374 150	0.27	[13]
56.059 091 8	53.281 146 1 ^b	112 004.36(10)	50 408.298 541	50 408.298 568	-0.83	This work
57.058 927 9	59.685 488 0 ^a	-86 979.65(10)	50 409.511 571	50 409.511 606	-1.05	[13]
57.928 485 7	55.281 096 2 ^b	96 147.45(10)	50 410.515 927	50 410.515 921	0.16	This work
59.670 607 4	58.686 495 7 ^a	31 248.46(10)	50 412.397 566	50 412.397 533	0.98	[13]
60.058 471 6	58.686 495 7 ^a	43 142.10(10)	50 412.794 295	50 412.794 325	-0.91	[13]
60.293 017 6	58.686 495 7 ^a	50 225.78(10)	50 413.030 581	50 413.030 563	0.53	[13]
60.650 219 1	59.685 488 0 ^a	29 146.52(10)	50 413.385 123	50 413.385 090	0.98	[13]
61.058 329 4	59.685 488 0 ^a	41 060.28(10)	50 413.782 523	50 413.782 553	-0.92	[13]
61.286 808 1	59.685 488 0 ^a	47 629.02(10)	50 414.001 633	50 414.001 613	0.60	[13]
62.607 490 3	61.683 374 2 ^a	25 337.93(10)	50 415.221 249	50 415.221 209	1.20	[13]
63.058 056 5	61.683 374 2 ^a	37 287.29(10)	50 415.619 836	50 415.619 861	-0.73	[13]
63.275 450 7	61.683 374 2 ^a	42 963.77(10)	50 415.809 184	50 415.809 168	0.46	[13]
63.928 418 3	60.280 988 0 ^b	100 361.22(10)	50 416.366 204	50 416.366 208	-0.13	This work
63.585 148 9	61.683 374 2 ^a	50 949.20(10)	50 416.075 549	50 416.075 508	1.21	[13]
64.057 924 6	62.682 248 5 ^a	35 576.29(10)	50 416.474 646	50 416.474 669	-0.71	[13]
64.270 208 5	62.682 248 5 ^a	40 864.94(10)	50 416.651 056	50 416.651 040	0.48	[13]
64.562 160 3	62.682 248 5 ^a	48 052.49(10)	50 416.890 807	50 416.890 765	1.26	[13]
65.057 794 9	63.681 060 4 ^a	33 970.77(10)	50 417.290 348	50 417.290 371	-0.69	[13]
65.265 193 5	63.681 060 4 ^a	38 904.19(10)	50 417.454 909	50 417.454 891	0.55	[13]
65.538 533 5	63.681 060 4 ^a	45 333.94(10)	50 417.669 382	50 417.669 338	1.35	[13]
66.057 666 6	64.679 793 0 ^a	32 463.28(10)	50 418.069 297	50 418.069 315	-0.53	[13]
66.260 353 7	64.679 793 0 ^a	37 069.78(10)	50 418.222 953	50 418.222 933	0.60	[13]
66.514 284 2	64.679 793 0 ^a	42 781.05(10)	50 418.413 461	50 418.413 412	1.48	[13]
67.057 538 9	64.679 793 0 ^a	54 778.70(10)	50 418.813 660	50 418.813 675	-0.47	[13]
69.928 367 4	65.280 888 7 ^b	99 201.62(10)	50 420.776 287	50 420.776 286	0.04	This work

Table S33: Predicted g_{th} and experimental g_{exp} factors of odd-parity $F = 3/2$ Rydberg states obtained from microwave spectroscopy in an atomic beam setup described in Sec. II A and from Ref. [13].

$\nu_{F_c=1}$	g_{exp}	g_{th}	Ref.
28.030 820 8	1.05(2)	1.037	[13]
28.071 220 1	1.48(2)	1.461	[13]
29.858 590 3	0.96(2)	0.954	[13]
30.840 632 3	0.97(2)	0.953	[13]
31.015 842 1	1.12(2)	1.115	[13]
31.068 424 0	1.39(2)	1.380	[13]
33.004 377 3	1.13(10)	1.159	This work
33.778 293 1	0.97(2)	0.951	[13]
34.754 702 3	0.98(2)	0.951	[13]
34.991 564 5	1.20(2)	1.196	[13]
35.065 658 8	1.29(2)	1.297	[13]
35.729 854 2	0.97(2)	0.951	[13]
37.677 229 1	0.98(2)	0.952	[13]
37.969 548 9	1.24(2)	1.238	[13]
38.064 095 2	1.25(2)	1.250	[13]
38.064 095 2	1.23(10)	1.250	This work
38.961 410 7	1.251(10)	1.249	This work
39.952 859 6	1.25(10)	1.258	This work
40.595 683 2	0.985(2)	0.956	This work
40.928 549 0	0.802(10)	0.809	This work
40.943 915 2	1.263(2)	1.262	This work
41.569 243 8	0.95(2)	0.958	[13]
41.928 131 1	0.844(3)	0.850	This work
41.934 801 1	1.235(2)	1.230	This work
42.062 475 9	1.22(2)	1.203	[13]
42.543 722 8	0.95(2)	0.961	[13]
42.923 452 3	1.26(10)	1.233	This work
42.929 475 5	0.847(10)	0.854	This work
43.913 466 9	1.28(2)	1.289	This work
43.928 970 1	0.807(4)	0.806	This work
44.902 607 5	1.293(3)	1.300	This work
44.928 839 0	0.80(10)	0.801	This work
45.891 173 6	1.297(4)	1.307	This work
45.891 173 6	1.30(2)	1.307	[13]
45.928 769 7	0.80(10)	0.800	This work
46.061 229 8	1.17(2)	1.169	[13]
46.454 674 2	0.99(2)	0.974	[13]
46.879 193 2	1.308(4)	1.311	This work
47.060 962 2	1.14(10)	1.162	This work
47.436 056 3	1.01(2)	0.978	This work
47.928 685 3	0.802(2)	0.799	This work
50.060 243 1	1.16(2)	1.143	[13]
52.362 808 4	1.02(2)	0.996	[13]
55.745 744 1	1.31(10)	1.336	This work
56.059 091 8	1.098(10)	1.115	This work
56.928 499 2	0.800(2)	0.799	This work
57.709 448 2	1.36(2)	1.338	[13]
58.058 770 3	1.12(2)	1.108	[13]
58.306 747 3	1.03(2)	1.016	[13]
58.690 348 8	1.41(2)	1.339	[13]
59.058 618 4	1.13(2)	1.104	[13]
59.299 646 5	1.04(2)	1.019	[13]
59.670 607 4	1.35(2)	1.339	[13]
60.058 471 6	1.11(2)	1.101	[13]
60.293 017 6	1.05(2)	1.022	[13]
60.650 219 1	1.36(2)	1.340	[13]
61.058 329 4	1.12(2)	1.098	[13]
61.286 808 1	1.05(2)	1.025	[13]
62.607 490 3	1.35(2)	1.340	[13]

Table S33 (*continued*)

$\nu F_c = 1$	g_{exp}	g_{th}	Ref.
63.058 056 5	1.10(2)	1.092	[13]
63.275 450 7	1.06(2)	1.032	[13]

9. ^{171}Yb P and F , $F = 5/2$

Table S34: Spectroscopic data of the odd-parity $F = 5/2$ Rydberg series obtained from microwave spectroscopy in an atomic beam setup described in Sec. II A. The transitions are from $i = |\nu, D, F = 3/2\rangle$ (^a) and $i = |\nu, D, F = 5/2\rangle$ (^b).

$\nu_{F_c=1}^f$	$\nu_{F_c=1}^i$	$\nu_{f \leftarrow i}$ (MHz)	$\tilde{\nu}_{\text{exp.}}$ (cm ⁻¹)	$\tilde{\nu}_{\text{th.}}$ (cm ⁻¹)	$E_{\text{exp.}} - E_{\text{th.}}$ (h · MHz)
29.723 686 5	30.283 095 1 ^b	-136 300.49(10)	50 319.010 053	50 319.010 054	-0.04
30.894 873 0	31.282 851 9 ^b	-84 962.57(10)	50 328.248 683	50 328.248 661	0.65
30.894 873 0	31.287 340 8 ^a	-85 927.51(10)	50 328.248 671	50 328.248 661	0.30
30.940 609 8	31.282 851 9 ^b	-74 783.86(10)	50 328.588 208	50 328.588 306	-2.95
31.890 935 7	32.282 646 5 ^b	-78 022.77(10)	50 335.318 251	50 335.318 243	0.24
31.939 622 1	32.282 646 5 ^b	-68 170.47(10)	50 335.646 888	50 335.646 939	-1.53
32.714 236 2	33.282 470 3 ^b	-104 067.63(10)	50 340.680 805	50 340.680 782	0.68
32.886 865 8	33.282 470 3 ^b	-71 881.43(10)	50 341.754 421	50 341.754 427	-0.18
32.938 842 0	32.282 646 5 ^b	124 519.97(10)	50 342.074 349	50 342.074 384	-1.06
33.710 889 2	34.282 317 3 ^b	-95 701.22(10)	50 346.654 115	50 346.654 096	0.56
33.882 669 9	34.282 317 3 ^b	-66 423.17(10)	50 347.630 725	50 347.630 741	-0.47
33.938 211 0	33.282 470 3 ^b	113 656.98(10)	50 347.943 316	50 347.943 347	-0.93
34.080 914 5	33.282 470 3 ^b	137 526.43(10)	50 348.739 515	50 348.739 540	-0.74
34.707 379 1	35.282 183 4 ^b	-88 261.34(10)	50 352.119 407	50 352.119 394	0.38
34.878 357 2	35.282 183 4 ^b	-61 547.08(10)	50 353.010 499	50 353.010 353	4.35
34.937 690 3	34.282 317 3 ^b	104 030.56(10)	50 353.316 450	50 353.316 483	-0.99
35.703 668 9	36.282 065 2 ^b	-81 627.17(10)	50 357.132 545	50 357.132 537	0.22
35.873 939 6	35.282 183 4 ^b	86 471.57(10)	50 357.947 869	50 357.947 779	2.71
35.937 253 8	35.282 183 4 ^b	95 467.48(10)	50 358.247 940	50 358.247 970	-0.88
36.699 721 1	37.281 960 3 ^b	-75 696.51(10)	50 361.741 922	50 361.741 919	0.07
36.936 882 6	36.282 065 2 ^b	87 822.98(10)	50 362.784 793	50 362.784 825	-0.94
37.080 001 3	38.281 866 7 ^b	-147 881.39(10)	50 363.404 544	50 363.404 523	0.65
37.695 497 6	38.281 866 7 ^b	-70 382.34(10)	50 365.989 635	50 365.989 634	0.01
37.936 563 3	37.281 960 3 ^b	80 976.35(10)	50 366.967 966	50 366.967 996	-0.88
37.936 563 3	39.281 782 8 ^b	-153 882.91(10)	50 366.967 979	50 366.967 996	-0.51
39.079 490 5	38.281 866 7 ^b	90 701.44(10)	50 371.362 811	50 371.362 795	0.49
40.079 259 7	39.281 782 8 ^b	84 000.12(10)	50 374.902 902	50 374.902 886	0.50
40.680 776 5	39.281 782 8 ^b	144 116.39(10)	50 376.908 165	50 376.908 186	-0.63
40.850 884 4	39.281 782 8 ^b	160 637.21(10)	50 377.459 240	50 377.459 276	-1.05
40.935 827 7	39.281 782 8 ^b	168 810.34(10)	50 377.731 866	50 377.731 894	-0.82
41.675 049 9	40.281 707 2 ^b	133 304.99(10)	50 380.034 406	50 380.034 426	-0.60
41.846 232 4	40.281 707 2 ^b	148 770.30(10)	50 380.550 273	50 380.550 301	-0.83
41.935 636 6	40.281 707 2 ^b	156 772.37(10)	50 380.817 194	50 380.817 222	-0.83
42.841 624 1	41.286 268 0 ^a	137 593.99(10)	50 383.428 508	50 383.428 518	-0.29
43.662 122 1	42.281 576 7 ^b	114 531.18(10)	50 385.654 488	50 385.654 511	-0.69
43.837 084 7	42.281 576 7 ^b	128 279.09(10)	50 386.113 069	50 386.113 085	-0.47
43.935 311 7	42.281 576 7 ^b	135 925.30(10)	50 386.368 119	50 386.368 138	-0.57
44.078 470 6	45.281 421 0 ^b	-88 770.33(10)	50 386.736 832	50 386.736 812	0.62
44.078 470 6	42.281 576 7 ^b	146 978.74(10)	50 386.736 823	50 386.736 812	0.33
45.646 971 5	44.252 270 0 ^b	101 091.48(10)	50 390.551 642	50 390.551 652	-0.30
45.828 305 4	44.286 097 1 ^a	110 995.74(10)	50 390.967 586	50 390.967 605	-0.55
45.935 046 0	44.252 270 0 ^b	120 832.89(10)	50 391.210 144	50 391.210 152	-0.23
46.638 475 9	45.281 421 0 ^b	92 012.94(10)	50 392.767 113	50 392.767 134	-0.61
46.638 475 9	48.281 299 5 ^b	-101 175.78(10)	50 392.767 119	50 392.767 134	-0.44
46.824 105 7	45.281 421 0 ^b	103 981.71(10)	50 393.166 348	50 393.166 352	-0.11
47.077 992 8	45.281 421 0 ^b	120 122.55(10)	50 393.704 749	50 393.704 738	0.31
47.820 053 9	46.281 377 3 ^b	97 248.93(10)	50 395.229 474	50 395.229 472	0.06
49.812 435 1	48.281 299 5 ^b	85 427.29(10)	50 398.991 527	50 398.991 517	0.30
49.934 638 6	48.281 299 5 ^b	91 908.49(10)	50 399.207 717	50 399.207 718	-0.04
50.077 590 2	48.281 299 5 ^b	99 430.44(10)	50 399.458 622	50 399.458 620	0.05
50.597 745 6	48.281 299 5 ^b	126 263.59(10)	50 400.353 680	50 400.353 696	-0.50
50.808 878 5	48.281 299 5 ^b	136 921.82(10)	50 400.709 200	50 400.709 192	0.25

Table S34 (*continued*)

$\nu_{F_c=1}^f$	$\nu_{F_c=1}^i$	$\nu_{f \leftarrow i}$ (MHz)	$\tilde{\nu}_{\text{exp.}}$ (cm $^{-1}$)	$\tilde{\nu}_{\text{th.}}$ (cm $^{-1}$)	$E_{\text{exp.}} - E_{\text{th.}}$ (h · MHz)
51.077 470 0	53.281 146 1 ^b	-102 150.71(10)	50 401.155 096	50 401.155 077	0.57
51.077 470 0	54.281 120 6 ^b	-144 454.70(10)	50 401.155 085	50 401.155 077	0.23
51.585 785 9	54.281 120 6 ^b	-119 726.43(10)	50 401.979 931	50 401.979 942	-0.33
51.805 491 1	54.281 120 6 ^b	-109 261.85(10)	50 402.328 992	50 402.328 974	0.53
52.802 269 5	50.281 232 2 ^b	121 290.47(10)	50 403.858 169	50 403.858 154	0.45
52.934 407 7	50.281 232 2 ^b	127 173.80(10)	50 404.054 416	50 404.054 412	0.13
53.559 660 1	50.281 232 2 ^b	154 425.52(10)	50 404.963 435	50 404.963 449	-0.42
55.530 563 7	53.281 146 1 ^b	91 982.81(10)	50 407.630 693	50 407.630 703	-0.30
55.793 527 0	53.281 146 1 ^b	102 016.62(10)	50 407.965 385	50 407.965 365	0.62
56.076 954 7	53.281 146 1 ^b	112 671.89(10)	50 408.320 807	50 408.320 811	-0.13
57.076 866 2	53.281 146 1 ^b	149 006.14(10)	50 409.532 787	50 409.532 789	-0.06
57.788 367 0	55.281 096 2 ^b	91 389.49(10)	50 410.357 218	50 410.357 147	2.14
57.934 114 0	55.281 096 2 ^b	96 338.09(10)	50 410.522 286	50 410.522 275	0.33
58.481 328 2	55.281 096 2 ^b	114 594.90(10)	50 411.131 268	50 411.131 275	-0.23
62.405 277 7	58.281 029 2 ^b	123 788.23(10)	50 415.039 481	50 415.039 481	-0.02
62.777 095 9	58.281 029 2 ^b	133 766.11(10)	50 415.372 307	50 415.372 280	0.81
62.933 893 5	58.281 029 2 ^b	137 920.08(10)	50 415.510 869	50 415.510 858	0.32
63.384 417 7	60.280 988 0 ^b	86 484.43(10)	50 415.903 324	50 415.903 325	-0.02
63.775 016 1	60.280 988 0 ^b	96 484.82(10)	50 416.236 901	50 416.236 879	0.68
63.933 855 2	60.280 988 0 ^b	100 498.62(10)	50 416.370 787	50 416.370 775	0.37
70.218 109 7	65.280 888 7 ^b	104 742.30(10)	50 420.961 104	50 420.961 103	0.05
70.760 195 0	65.280 888 7 ^b	114 926.84(10)	50 421.300 824	50 421.300 803	0.62
70.933 613 4	65.280 888 7 ^b	118 135.08(10)	50 421.407 839	50 421.407 836	0.09
73.075 840 3	68.280 823 7 ^b	89 564.00(10)	50 422.667 789	50 422.667 799	-0.30
73.136 577 7	68.280 823 7 ^b	90 587.36(10)	50 422.701 925	50 422.701 916	0.25
74.075 752 8	68.280 823 7 ^b	106 083.51(10)	50 423.218 820	50 423.218 835	-0.43
74.108 258 5	68.280 823 7 ^b	106 610.97(10)	50 423.236 415	50 423.236 375	1.20
75.080 052 9	68.280 823 7 ^b	122 016.99(10)	50 423.750 304	50 423.750 276	0.84
75.933 393 2	68.280 823 7 ^b	135 059.98(10)	50 424.185 371	50 424.185 363	0.24
75.075 068 0	68.280 823 7 ^b	121 937.70(10)	50 423.747 659	50 423.747 691	-0.95
76.075 891 6	68.280 823 7 ^b	137 195.11(10)	50 424.256 592	50 424.256 595	-0.09
77.075 788 9	68.280 823 7 ^b	151 847.80(10)	50 424.745 353	50 424.745 360	-0.21

Table S35: Predicted g_{th} and experimental g_{exp} factors of odd-parity $F = 5/2$ Rydberg states obtained from microwave spectroscopy in an atomic beam setup described in Sec. II A.

$\nu_{F_c=1}$	g_{exp}	g_{th}
37.936 563 3	1.052(6)	1.059
40.079 259 7	1.194(3)	1.200
40.850 884 4	0.761(2)	0.764
41.675 049 9	1.089(2)	1.096
41.935 636 6	1.044(2)	1.043
43.662 122 1	1.078(10)	1.081
43.837 084 7	0.793(10)	0.794
43.935 311 7	1.033(3)	1.038
46.638 475 9	1.048(9)	1.055
47.820 053 9	0.833(10)	0.838
49.934 638 6	1.043(10)	1.027
51.585 785 9	1.007(3)	1.008
51.805 491 1	0.876(2)	0.882
55.530 563 7	0.978(2)	0.974
55.793 527 0	0.917(10)	0.920
62.405 277 7	0.932(7)	0.930
62.777 095 9	0.977(10)	0.968

Table S35 (*continued*)

$\nu_{F_c=1}$	g_{exp}	g_{th}
62.933 893 5	1.027(6)	1.015
73.075 840 3	1.186(13)	1.200
73.136 577 7	0.885(6)	0.897
74.075 752 8	1.173(4)	1.200
74.108 258 5	0.890(10)	0.897
75.075 068 0	1.125(11)	1.155
75.080 052 9	0.937(3)	0.941
76.075 891 6	1.203(4)	1.199
77.075 788 9	1.200(10)	1.200

10. ^{171}Yb $F, F = 7/2$

Table S36: Spectroscopic data of the $|\nu, \ell = 3, F = 7/2\rangle$ Rydberg series obtained from microwave spectroscopy in an atomic beam setup described in Sec. II A. The transitions are from $i = |\nu, D, F = 5/2\rangle$ states.

$\nu_{F_c=1}^f$	$\nu_{F_c=1}^i$	$\nu_{f \leftarrow i}$ (MHz)	$\tilde{\nu}_{\text{exp.}}$ (cm $^{-1}$)	$\tilde{\nu}_{\text{th.}}$ (cm $^{-1}$)	$E_{\text{exp.}} - E_{\text{th.}}$ ($\text{h} \cdot \text{MHz}$)
30.885 083 7	31.282 851 9	-87 145.34(10)	50 328.175 873	50 328.175 768	3.16
30.942 905 9	31.282 851 9	-74 269.75(10)	50 328.605 357	50 328.605 317	1.18
31.881 374 4	32.282 646 5	-79 965.79(10)	50 335.253 439	50 335.253 514	-2.27
31.941 644 8	32.282 646 5	-67 759.09(10)	50 335.660 610	50 335.660 563	1.42
32.711 596 7	33.282 470 3	-104 564.56(10)	50 340.664 229	50 340.664 234	-0.15
32.877 558 5	33.282 470 3	-73 606.58(10)	50 341.696 876	50 341.696 973	-2.91
32.940 622 4	32.282 646 5	124 849.84(10)	50 342.085 352	50 342.085 317	1.06
33.708 047 5	34.282 317 3	-96 190.18(10)	50 346.637 805	50 346.637 814	-0.28
33.873 641 1	34.282 317 3	-67 952.65(10)	50 347.579 707	50 347.579 779	-2.13
33.939 775 7	33.282 470 3	113 922.24(10)	50 347.952 164	50 347.952 132	0.96
34.704 308 2	35.282 183 4	-88 745.27(10)	50 352.103 264	50 352.103 271	-0.20
34.939 062 7	34.282 317 3	104 244.01(10)	50 353.323 570	50 353.323 546	0.73
35.700 342 0	36.282 065 2	-82 108.64(10)	50 357.116 484	50 357.116 492	-0.22
35.938 453 9	35.282 183 4	95 639.08(10)	50 358.253 664	50 358.253 645	0.59
36.696 111 9	37.281 960 3	-76 177.27(10)	50 361.725 885	50 361.725 892	-0.19
36.937 928 0	36.282 065 2	87 960.84(10)	50 362.789 392	50 362.789 377	0.43
37.691 580 4	38.281 866 7	-70 863.81(10)	50 365.973 575	50 365.973 581	-0.19
37.857 168 1	39.281 782 8	-163 478.85(10)	50 366.647 892	50 366.647 835	1.72
37.937 469 2	37.281 960 3	81 086.78(10)	50 366.971 650	50 366.971 637	0.37
37.937 469 2	39.281 782 8	-153 772.47(10)	50 366.971 662	50 366.971 637	0.75
38.852 926 9	40.281 707 2	-151 857.99(10)	50 370.522 393	50 370.522 337	1.68
40.675 793 3	39.281 782 8	143 629.54(10)	50 376.891 925	50 376.891 938	-0.37
40.844 435 4	39.281 782 8	160 017.04(10)	50 377.438 554	50 377.438 508	1.36
40.936 389 3	39.281 782 8	168 865.00(10)	50 377.733 690	50 377.733 690	-0.02
41.669 671 6	40.281 707 2	132 816.37(10)	50 380.018 107	50 380.018 115	-0.23
41.840 229 2	40.281 707 2	148 233.02(10)	50 380.532 352	50 380.532 317	1.04
41.936 103 3	40.281 707 2	156 814.83(10)	50 380.818 610	50 380.818 610	-0.01
42.836 078 9	41.281 638 8	137 563.91(10)	50 383.413 066	50 383.413 037	0.85
43.655 914 6	42.281 576 7	114 040.96(10)	50 385.638 136	50 385.638 140	-0.11
43.832 005 3	42.281 576 7	127 883.35(10)	50 386.099 869	50 386.099 849	0.58
43.935 611 9	42.281 576 7	135 949.23(10)	50 386.368 918	50 386.368 915	0.06
45.639 914 0	44.252 270 0	100 603.43(10)	50 390.535 362	50 390.535 363	-0.02
45.639 914 0	44.281 468 5	98 388.83(10)	50 390.535 367	50 390.535 363	0.14
45.824 162 3	44.281 468 5	111 063.84(10)	50 390.958 160	50 390.958 156	0.12
45.935 205 5	44.252 270 0	120 844.12(10)	50 391.210 519	50 391.210 513	0.17
46.630 998 4	45.281 421 0	91 528.65(10)	50 392.750 959	50 392.750 952	0.19
46.820 423 2	45.281 421 0	103 745.65(10)	50 393.158 474	50 393.158 479	-0.13
46.935 027 6	45.281 421 0	111 065.79(10)	50 393.402 648	50 393.402 645	0.08
49.810 050 2	48.281 299 5	85 299.53(10)	50 398.987 266	50 398.987 282	-0.50
49.810 050 2	52.281 173 1	-122 386.39(10)	50 398.987 270	50 398.987 282	-0.37
49.934 573 2	48.281 299 5	91 905.08(10)	50 399.207 603	50 399.207 603	0.01
49.934 573 2	52.281 173 1	-115 780.71(10)	50 399.207 611	50 399.207 603	0.26
50.588 725 9	48.281 299 5	125 805.68(10)	50 400.338 405	50 400.338 410	-0.15
50.806 886 5	48.281 299 5	136 820.95(10)	50 400.705 835	50 400.705 858	-0.69
52.563 426 2	50.281 232 2	110 542.26(10)	50 403.499 647	50 403.499 651	-0.12
52.934 209 2	50.281 232 2	127 164.91(10)	50 404.054 119	50 404.054 118	0.05
54.535 266 7	52.281 173 1	97 439.90(10)	50 406.319 885	50 406.319 895	-0.29
54.795 634 3	52.281 173 1	107 926.44(10)	50 406.669 679	50 406.669 708	-0.89
54.934 003 6	52.281 173 1	113 439.91(10)	50 406.853 588	50 406.853 592	-0.10
57.933 736 5	55.281 096 2	96 324.93(10)	50 410.521 847	50 410.521 849	-0.06
63.372 720 1	60.280 988 0	86 181.29(10)	50 415.893 213	50 415.893 241	-0.84
63.933 299 0	60.280 988 0	100 483.94(10)	50 416.370 298	50 416.370 308	-0.31
69.932 899 7	65.280 888 7	99 288.25(10)	50 420.779 177	50 420.779 194	-0.53
70.206 047 7	65.280 888 7	104 511.80(10)	50 420.953 416	50 420.953 454	-1.16
70.761 859 6	65.280 888 7	114 956.93(10)	50 421.301 828	50 421.301 835	-0.20

Table S36 (*continued*)

$\nu_{F_c=1}^f$	$\nu_{F_c=1}^i$	$\nu_{f \leftarrow i}$ (MHz)	$\tilde{\nu}_{\text{exp.}}$ (cm $^{-1}$)	$\tilde{\nu}_{\text{th.}}$ (cm $^{-1}$)	$E_{\text{exp.}} - E_{\text{th.}}$ (h · MHz)
70.932 824 7	65.280 888 7	118 119.86(10)	50 421.407 332	50 421.407 351	-0.59

Table S37: Predicted g_{th} and experimental g_{exp} factors of $|\nu, \ell = 3, F = 7/2\rangle$ Rydberg states obtained from microwave spectroscopy in an atomic beam setup described in Sec. II A.

$\nu_{F_c=1}$	g_{exp}	g_{th}
32.711 596 7	0.844(6)	0.868
33.708 047 5	0.864(9)	0.871
37.857 168 1	1.295(10)	1.265
37.937 469 2	1.013(4)	1.024
41.669 671 6	0.886(7)	0.909
41.936 103 3	1.032(4)	1.035
45.639 914 0	0.940(6)	0.942
45.824 162 3	1.172(2)	1.189
45.935 205 5	1.028(3)	1.043
49.810 050 2	1.136(3)	1.147
49.934 573 2	1.037(3)	1.049
54.535 266 7	1.014(4)	1.022
54.795 634 3	1.098(4)	1.098
54.934 003 6	1.046(5)	1.055

11. ^{171}Yb G, $F = 5/2$

Table S38: Spectroscopic data of the $|\nu, \ell = 4, F = 5/2\rangle$ Rydberg series obtained from microwave spectroscopy in an atomic beam setup described in Sec. II A. The transitions are two-step: from a $i = |\nu, D, F = 5/2\rangle$ state and via an intermediate $|\nu, F, F = 7/2\rangle$ state.

$\nu_{F_c=1}^f$	$\nu_{F_c=1}^i$	$\nu_{f \leftarrow i}$ (MHz)	$\tilde{\nu}_{\text{exp.}}$ (cm^{-1})	$\tilde{\nu}_{\text{th.}}$ (cm^{-1})	$E_{\text{exp.}} - E_{\text{th.}}$ ($\text{h} \cdot \text{MHz}$)
34.973 990 7	36.282 065 2	-190 437.84(10)	50 353.503 011	50 353.503 007	0.13
37.973 974 4	39.281 782 8	-149 380.70(10)	50 367.118 156	50 367.118 160	-0.13
40.973 961 6	42.281 576 7	-119 329.68(10)	50 377.853 730	50 377.853 730	-0.01

12. ^{171}Yb $G, F = 7/2$

Table S39: Spectroscopic data of the $|\nu, \ell = 4, F = 7/2\rangle$ Rydberg series obtained from microwave spectroscopy in an atomic beam setup described in Sec. II A. The transitions are two-step: from a $i = |\nu, D, F = 5/2\rangle$ state and via an intermediate $|\nu, F, F = 7/2\rangle$ state.

$\nu_{F_c=1}^f$	$\nu_{F_c=1}^i$	$\nu_{f \leftarrow i}$ (MHz)	$\tilde{\nu}_{\text{exp.}}$ (cm^{-1})	$\tilde{\nu}_{\text{th.}}$ (cm^{-1})	$E_{\text{exp.}} - E_{\text{th.}}$ ($\text{h} \cdot \text{MHz}$)
34.892 428 7	36.282 065 2	-203 026.45(10)	50 353.083 100	50 353.083 097	0.10
34.973 831 5	36.282 065 2	-190 462.24(10)	50 353.502 197	50 353.502 190	0.21
34.974 270 8	36.282 065 2	-190 394.75(10)	50 353.504 449	50 353.504 444	0.14
37.869 540 6	39.281 782 8	-161 981.08(10)	50 366.697 853	50 366.697 859	-0.21
37.973 815 0	39.281 782 8	-149 399.95(10)	50 367.117 514	50 367.117 521	-0.23
37.974 255 0	39.281 782 8	-149 346.93(10)	50 367.119 282	50 367.119 285	-0.08
40.973 802 0	42.281 576 7	-119 345.14(10)	50 377.853 214	50 377.853 221	-0.20
40.974 242 6	42.281 576 7	-119 302.90(10)	50 377.854 623	50 377.854 627	-0.11
42.973 794 8	45.281 421 0	-176 942.50(10)	50 383.795 725	50 383.795 728	-0.08
42.974 235 8	45.281 421 0	-176 905.82(10)	50 383.796 949	50 383.796 947	0.04
45.973 785 8	48.281 299 5	-145 225.66(10)	50 391.297 773	50 391.297 763	0.32

13. ^{171}Yb $G, F = 9/2$

Table S40: Spectroscopic data of the $|\nu, \ell = 4, F = 9/2\rangle$ Rydberg series obtained from microwave spectroscopy in an atomic beam setup described in Sec. II A. The transitions are two-step: from a $i = |\nu, D, F = 5/2\rangle$ state and via an intermediate $|\nu, F, F = 7/2\rangle$ state.

$\nu_{F_c=1}^f$	$\nu_{F_c=1}^i$	$\nu_{f \leftarrow i}$ (MHz)	$\tilde{\nu}_{\text{exp.}}$ (cm^{-1})	$\tilde{\nu}_{\text{th.}}$ (cm^{-1})	$E_{\text{exp.}} - E_{\text{th.}}$ ($\text{h} \cdot \text{MHz}$)
34.892 445 8	36.282 065 2	-203 023.95(10)	50 353.083 184	50 353.083 185	-0.05
34.974 263 0	36.282 065 2	-190 396.26(10)	50 353.504 398	50 353.504 404	-0.17
34.974 625 6	36.282 065 2	-190 340.14(10)	50 353.506 270	50 353.506 264	0.19
37.869 552 3	39.281 782 8	-161 979.41(10)	50 366.697 908	50 366.697 907	0.05
37.974 242 1	39.281 782 8	-149 348.46(10)	50 367.119 231	50 367.119 233	-0.06
37.974 611 0	39.281 782 8	-149 304.28(10)	50 367.120 705	50 367.120 712	-0.20
40.974 225 7	42.281 576 7	-119 304.20(10)	50 377.854 580	50 377.854 573	0.21
40.974 599 5	42.281 576 7	-119 268.84(10)	50 377.855 759	50 377.855 765	-0.18
42.974 216 7	45.281 421 0	-176 907.14(10)	50 383.796 905	50 383.796 894	0.31
42.974 593 2	45.281 421 0	-176 876.28(10)	50 383.797 934	50 383.797 936	-0.04
45.974 585 1	48.281 299 5	-145 171.52(10)	50 391.299 579	50 391.299 568	0.33

14. ^{171}Yb $D, F = 3/2$

Table S41: Experimental ($\alpha_{0,\text{exp.}}$) and predicted ($\alpha_{0,\text{theo.}}$) static dipole polarizabilities of $|\nu, \ell = 2, F = 3/2\rangle$ Rydberg states of ^{171}Yb , scaled by $\nu_{F_c=1}^7$. The experimental values for $\alpha_{0,\text{exp.}}$ are obtained by measurement of quadratic Stark shifts. Prediction for the static dipole polarizability $\alpha_{0,\text{theo.}}$ are obtained from a non-perturbative diagonalization of the atomic Hamiltonian including electric fields.

$\nu_{F_c=1}$	$m_F = 1/2$		$m_F = 3/2$	
	$\alpha_{0,\text{exp.}}/\nu_{F_c=1}^7$ ($h \cdot \text{mHz}/(\text{V/cm})^2$)	$\alpha_{0,\text{theo.}}/\nu_{F_c=1}^7$ ($h \cdot \text{mHz}/(\text{V/cm})^2$)	$\alpha_{0,\text{exp.}}/\nu_{F_c=1}^7$ ($h \cdot \text{mHz}/(\text{V/cm})^2$)	$\alpha_{0,\text{theo.}}/\nu_{F_c=1}^7$ ($h \cdot \text{mHz}/(\text{V/cm})^2$)
29.2877938	-0.70(8)	-0.722	—	—
31.2873408	-0.70(10)	-0.709	-0.16(5)	-0.133
33.2870187	-0.67(10)	-0.689	-0.14(4)	-0.135
35.2867706	-0.67(10)	-0.661	-0.16(10)	-0.137
39.2864065	-0.55(2)	-0.555	-0.19(10)	-0.138
40.2863344	-0.50(10)	-0.505	-0.17(10)	-0.138
41.2862680	-0.45(3)	-0.435	-0.19(10)	-0.138
42.2862067	-0.33(10)	-0.328	-0.17(3)	-0.137
43.2861499	-0.16(4)	-0.140	-0.15(4)	-0.136
44.2860971	0.22(7)	0.273	-0.15(4)	-0.135
45.2860479	1.92(25)	1.965	-0.14(7)	-0.134
46.2860020	—	—	-0.15(7)	-0.132
47.2859589	-2.23(34)	-2.103	-0.17(7)	-0.130
48.2859185	-1.65(14)	-1.545	-0.15(5)	-0.128

15. ^{171}Yb $D, F = 5/2$

Table S42: Experimental ($\alpha_{0,\text{exp.}}$) and predicted ($\alpha_{0,\text{theo.}}$) static dipole polarizabilities of $|\nu, \ell = 2, F = 5/2\rangle$ Rydberg states of ^{171}Yb , scaled by $\nu_{F_c=1}^7$. The experimental values for $\alpha_{0,\text{exp.}}$ are obtained by measurement of quadratic Stark shifts. Prediction for the static dipole polarizability $\alpha_{0,\text{theo.}}$ are obtained from a non-perturbative diagonalization of the atomic Hamiltonian including electric fields.

$\nu_{F_c=1}$	$m_F = 1/2$		$m_F = 3/2$		$m_F = 5/2$	
	$\alpha_{0,\text{exp.}}/\nu_{F_c=1}^7$ ($h \cdot \text{mHz}/(\text{V/cm})^2$)	$\alpha_{0,\text{theo.}}/\nu_{F_c=1}^7$ ($h \cdot \text{mHz}/(\text{V/cm})^2$)	$\alpha_{0,\text{exp.}}/\nu_{F_c=1}^7$ ($h \cdot \text{mHz}/(\text{V/cm})^2$)	$\alpha_{0,\text{theo.}}/\nu_{F_c=1}^7$ ($h \cdot \text{mHz}/(\text{V/cm})^2$)	$\alpha_{0,\text{exp.}}/\nu_{F_c=1}^7$ ($h \cdot \text{mHz}/(\text{V/cm})^2$)	$\alpha_{0,\text{theo.}}/\nu_{F_c=1}^7$ ($h \cdot \text{mHz}/(\text{V/cm})^2$)
27.2840767	-0.78(9)	-0.858	—	—	—	—
30.2830568	-0.89(10)	-0.880	-0.56(3)	-0.616	—	—
33.2824685	-0.87(10)	-0.894	-0.63(3)	-0.630	-0.104(4)	-0.100
36.2820774	-0.94(3)	-0.903	-0.62(3)	-0.638	-0.11(10)	-0.110
39.2818018	-0.90(2)	-0.906	-0.64(3)	-0.643	-0.13(2)	-0.116
42.2815999	-0.90(2)	-0.906	-0.59(5)	-0.644	-0.13(4)	-0.121
45.2814471	-0.91(2)	-0.901	-0.66(5)	-0.642	-0.14(6)	-0.123
48.2813279	-0.88(10)	-0.891	-0.62(5)	-0.635	—	—